UNIVERSITÀ
DEGLI STUDI
FIRENZE

DOTTORATO DI RICERCA IN SCIENZE DELLA TERRA

CICLO XXIX

COORDINATORE Prof. LORENZO ROOK

Study of CO_2 leakage from gas reservoirs through the further development of a gas flux device and the role of CO_2 on cap rock integrity and cement/casing degradation by Reaction-Path- and Reactive-Transport-Modeling

Settore Scientifico Disciplinare GEO/08 (Geochimica e Vulcanologia)

Dottorando
Dott. Ana Hernández Rodríguez

Tutore
Prof. Orlando Vaselli

Coordinatore
Prof. Lorenzo Rook

Anni 2013/2016

TITLE: Study of CO_2 leakage from gas reservoirs through the further development of a gas flux device and the role of CO_2 on cap rock integrity and cement/casing degradation by Reaction-Path- and Reactive-Transport-Modeling.

Ph.D STUDENT: Ana Hernández Rodríguez [(1), (2)].

TUTOR: Orlando Vaselli [(2)].

CO-TUTORS: Luigi Marini [(1)], Giordano Montegrossi [(2)], Bruno Huet [(4)], Giorgio Virgili [(1)].

INSTITUTIONS:

[(1)] West Systems s.r.l., Viale Donato Giannotti 24, I-50126 Florence, Italy.

[(2)] Dipartimento di Scienze della Terra, Università di Firenze, Via La Pira 4, I-50121, Florence, Italy.

[(3)] CNR-IGG. Via La Pira 4, I-50121, Florence, Italy.

[(4)] LafargeHolcim Research Center, 95 Rue du Montmurier, 38070 Saint-Quentin-Fallavier, France

REVIEWERS:

Andri Stefansson, University of Iceland, Institute of Earth Sciences, Reykjavík, Iceland

Marìa José Gimeno, Department of Earth Sciences, University of Zaragoza, Spain

TABLE OF CONTENTS

EXTENDED ABSTRACT

My PhD Thesis is focused on the study of three distinct aspects related to geological CO_2 storage, namely:

(i) wellbore cement alteration and well integrity by using Reaction Path and Reactive Transport Modeling;

(ii) cement carbonation by means of laboratory experiments;

(iii) monitoring of CO_2 leakage from the deep reservoirs where CO_2 is injected, by using the accumulation chamber method.

For what concerns **wellbore cement alteration and well integrity**, this study presents the results obtained in the natural analogue for the geological storage of CO_2 of Sant'Albino, Southern Tuscany, which is affected by intense CO_2 degassing and where a thermal spa and a CO_2 production plant are present. Reaction Path Modelling (RPM) of cement hydration and carbonation as well as Reactive Transport Modelling (RTM) of cement alteration were used to investigate the processes occurring near a hypothetical average production well with a damaged leaking zone, affecting casing and cement, assuming a defined composition of class G Portland cement. It turns out that the advective flow of CO_2 from the damaged zone, first, leads to completion of cement carbonation and, second, promotes further cement alteration through considerable dissolution of carbonate minerals. These processes takes place in a relatively short time, in the order of some years. The ultimate consequence of these CO_2-promoted comparatively fast chemical reactions is, most likely, the CO_2 leakage to the surface.

Regarding **cement carbonation**, three types of laboratory experiments were carried out at room temperature and different P_{CO2} values, in the range 1 to 51 bar, on G-class Portland cement. Cement hydration (accompanied by limited carbonation) was carried out for 28 days at atmospheric conditions. Afterwards, cement carbonation was investigated using a micro-reactor by reacting, in separate runs, cement powder samples, under stirred conditions, and massive samples, under stagnant conditions, with pure CO_2(g) and MilliQ water. After the completion of each experiments, analyses were performed on both, the aqueous solution (IC, ICP-OES, acidimetric titration) and the solids (XRD, SEM, TGA/DTA). In type 1 experiments cement powder was reacted at 11 bar P_{CO2}, for 1, 3, 6, 21, 67, 97 and 120 hours. Portlandite was present only in the hydrated cement paste and was converted to $CaCO_3$ in less than one hour. In type 2 experiments cement powder was reacted for 6 hours at P_{CO2} of 1, 11, 31 and 51 bar. The extent of cement carbonation was similar at all P_{CO2} values. The experiments of type 3 were performed with cement cube samples at 11 bar P_{CO2} for 6,

24 and 210 hours. The average carbonation depth attained 0.23 mm in 1 day and resulted to be linearly related to the square root of reaction time indicating that cement carbonation rate is controlled by diffusion (Fickian behavior).

Concerning the **monitoring of CO_2 leakage from the deep reservoirs where CO_2 is injected**, three different types of laboratory experiments were carried out to improve the present understanding of the accumulation chamber method. In particular, in type A experiments a standard gas mixture was continuously injected, at constant flux, into the accumulation chamber, mimicking the soil CO_2 flux measurements performed in field surveys. In type B experiments, a standard gas mixture was initially injected into the accumulation chamber for a short lapse of time, to achieve a relatively high CO_2 concentration inside the accumulation chamber; then the injection of the standard gas mixture was stopped and the CO_2 concentration inside the chamber was monitored for a sufficient interval of time. The type C experiments, which are a modified version of those of type B, including the use of a plaster to seal the chamber-desk interface, to verify the absence of gas leakage in the system.In both types of experiments A and B, the accumulation chamber appears to be flushed by a considerable flux of atmospheric air, which is virtually constant in each experiment but is different from experiment to experiment. We underscore that the occurrence of this air flux through the accumulation chamber (i) has no effect on the determination of the soil CO_2 flux on the basis of the initial slope (at time zero) of the CO_2 concentration-time curve, but (ii) it complicates the evaluation of the two components of the soil CO_2 flux, namely the CO_2 molar fraction of soil gas and the flux of the soil gas mixture. Atmospheric air enters and leaves the accumulation chamber chiefly through the interface between the chamber rim and the surface onto which the chamber rests whereas the pressure compensation device is considered a less likely pathway for atmospheric air. The air flux appears to be controlled by the membrane pump flowrate in type B experiments, in which there is only a gas flow driven by the membrane pump, from the accumulation chamber to the CO_2 analyzer and back again into the chamber, whereas no gas flow enters the chamber from below. In type A experiments, there is both a gas flow entering the chamber from below and a gas flow driven by the membrane pump. Consequently, the gas exchanges between the chamber and the atmosphere are probably more complex than in the the experiments of type B, leading to a relation between the air flux and the gas flow entering the chamber from below, when this is relatively high (1.67 to 6.67 $cm^3\ s^{-1}$). A possible way to obtain the two components of the soil CO_2 flux is presented although it must be improved. The implications related to the knowledge of both the CO_2 molar fraction of soil gas and the flux of the soil gas mixture are discussed.

ACKNOWLEDGEMENTS

This PhD is dedicated to my lovely parents Isabel and Jose, who have always supported me unconditionally, not only during the PhD but also during everything I have done so far, wherever.

I would like to thank my supervisor Luigi Marini for everything I have learnt, all the patience, dedication and support he has gave me during these years. I would like to thank also, West Systems and the technical director Giorgio Virgili to gave me the opportunity to work there. I thank all my colleagues from West Systems who supported me and shared this experience with me. Also, I have to thank everybody from the Earth Science department at the University of Florence and CNR-IGG; Orlando Vaselli, Giordano Montegrossi, Andrea Orlando and all the people who help me; Stefania Venturi, Giulia Dotta, Francesco Capecchiacci, Jacopo Cabassi and Franco Tassi for all the help and advices.

There are also more people that I met during this period that I want to express my gratitude: Francesca, Alex and Tere, Beatrice, Luca and Rosella, Carlos and Benedetta, all the fellows from the CO_2 REACT and MINSC projects who I shared with very nice moments.

I would like to thank Bruno Huet and Alexander Pisch from Lafarge-Holcim research center in Lyon, for allowing me to develop part of my research with them, for their assistance, kindness and hospitality during my stay there.

An especial mention and thanks to my Mentor in geochemist; the exceptional Professor Manolo Prieto, from the University of Oviedo.

To my biggest support in Italy during my stay, my friend Fernando Berro, I do thank his generosity and support, and the all great and bad moments we shared together. Also, my Sardinian friend Maria who helped me to communicate in Italian and gave me a warm welcome since the beginning, together with my special friend Elizabeth, for her warmth, generosity and the joy she radiates. I also want to give a huge thank to my *"Italian brother"* Francesco Maffei and his family for all the support and affection I received from them.

Thanks to my inseparable "*A Team"*; my twin Inés, my sister Zaida and my brothers Javier and Alfonso, thanks for all the love, support and wonderful moments they always give me. I would also like to say thanks to my other "sister" Gemy for being always there, for her support in the distance, the long phone conversation, etc. I want to thank my lovely friends Juanjo, Andrea and Marta for all

their support from the distance and I want to dedicate a few special words to my little sweeties Elaia and Simón.

I want to dedicate some words for all the people who supported me during these years in the distance, Tía Chiqui, Beni, Yoli, Laure, and two people who are not here my grantmother Isa and my uncle Javi.

The most special and important thanks are for my boyfriend Mariano, who despite the distance and all the difficulties during this period he has always been supporting me and giving me the faith and love I have always needed.

The last acknowledgement is for the European Commission which has supported the CO_2 REACT Marie Curie Initial Training network, together with all the fellows, supervisors and managers within the project.

1.1 Changes in atmospheric CO_2 concentration with time.

Time changes in atmospheric CO_2 concentration have been monitored since 1957 (Keeling et al., 1995; Keeling and Whorf, 2003). Estimates of atmospheric CO_2 during the Earth's history have been obtained using CO_2 proxies data. Although the uncertainties of these data grow considerably with increasing time before present, the available picture leaves no doubt on the continuous increase of atmospheric CO_2 concentration after the industrial revolution (Figure 1.1).

The monthly average atmospheric CO_2 concentration in January - October 2016 has attained 401-408 ppmv based on the measurements of NOAA (National Oceanic & Atmospheric Administration) and Scripps Institution of Oceanography (SIO) with an increase of 28% approximately compared to the 312-318 ppmv in 1958 (https://www.co2.earth/monthly-co2). The current atmospheric CO_2 levels are approximately 46% higher than the ~277 ppmv of the years 1740-1780, before the industrial revolution (Figure 1.1)

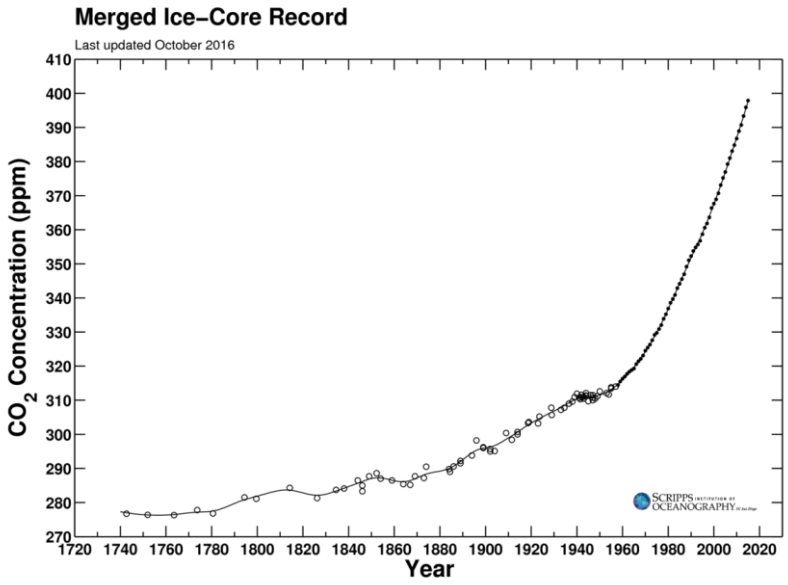

Figure 1. 1. Atmospheric CO_2 record based on ice core data before 1958 (Etheridge et. al., 1996; MacFarling Meure et al., 2006) and yearly averages of direct observations from Mauna Loa and the South Pole after and including 1958 (from Scripps CO_2 Program).

Ice core records provide a high-resolution proxy record of the atmospheric CO_2 concentration during the past. Atmospheric CO_2 concentration was close to 280 ± 5 ppmv during the past 1000 years (Siegenthaler et al., 1988; Neftel et al., 1994; Barnola et al., 1995; Etheridge et al., 1996). The Taylor Dome Antarctic ice core indicates that atmospheric CO_2 concentration varied between 260

and 280 ppmv during the past 11,000 years (Smith et al., 1999; Indermühle et al., 1999) and similar values are suggested by ice core BH7 near Vostok (Peybernès et al., 2000). Study of the Vostok Antarctic ice core indicates that during the last four glacial – interglacial cycles, i.e., during the past 420,000 years, atmospheric CO_2 concentration oscillated between 180 and 300 ppmv and it was high during the interglacial periods and low during the glacial ones (Figure 1.2; Petit et al., 1999; Fischer et al., 1999). In spite of these large changes, atmospheric CO_2 concentration was always lower than at present.

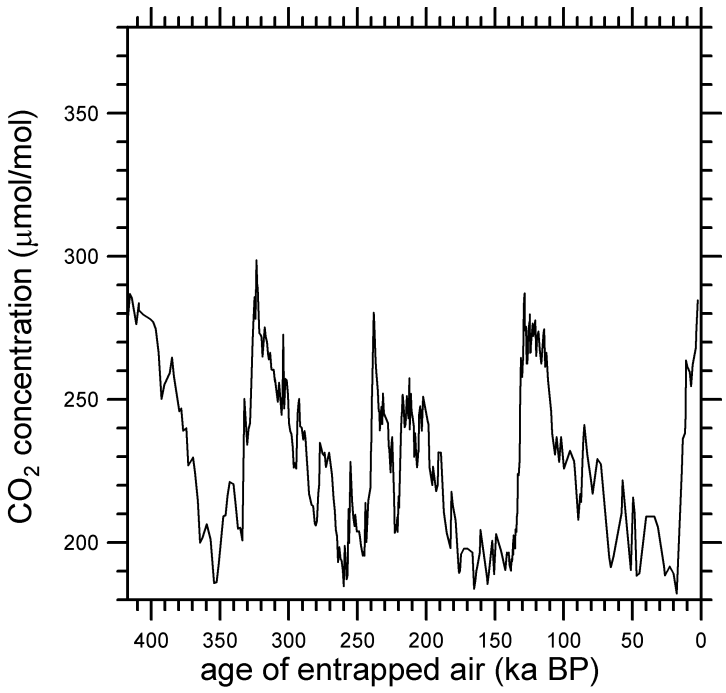

Figure 1.2. Carbon dioxide concentration in the air bubbles trapped in the Vostok Antarctic ice core (data from Barnola et al., 2003 and references therein).

Many types of proxy records were combined to reconstruct the atmospheric CO_2 levels from thousands to many millions of years ago. Hönisch et al. (2009) analyzed a sediment core obtained from the bottom of the Atlantic ocean westward of Sierra Leone. From the ancient shells of *Globigerinoides ruber* in the sediment core, these authors developed a high-resolution record of the oxygen isotope ratio, indicating that atmospheric CO_2 levels fluctuated between 213 and 283 ppmv (± 30 ppmv approximately) during the period between 900,000 years ago and 2.1 million years ago. This is similar to the range of 180 to 300 ppmv established by the ice core record. Atmospheric CO_2 levels during the Pliocene, between 2.6 and 5.3 million years ago, seem to be similar to the present day levels (Zhang et al., 2014). Evidence suggests that it has likely been millions of years since atmospheric CO_2 was higher than today (Hönisch et al., 2009; Zhang et al., 2013; Zhang et al, 2014).

1.2. The causes of the increase in atmospheric CO_2 concentration and future predictions

The increase in atmospheric CO_2 concentration from the industrial revolution is unanimously attributed to the burning of fossil fuels, coal, natural gas, and oil, and subordinately to the production of cement. The annual global emission of CO_2 from burning of fossil fuels and cement production has been evaluated for the period of time from 1751 to 1999 (Marland et al., 2000) with average values of $5.4 \pm 0.3 \times 10^{15}$ g C/year during the 1980s and $6.3 \pm 0.4 \times 10^{15}$ g C/year during the 1990s. Fossil fuel emissions (including cement production) accounted for about 91% of total CO_2 emissions from human sources in 2014. This portion of emissions originates from coal (42%), oil (33%), gas (19%), cement (6%) and gas flaring (1%). In 2013, the largest national contributions to the net growth in total global emissions (https://www.co2.earth/global-co2-emissions) were China (58% of the growth), USA (20% of the growth), India (17% of the growth), and EU28 (11% of the growth).

Since anthropogenic emissions are assumed to be responsible of the rise in atmospheric CO_2 concentration, it is instructive to compare the rate of both anthropogenic emissions and atmospheric CO_2 content (Figure 1.3). This comparison shows that the rates of increase in atmospheric CO_2 are less than the emission, suggesting that the emitted CO_2 is partly taken up by the two carbon reservoirs acting as sinks, that is the oceanic waters and the terrestrial ecosystems.

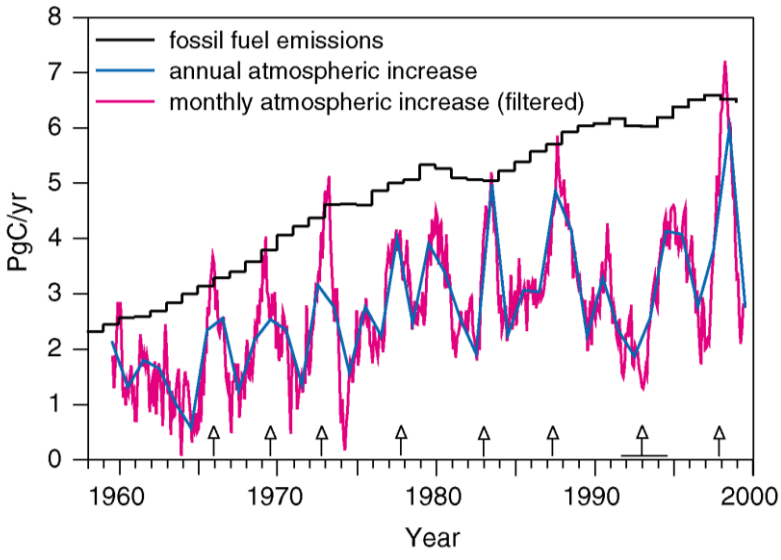

Figure 1.3. Comparison of fossil fuel emissions and the rate of rise in atmospheric CO_2 concentration The annual atmospheric increase is the measured increment during a calendar year whereas the monthly atmospheric increases was filtered to eliminate the seasonal cycle. Vertical arrows indicate El Niño events. (from Prentice et al., 2001)

To a first approximation, about a half of the human-induced emissions is absorbed relatively fast by both the oceans and the terrestrial ecosystems, whereas the rest remains in the atmosphere. Absorption of CO_2 in marine waters causes their acidification (Figure 1.4) and potential negative impacts to the marine plants and animals.

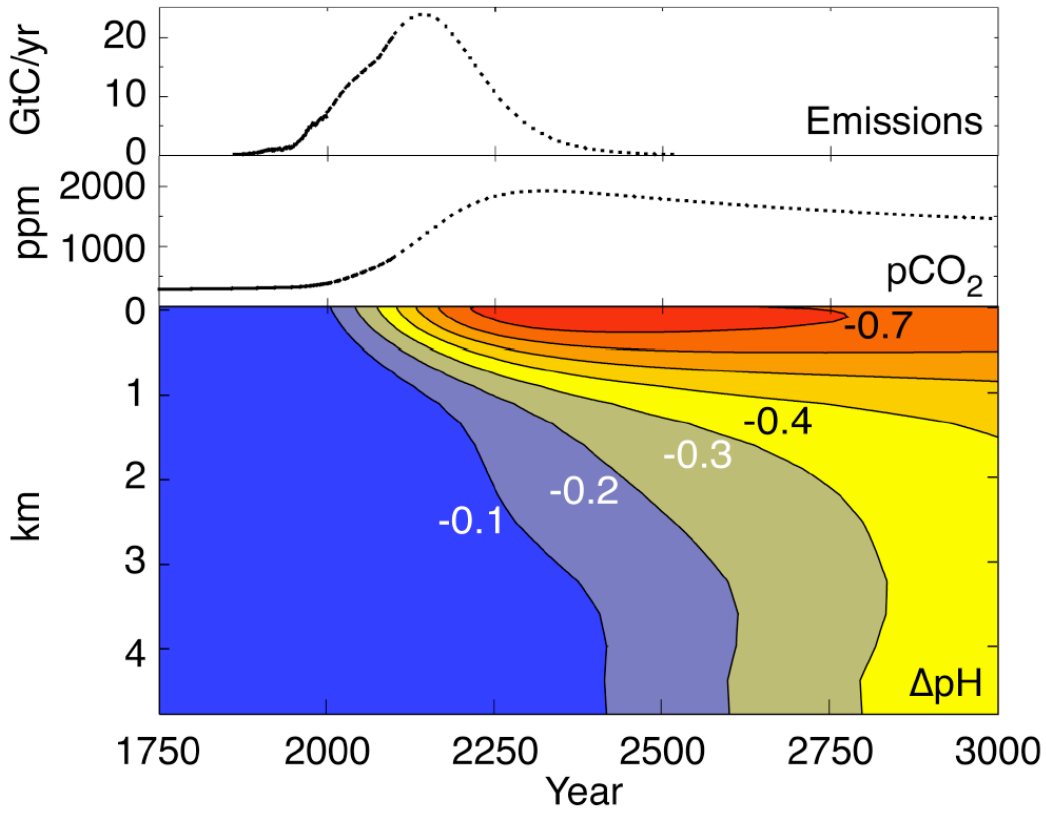

Figure 1.4. Model simulation of long-term changes in ocean pH (bottom panel), as a result of the CO_2 emissions shown in the top panel. The pCO_2 in the middle panel is the atmospheric concentration of CO_2 (from Caldeira and Wickett, 2003)

The main natural processes that remove CO_2 continuously from the atmosphere are explained by the following reactions (IPCC report 2014):

i. Land uptake: Photosynthesis-respiration, with a time scale of $1\text{-}10^2$ years:

$$6CO_2 + 6\,H_2O + \text{Photons} \rightarrow C_6H_{12}O_6 + 6O_2 \quad (1.1)$$
$$C_6H_{12}O_6 + 6O_2 \rightarrow 6CO_2 + 6\,H_2O + \text{heat} \quad (1.2)$$

ii. Ocean invasion: Seawater buffer, with a time scale of $1\text{-}10^3$ years:

$$CO_2 + CO_3^{-2} + H_2O \leftrightarrow 2HCO_3^- \quad (1.3)$$

iii. Reaction with calcium carbonate, with a time scale of $10^3\text{-}10^4$ years :

$$CO_2 + CaCO_3 + H_2O \leftrightarrow Ca^{2+} + 2HCO_3^- \quad (1.4)$$

iv. Silicate weathering, with a time scale of 10^4-10^6 years:

$$CO_2 + CaSiO_3 \rightarrow CaCO_3 + SiO_2 \qquad (1.5)$$

The short-term carbon cycle has been modeled by several authors (see Prentice et al., 2001 and references therein) taking into account the complex interactions among relevant processes. The aim of this exercise is to evaluate the possible responses of the carbon cycle to climate changes and to predict possible future variations in fluxes between different reservoirs. These carbon cycle models have been developed and tested against available data and then used for future predictions, until the end of the century, assuming reasonable emissions scenarios (e.g., Figure 1.5).

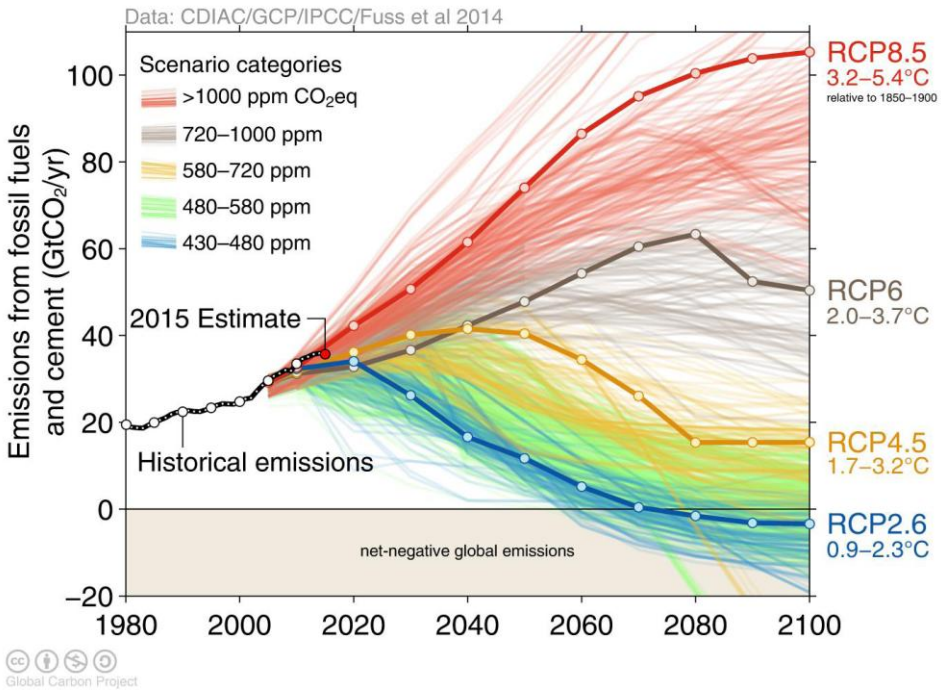

Figure 1.5. Over 1000 scenarios from the IPCC Fifth Assessment Report are shown, including the Representative Concentration Scenarios (RCP). The four RCPs in the graphic are summarized in this SI (i.e. 2.6, 4.5, 6.0 and 8.5 W/m^2) and they are referred to the radiative forcing of the Greehouse Gases Emissions. From Fuss et al., 2014; CDIAC (Carbon Dioxide Information Analysis Center); Global Carbon Budget, 2015 (see http://www.globalcarbonproject.org/carbonbudget/archive/2015/GCP_budget_2015_v1.02.pdf).

Oceanic models indicate that ocean uptake increases with time but the uptake/emissions ratio decreases with time. Terrestrial model suggests that the rate of uptake by the land increases until 2050 and stabilizes afterwards. Both the ocean uptake and the terrestrial uptake decrease if climate-change feedbacks are taken into account in modeling. To quantify these effects coupled models are needed.

The rise in atmospheric CO_2 concentration has caused an increase in the trapping of infrared radiations emitted from the Earth surface, with respect to the preindustrial situation. Indeed, more than half of this increase in infrared absorption is attributed to CO_2, while the remaining part is probably controlled by other atmospheric gases, chiefly CH_4, N_2O, and chlorofluorocarbons.

The effects of this increased infrared absorption on the Earth climate involve several feedback mechanisms. However, there is little doubt that increased trapping enhances the atmospheric greenhouse effect, thus leading to global warming and climate change, which is the challenge for the present and the future generations. Therefore, anthropic CO_2 inputs into the atmosphere have to be drastically reduced, and several strategies have to be undertaken to this purpose, as we do not have a single magic option.

1.3. The Carbon Capture Storage

The Carbon Capture Storage (CCS) is the most promising technology to reduce the release of CO_2 to the atmosphere from fossil fuels burning, cement production and other industrial processes. The CO_2 by-product of fossil fuel burning can be stored by returning the released carbon back to a geological reservoir.

As discussed by Benson and Cole (2008), the large sedimentary basins are the best candidates for geological carbon storage, due to the very high pore volume and connectivity and their wide distribution worldwide. Many sedimentary rock formations of different textures and mineralogical and chemical compositions provide both, the volume to store the CO_2 and the seals to trap it at depth. Possible reservoirs comprise depleted oil and gas reservoirs, saline aquifers, and coal beds. Suitable formations should be deeper than 800 m approximately, have a seal of suitable thickness and extension, have sufficient porosity to store large CO_2 volumes, and be sufficiently permeable to allow injection at high flow rates. Injection of CO_2 at depths greater than 800 meters has two advantages due to the high pressures present at these depths: CO_2 density is high enough to allow effective pore filling and to decrease the buoyancy difference with respect to the in situ fluids.

In 1996, Statoil began to inject a million metric tons per year of CO_2 into an aquifer 800 meters below the North Sea at Sleipner (Torp and Gale, 2004). The CO_2 was separated from natural gas to meet specifcations for sale in Europe. Statoil could have emitted the CO_2 into the atmosphere and paid a tax of $50 per ton, but they opted instead to inject CO_2 into a deep aquifer. Afterwards, other CO_2 injection projects have been linked with enhance oil (EOR) or gas recovery (EGR) such as at Weyburn EOR site in Canada (1.8 Mt per year since 2000), at the Salah site in

Algeria (about 1 Mt per year since 2004) and at the Cranfield EOR in Mississippi, USA (DePaolo and Cole, 2013). Furthermore, the team of the CarbFix project has demonstrated that over 95% of the CO_2 captured and injected at Hellisheidi geothermal power plant in Iceland was mineralized within two years (see https://www.or.is/english/carbfix-project).

There is also a number of research projects focused on the potential issues and challenges of CCS, as the CO_2-REACT European Network on geological carbon storage, which is founding the research of this PhD Thesis. The project combines observations of real rock cores, with experiments exploring mineral-fluid interaction, and with computational studies and fundamental theory to understand dissolution, precipitation and mass transport in the subsurface. CO_2-REACT also explores CO_2 capture and optimal conditions for injecting pure CO_2 or CO_2-rich gases into porous rocks. Advances are tested at field scale at the CarbFix pilot site (Iceland) and on limestone and chalk cores. This combined approach enables CO_2-REACT to attain its main research aim: to develop practical knowledge and predictive tools for successful, long term, geological CO_2 storage that can be integrated into industrial processes.

For CCS to be successful, three basic conditions have to be met by the storage medium: (1) capacity, (2) injectivity, and (3) confinement (Bachu, 2003, 2010; IPCC, 2005). The last condition is critical because CO_2 leakage may (IPCC, 2005) impact other resources, potable groundwater, vegetation and animal life, and human health, notwithstanding the global aspect of the return of CO_2 to the atmosphere, even if it is at acceptable levels (Celia and Bachu, 2003; IPCC, 2005). Injected CO_2 tends to migrate upwards through the porous media of the permeable reservoir rocks. Hence, to first guarantee the confinement of CO_2 underground for a long-midterm scale, it is necessary that the host rocks are overlain by impermeable rock layers. Normally this requirement is achieved in many geological environments worldwide (DOE, 2012). Evidence from natural CO_2 reservoirs and numerical models suggests that injected CO_2 can be stored in geological formations for time scales well over 1000 years (Wilson and Johnson, 2003; Keith and Giardina, 2005).

Possible pathways for CO_2 leakage are both natural (e.g., active faults and open fractures) and manmade, mainly boreholes (Celia and Bachu, 2010). The potential for CO_2 leakage through existing wells, either active or abandoned, is especially important in sedimentary basins which have been the subject of hydrocarbon exploration and production. Well integrity may be compromised due to poor completion, abandonment, and wrong operations. Crow et al. (2010) defined "wellbore integrity" as a condition that maintains isolation of geological formations and prevents vertical escape of fluids.

Globally there are several natural accumulations of CO_2 in geological reservoirs situated in different geological environments, which are excellent natural laboratories to be observed and studied.

The important questions that may be answered with observations from these natural analogues include the nature, magnitude and rates of geochemical processes that involve the CO_2 in geological reservoirs including: (i) CO_2 dissolution into formation brine, (ii) silicate dissolution/precipitation reactions acting as buffers of acidity and solutes and (iii) carbonate dissolution/precipitation (Bickle et al., 2013). These three processes mention before can be expressed by simple reactions (DePaolo and Cole, 2013). The CO_2 dissolved into the aqueous phase undergoes a partial dissociation according to the following reaction:

$$CO_2 + H_2O = H^+_{(aq)} + HCO_3^-{}_{(aq)} \quad (1.6)$$

Nevertheless, due to the high CO_2 partial pressure, the pH of the aqueous solution may attain values close to 3. Then the acid brine might react with silicate and carbonate minerals contained in the rock formation, which will neutralize the brine through the following simplified reactions:

$$H^+_{(aq)} + CaAl_2Si_2O_8 + H_2O = Ca^{2+}_{(aq)} + Al_2Si_2O_5(OH)_4 \quad (1.7)$$

$$H^+_{(aq)} + CaCO_{3(aq)} = Ca^{2+}_{(aq)} + HCO_3^-{}_{(aq)} \quad (1.8)$$

1.4. Subjects and objectives of this research

One of the major risks related to the geological sequestration of CO_2 is the leakage of CO_2-rich gases from the deep reservoirs in which they have been disposed. This risk can be mitigated monitoring the flux of CO_2 from soil using the accumulation chamber method. The use of this methodology in a natural analogue for the geological CO_2 storage has been one of the objectives of this PhD.

These CO_2 gas studies, which are presented in chapter 2 of my PhD thesis, were performed in a natural analogue for the geological CO_2 storage, which is affected by intense CO_2 degassing and where both. a thermal spa and a CO_2 production plant are present. This natural analogue is located in the Sant'Albino area, Southern Tuscany. The production wells (run by the company Air Liquide) extract 96 t d^{-1} of CO_2 on average (Frondini et.al, 2009), whereas the bubbling pools located inside the thermal spa area discharge a CO_2 flux in the order of 10-100 t d^{-1} according to the INGV-DPCV5 catalogue of Italian gas emissions (see http://googas.ov.ingv.it/).

In three selected zones of the study area (Salcheto, Acqua Puzzola and Terme di Montepulciano spa), the diffuse CO_2 flux from soil was measured by means of the accumulation chamber method and mapped to assess the natural CO_2 leakage. Also, diffuse CO_2 fluxes data from soil were used to

estimate as a first approximation, the vertical permeability of the cap-rock overlying the Sant'Albino gas reservoir (see *chapter 2*).

In addition, new laboratory experiments with the accumulation chamber method were carried out to improve the understanding of this method (see c*hapter 4*) and the possible implications in surface monitoring of CO_2 geological sequestration sites, as well as other geo-scientific purposes (geothermal exploration, volcanic surveillance).

In principle, the CO_2 time series acquired using the accumulation chamber method can be used to obtain not only the CO_2 flux from soil, F_{CO_2}, but also its two components, namely the CO_2 molar fraction of soil gas, $X_{CO_2,G}$, and the flux of the soil gas mixture, F_G. Note that only two of the three variables F_{CO_2}, F_G, and $X_{CO_2,G}$ are independent, as they are linked by the simple relation:

$$F_{CO_2} = F_G \cdot X_{CO_2,G} \tag{1.9}$$

Consequently, it should be possible to understand if high F_{CO_2} values are controlled by either (i) high F_G values or (ii) high $X_{CO_2,G}$ values or (iii) high values of both variables and, conversely, if low F_{CO_2} values are due to either (a) low F_G values or (b) low $X_{CO_2,G}$ or (c) low values of both parameters.

Well integrity can be compromised also by CO_2-driven chemical reactions. Initially, these chemical reactions are due to the thermodynamic incompatibility between the acidic CO_2-rich fluids and the alkaline Portland cement pore fluids. At later stages, CO_2-driven chemical reactions may lead to cement carbonation and alteration and consequently to gas leakages.

Cement carbonation studies are presented in *chapter 2* where reaction path and reactive transport modelling are used to investigate the processes occurring near a hypothetical average production well with a damaged zone affecting both, casing and cement.

In addition, a discussion of the laboratory experiments on cement carbonation, which were performed using class G Portland cement at different partial pressures of CO_2 and different times of exposure is presented in *chapter 3*.

The Ph.D. was mainly carried out in the West Systems laboratories at Pontedera, in the Department of Earth Sciences of the University of Florence and in the Florence section of the Institute of Geosciences and Earth Resources of the National Research Council of Italy. The Ph.D. work has also benefitted of the research carried out during the secondment period at the Lafarge-Holcim Research Center in Saint-Quentin-Fallavier, France.

Summing up, my PhD Thesis consists of five chapters, three of which are scientific research manuscripts whereas the remaining two are the general introduction and conclusions. *Chapter 2* has been submitted to *Chemical Geology*. *Chapter 4* has been submitted to *Journal of Volcanology and Geothermal Research*. *Chapter 3* will be submitted to an internal journal before the defence of my PhD Thesis.

References

Bachu, S.(2003). Screening and ranking of sedimentary basins for sequestration of CO_2 in geological media in response to climate change. Environmental Geology, 44(3), 277-289.

Bachu, S. (2010). Screening and selection criteria, and characterisation for CO_2 geological storage. Developments and innovation in carbon dioxide (CO_2) capture and storage technology, 2, 27-56.

Barnola J.-M., Anklin M., Porcheron J., Raynaud D., Schwander J., Stauffer B. (1995) CO_2 evolution during the last millenium as recorded by Antarctic and Greenland ice. Tellus Series B-Chemical and Physical Meteorology, 47, 264-272.

Barnola J.-M., Raynaud D., Lorius C., Barkov N.I. (2003) Historical CO_2 record from the Vostok ice core. In Trends: A Compendium of Data on Global Change. Carbon Dioxide Information Analysis Center, Oak Ridge National Laboratory, U.S. Department of Energy, Oak Ridge, Tenn., U.S.A.

Benson, S.M., & Cole, D.R. (2008). CO_2 sequestration in deep sedimentary formations. Elements, 4(5), 325-331.

Bickle, M., Kampman, N., & Wigley, M. (2013). Natural analogues. Reviews in Mineralogy and Geochemistry, 77(1), 15-71.

Caldeira, K., & Wickett, M.E. (2003). Oceanography: anthropogenic carbon and ocean pH. Nature, 425(6956), 365-365. Caldeira and Wickett, Nature.

Celia, M.A., & Bachu, S. (2003). Geological sequestration of CO_2: is leakage unavoidable and acceptable. In GHGT-6: Sixth International Conference on Greenhouse Gas Control Technologies, October 2003.

Celia, M.A., & Bachu, S. (2010). Field-scale application of a semi-analytical model for estimation of CO_2 and brine leakage along old wells - International Journal of Greenhouse Gas Control.

Crow, W., Carey, J.W., Gasda, S., Williams, D.B., & Celia, M. (2010). Wellbore integrity analysis of a natural CO_2 producer. International Journal of Greenhouse Gas Control, 4(2), 186-197.

DePaolo, D.J., & Cole, D.R. (2013). Geochemistry of geologic carbon sequestration: an overview. Reviews in Mineralogy and Geochemistry, 77(1), 1-14.

DOE (2012). Department of Energy of the Energy, Office of fossil Energy, Carbon Utilization and Storage Atlas, The United States 2012, 4th Edition.

Etheridge D.M., Steele L.P., Langenfelds R.L., Francey R.J., Barnola J.M., Morgan V.I. (1996) Natural and anthropogenic changes in atmospheric CO_2 over the last 1000 years from air in Antarctic ice and firn. Jour. Geophys. Res. - Atmosphere, 101, 4115-4128.

Fischer H., Whalen M., Smith J., Mastroianni D., Deck B. (1999) Ice core records of atmospheric CO_2 around the last three glacial terminations. Science, 283, 1712-1714.

Frondini F., Caliro S., Cardellini C., Chiodini G., Morgantini N. (2009) Carbon dioxide degassing and thermal energy release in the Monte Amiata volcanic-geothermal area (Italy). Applied Geochemistry, 24, 860-875.

Fuss, S., Canadell, J.G., Peters, G.P., Tavoni, M., Andrew, R.M., Ciais, P., Robert B. Jackson, R.B., Jones C.D., Kraxner, Nakicenovic, F.N., Le Quéré, C., Raupach, M.R., Sharifi, A., Smith, P., & Yamagata Y.(2014). Betting on negative emissions. Nature Climate Change, 4(10), 850-853.

Hönisch, B., Hemming, N.G., Archer, D., Siddall, M., & McManus, J.F. (2009). Atmospheric carbon dioxide concentration across the mid-Pleistocene transition. Science, 324(5934), 1551-1554.

Indermühle A., Stocker T.F., Joss F., Fischer H., Smith H.J., Wahlen M., Deck B., Mastroianni D., Tschumi J., Blunier T., Meyer R., Stauffer B. (1999) Holocene carbon-cycle dynamics based on CO_2 trapped in ice at Taylor Dome, Antarctica. Nature, 398, 121-126.

Intergovernmental Panel on Climate Change, (2005). IPCC special report on carbon capture and storage, United Nations Framework Convention on Climate Change, ISBN 92-9169-119-4.

Keeling C.D., Whorf T.P., Wahlen M., Vanderplicht J. (1995) Interannual extremes in the rate of rise of atmospheric carbon dioxide since 1980. Nature, 375, 666-670.

Keeling, C.D., & Whorf, T.P. (2003). Atmospheric CO_2 Concentrations—Mauna Loa Observatory, Hawaii, 1958–2002 (revised July 2003).

Keith, D.W.; Giardina, J.A.; Morgan, M.G.; Wilson, E.J (2005). Regulating the Underground Injection of CO_2. Environmental Science & Technology., 39, 499A-505°.

MacFarling Meure, C., Etheridge, D., Trudinger, C., Steele, P., Langenfelds, R., Van Ommen, T., Smith, A., Elkins, J. (2006). Law Dome CO_2, CH_4 and N_2O ice core records extended to 2000 years BP. Geophysical Research Letters, 33(14).

Marland B., Boden T.A., Andres R.J. (2000) Global, regional, and national CO_2 emissions. In: Trends: A compendium of data on global change. Carbon Dioxide Information Analysis Center, Oak Ridge National Laboratory, Oak Ridge, Tenn., USA.

Neftel A., Friedli H., Moor E., Lötscher H., Oeschger H., Siegenthaler U., Stauffer B. (1994) Historical CO_2 record from the Simple station ice core. In: T.A. Boden, D.P. Kaiser, R.J. Sepanski, F.W. Stoss (eds.) Trends '93: A Compendium of Data on Global Change. Carbon Dioxide Information Analysis Center, Oak Ridge National Laboratory, Oak Ridge, Tenn., USA, 11-14.

Petit J.R., Jouzel J., Raynaud D., Barkov N.I., Barnola J.M., Basile I., Bender M., Chappellaz J., Davis M., Delaygue G., Delmotte M., Kotlyakov V.M., Legrand M., Lipenkov V.Y., Lorius C., Pepin L., Ritz C., Saltzman E., Stievenard M. (1999). Climate and atmospheric history of the past 420,000 years from the Vostok ice core, Antarctica. Nature, 399, 429-436.

Peybernès N., Michel E., Barnola J.-M., Delmotte M., Chappellaz J., Raynaud D. (2000) . Information on carbon cycle during the last 8000 years deduced from CO_2, $\delta 13$ CO_2, and CH_4 profiles obtained on a Vostok ice core. EGS, Nice, France, 25-26 April 2000.

Prentice I.C., Farquhar G.D., Fasham M.J.R., Goulden M.L., Heimann M., Jaramillo V.J., Kheshgi H.S., Le Quéré C., Scholes R.J., Wallace D.W.R., Archer D., Ashmore M.R., Aumont O., Baker D., Bender M., Bopp L.P., Bousquet P., Caldeira K., Ciais P., Cox P.M., Cramer W., Dentener F., Enting I.G., Field C.B., Friedlingstein P., Holland E.A., Houghton R.A., House J.I., Ishida A., Jain A.K., Janssens I.A., Joos F., Kaminski T., Keeling C.D., Keeling R.F., Kicklighter D.W., Kohfeld K.E., Knorr W., Law R., Lenton T., Lindsay K., Maier-Reimer E., Manning A.C., Matear R.J., McGuire A.D., Melillo J.M., Meyer R., Mund M., Orr J.C., Piper S., Plattner K., Rayner P.J., Sitch S., Slater R., Taguchi S., Tans P.P., Tian H.Q., Weirig M.F., Whorf T., Yool A. (2001). The Carbon Cycle and Atmospheric Carbon Dioxide. In:

Houghton J.T., Ding Y., Griggs D.J., Noguer M., Van der Linden P.J., Dai X., Maskell K.,Johnson C.A. (eds.). Climate Change (2001): The Scientific Basis. Cambridge University Press, Cambridge, UK, 183-238 (available at http://www.ipcc.ch).

Siegenthaler U., Friedli H., Lötscher H., Moor E., Neftel A., Oeschger H., Stauffe B. (1988) Stable-isotope ratios and concentration of CO_2 in air from polar ice cores. Annals of Glaciology, 10, 1-6.

Smith H.J., Fischer H., Wahlen M., Mastroianni D., Deck B. (1999). Dual modes of the carbon cycle since the Last Glacial Maximum. Nature, 400, 248-250.

Torp, T.A., & Gale J. (2004). Demonstrating storage of CO_2 in geological reservoirs: the Sleipner and SACS projects. Energy, 29(9), 1361-1369.

Wilson, E.J.; &Johnson, T.L. (2003); Keith, D. W. Regulating the ultimate sink: Managing the risks of geologic CO_2 storage. Environmental Science & Technology 37, 3476-3483.

Zhang, Y.G., Pagani, M., Liu, Z., Bohaty, S.M., & DeConto, R. (2013). A 40-million-year history of atmospheric CO_2. Phil. Trans. R. Soc. A, 371(2001), 20130096.

Zhang, Y.G., Pagani, M., & Liu, Z. (2014). A 12-million-year temperature history of the tropical Pacific Ocean. Science, 344(6179), 84-87.

C*hapter* 2- A STUDY ON WELLBORE CEMENT CARBONATION BY CO_2 LEAKAGE IN A NATURAL ANALOGUE FOR THE GEOLOGICAL CO_2 STORAGE

Abstract

This study presents the results obtained by studying well integrity in the natural analogue for the geological storage of CO_2 of Sant'Albino, Southern Tuscany, which is affected by intense CO_2 degassing and where a thermal spa and a CO_2 production plant are present. Reaction Path Modelling (RPM) of cement hydration and carbonation as well as Reactive Transport Modelling (RTM) of cement alteration were used to investigate the processes occurring near a hypothetical average production well with a damaged leaking zone, affecting casing and cement, assuming a defined composition of class G Portland cement. The results indicate that the advective flow of CO_2 from the damaged zone, leads to the completion of cement carbonation and promotes further cement alteration through considerable dissolution of carbonate minerals. These two processes takes place in a relatively short time, in the order of some years. The ultimate consequence of these CO_2-promoted comparatively fast chemical reactions is, most likely, the CO_2 leakage to the surface.

Keywords: carbon dioxide; cement alteration; gas leakage; reaction path modelling; reactive transport modelling.

2.1. Introduction

Ideally, the basic premise of geological CO_2 sequestration is the absence of leaks from the reservoir where CO_2 is stored. Since this ideal condition is never completely attained in the real world, the presence of very low leak rates is actually the fundament requirement for effective geological CO_2 storage.

Among the possible leakage paths, injection wells, monitoring wells, and other wells present in the area of interest are of utmost concern because all boreholes pierce the impervious cap-rock covering the reservoir where CO_2 is stored. Irrespective of the well type, all the boreholes, especially the old ones, may be affected by imperfect completion or other flaws and damages. Usually, the conceptual model adopted for leakage assumes that CO_2 traveling through the reservoir, meets a well and may leak towards the surface via (i) the interface between cement and rock, (ii) the permeable cement matrix, (iii) fractures/defects in the cement, (iv) the interface between cement and the casing strings, and (v) discontinuities within the casing strings (Carey, 2013).

Leakage pathways may also result from, or be enhanced by, CO_2-promoted chemical reactions owing to the aggressiveness of CO_2 towards the materials employed in the well construction, usually Portland cement and casing strings of low-carbon steel. Therefore, cement alteration (i.e., the chemical reactions affecting cement after carbonation completion) and steel corrosion and their impact on well integrity are pivotal issues in risk analysis of CO_2 storage sites (e.g. Chiaramonte et al 2008; Viswanathan et al. 2008; Crow et al., 2010; Zhang and Bachu, 2011; Newell and Carey, 2012; Carey, 2013).

During the last years, several field investigations, laboratory experiments, and modeling studies were focused on the chemical reactions involving CO_2, Portland cement, and steel and impacting wellbore integrity in CO_2 sequestration scenarios (see the reviews performed by Zhang and Bachu, 2011; and Carey, 2013). Some studies have investigated the gas-solid reactions of supercritical CO_2 with cement and/or steel. Nevertheless, the main interest is on water-mediated reactions due to the ubiquity of water in wellbores and their surroundings, under conditions intermediate between the limiting states of saturation (e.g. in aquifers) and dryness (e.g., close to the CO_2 injection zones). These intermediate situations are conveniently described by the residual state condition, in which the water phase is discontinuous and isolated with thin films of water surrounding the solid particles and the gas bubbles as in soils (e.g., Fairbridge and Finkl, 1979).

Most reactive transport modeling (RTM) investigations of cement-CO_2 interactions carried out so far (e.g., Carey and Lichtner, 2007; Carey et al., 2007; Huet et al., 2010; Corvisier et al., 2010;

McNab and Carroll, 2011; Deremble et al., 2011; Geloni et al., 2011; Wilson et al., 2011; Gherardi et al., 2012; Fabbri et al., 2012; Raoof et al., 2012; Jacquemet et al., 2012; Brunet et al., 2013; Wertz et al., 2013) are based on the assumption that CO_2 comes in contact and reacts with cement through diffusion. These previous studies reproduce to a satisfactory extent the fundamental reactions occurring in CO_2-cement systems, namely destruction of portlandite and calcium-silicate-hydrates (CSH phases) accompanied by concurrent production of calcite and amorphous silica (e.g., Richardson, 1988; Papadakis et al., 1989). The alteration of fractured class-G cement flowed by CO_2-rich brines was also investigated through laboratory experiments and RTM (e.g., Luquot, 2013; Abdoulghafour et al., 2013, 2016). These studies showed that the fracture aperture has a strong influence on the cement alteration patterns, with (i) the self-heal of low-aperture fractures due to calcite precipitation and (ii) the development of preferential pathways in high-aperture fractures mainly lined by amorphous silica.

In this work, we intend to evaluate the effect of an advective $CO_2(g)+H_2O(l)$ bi-phase flow on cement alteration, referring to a hypothetical average production well with a damaged zone and focusing on a natural analogue for the geological CO_2 storage. The case study is located in the Sant'Albino area, Southern Tuscany, which is affected by intense CO_2 degassing and where both the Terme di Montepulciano spa and the Air Liquide CO_2 production plant are present. The Air Liquide production wells extract 96 t d^{-1} of CO_2 on average (Frondini et.al, 2008), whereas the bubbling pools located inside the Terme di Montepulciano spa discharge a CO_2 flux in the order of 10-100 t d^{-1} according to the INGV-DPCV5 catalogue of Italian gas emissions (see http://googas.ov.ingv.it/).

Although none of the CO_2 production wells of the Sant'Albino plant have any problem, we assume that the hypothetical average production well of interest has a damaged zone affecting casing and cement. The considered well is assumed to be 100 m deep and to have a 20 m-thick production zone. The damaged zone is assumed to be situated at 53 m depth to study in detail the alteration of class G Portland cement of defined composition. The results obtained in this work on fluid-cement interactions under relatively high P_{CO2} conditions in a natural analogue, may be exported to geological CO_2 storage sites.

2. 2. Geological setting of the study area

As shown in Figure 2.1, the Sant'Albino thermal area is located along the NW-SE trending Rapolano-Cetona ridge, where the non-metamorphic succession of the Tuscan domain crops out. This succession includes, from bottom to top: (a) Dolostones, dolomitic limestones and anhydrites of Late Triassic; (b) Limestones and dolomitic limestones of Rhaetian-Early Liassic; (c) Marls, shales, nodular limestones, cherty limestones, radiolarites, calcilutites and calcarenites of Early Liassic-Early Cretaceous; (d) Shales and marls, Quartz-rich calcilutites and nummulites calcarenites of Early Cretaceous-Oligocene; (e) The internal sandstone flysch of Chattian-Aquitanian; and (f) The external sandstone flysch of Chattian-Langhian.

The Rapolano-Cetona ridge separates: (i) the Siena-Radicofani basin to the East, where the clays, silty-marly clays, conglomerates, sandstones, and bioclastic limestones of Zanclean-Piacenzian are exposed to the surface, from (ii) the Valdichiana basin to the East, where the fluvial-lacustrine conglomerates, sandstones, siltstones, clays and limestones of Ruscinian-Villafranchian crop out.

The Sant'Albino horst is delimited by NW- and NE-trending fault systems that have also considerable influence on fluid circulation at different depths and scales. Among the deepest carbonate units of the non-metamorphic Tuscan succession, only the following ones are present in the Sant'Albino area: (i) Calcare Selcifero (cherty limestones); (ii) Diaspri (radiolarites); (iii) Maiolica (limestones with silica nodules); (iv) Marne a *Posydonomia* (*Posydonomia* bearing marls, shales and marly limestones); and (v) Scaglia Toscana (shales and marls, Quartz-rich calcilutites and nummulites calcarenites). In general, these carbonate units have high secondary permeability and act as water and CO_2 reservoirs. In particular, the main production zone of the Sant'Albino CO_2 wells corresponds to the lower part of the Calcare Selcifero and the upper part of the Marne a *Posydonomia*.

The Pliocene-Quaternary. Clays, as well as the shales and siltstones of the Santa Fiora flyschoid unit (Upper Cretaceous), constitute the impermeable cap-rock. Additionally, relatively extensive travertine deposits occur close to the surface in some parts of the study area.

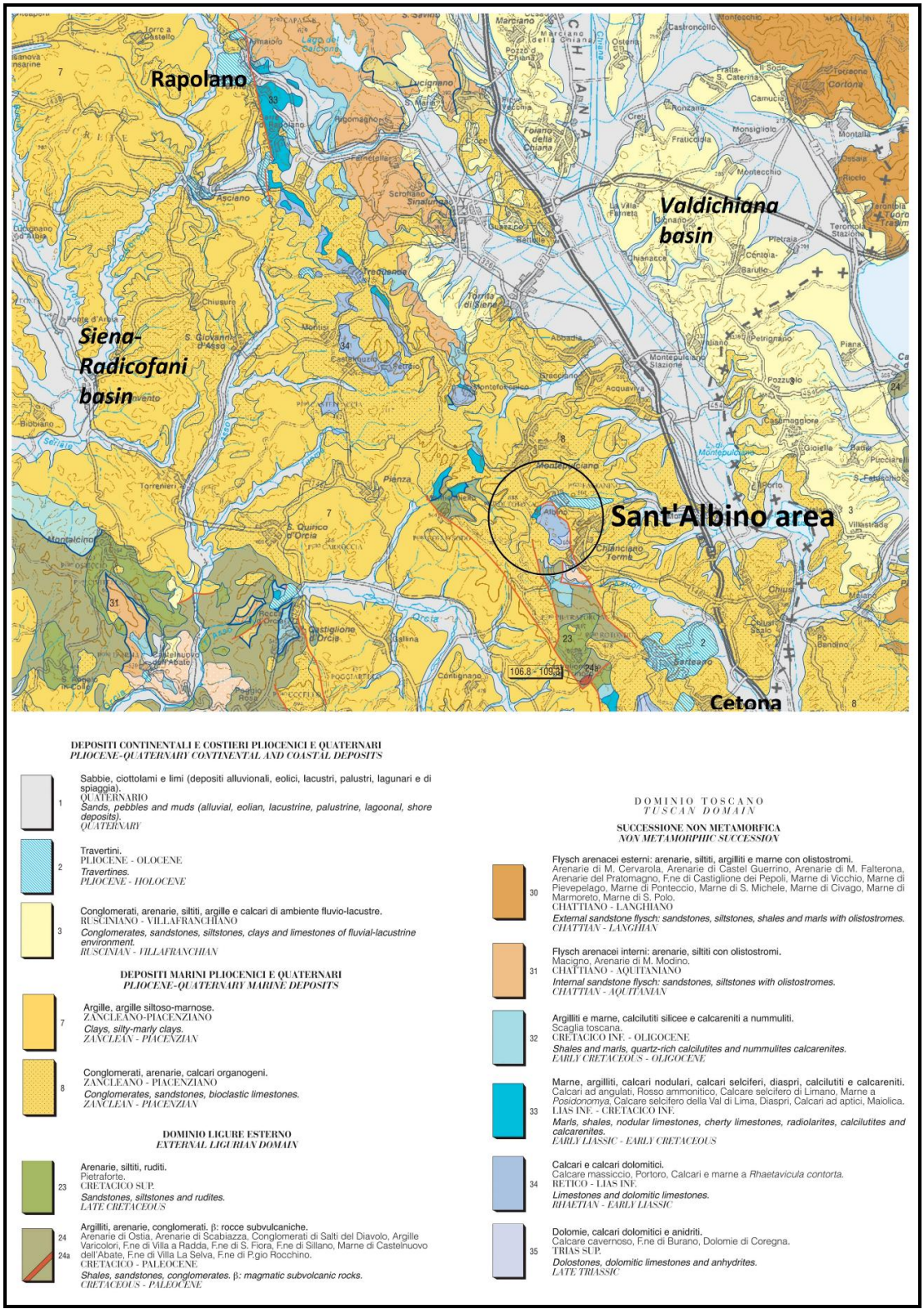

Figure 2.1. Geological map of the Tuscany Region at the scale 1:250,000, showing the location of the Sant'Albino area along the NW-trending Rapolano-Cetona ridge separating the Siena-Radicofani basin from the Valdichiana basin (Carmignani, L., & Lazzarotto, A., 2004).

2. 3. Methods

2.3.1. Measurement of CO_2 soil flux and data processing

In three selected zones of the studied area (Salcheto, Acqua Puzzola and Terme di Montepulciano spa), the diffuse CO_2 flux from soil was measured by means of the accumulation chamber method (Chiodini et al., 1998) using two West Systems fluxmeters (Figure 2.2) to assess the natural CO_2 leakage.

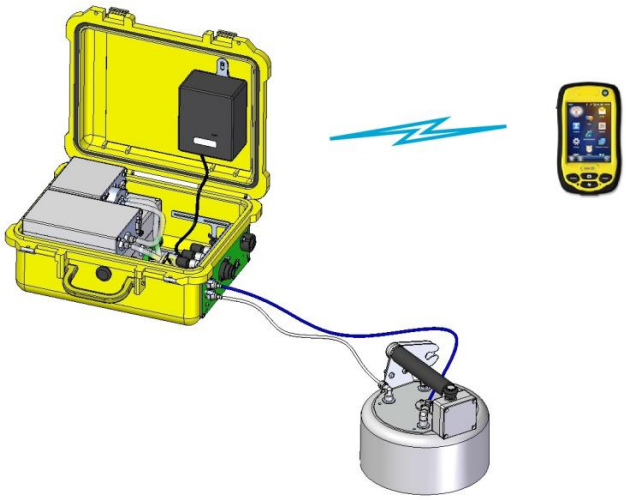

Figure 2.2. The West Systems portable CO_2 fluxmeter (from the Handbook of the West Systems CO_2 fluxmeter).

The chamber is set on the soil and is gently pressed onto it to minimize the entrance of atmospheric air, which occurs everywhere (Hernández-Rodríguez et al., 2016). The chamber is equipped with a fan ensuring the homogenization of the gas mixture inside the chamber. The gas mixture is continuously extracted from the chamber, sent to the CO_2 analyzer, and then injected again into the chamber by a membrane pump through inlet and outlet tubes. A palmtop computer with an integrated GPS acquires the data of interest (time, CO_2 concentration, pressure and temperature in the measuring cell of the CO_2 analyzer, ambient temperature, barometric pressure, and geographical coordinates) with the frequency of one record per second. The palmtop communicates with the CO_2 analyzer through either a wired or a wireless connection. Also, the palmtop computer allows the operator to elaborate the data on site and to obtain the CO_2 flux from soil from the initial slope (at time zero) of the CO_2 concentration-time curve.

The measured diffuse CO_2 flux data in the three selected zones of the Sant'Albino area were (i) processed using log probability plots and partitioned in different log-normal populations following the approach of Sinclair (1974, 1976) and (ii) mapped by using geostatistical tools, namely

semivariograms and Kriging (e.g., Sinclair and Blackwell, 2002) adopting the thresholds obtained by the Sinclair's partitioning procedure.

Diffuse CO_2 fluxes data from soil were used to estimate as a first approximation the vertical permeability of the cap-rock overlying the Sant'Albino gas reservoir, using the Darcy's law and following the guidelines of Collins (1961), from which the subsequent part of this section is derived. The Darcy's law is valid for gases if the flowrate, Q, is taken as the volumetric flowrate at the mean flowing pressure $p = (p_A+p_B)/2$ and if p is sufficiently large. Assuming that gravitational effects are negligible (which is a reasonable assumption for gases), the Darcy's law for an isothermal flow of ideal gases can be written as follows:

$$Q_A \cdot p_A = -\frac{k \cdot A}{\mu \cdot z} \cdot \frac{p_A^2 - p_B^2}{2}, \qquad (2.1)$$

where Q_A is the volumetric gas flux [$cm^3\ s^{-1}$] at pressure p_A (1 atm in the case of interest), k is the permeability [D] of the porous medium (i.e., the cap-rock), A is the surface area of the accumulation chamber [cm^2], μ is the dynamic viscosity of CO_2 [cP], and z is the vertical length [cm].

In the case of gases, the fluid does not stick to the walls of the pores and a phenomenon known as slip occurs. This slipping of the gases along the pore walls give rise to an apparent dependence of permeability on pressure, which is known as Klinkenberg effect. In fact, Klinkenberg proposed the following relation between permeability and pressure:

$$k = k_\infty \cdot \left(1 + \frac{b}{p}\right) \qquad (2.2)$$

where k_∞ is the permeability as measured for incompressible fluids (liquids), and b is a constant characteristic of both the porous medium and the gas. From Equation (2.2), it is clear that slip can be neglected for sufficiently high p values. Equation (2.1) can be solved for k if p_B and z are known (see section 2.4.1). Due to the uncertainties on these two parameters in the case of interest, it is inappropriate to discuss if either k is representative of k_∞ or it is not.

The measured CO_2 flux data were also used to constrain CO_2 saturation in the soil (see section 2.3.3).

2.3.2. Reaction Path Modeling (RPM).

Isothermal (25°C) RPM was carried out to simulate, first, progressive hydration of cement minerals and, second, cement carbonation reactions. Since class G Portland cement is normally used at the high pressures and high temperatures typical of oil and gas reservoirs, this cement type has been adopted in this study referring to the mineralogical composition given in Table 2.1 (from Thomas and Jennings, 2014).

Table 2.1. Mineralogical composition of the Portland cement adopted in this study (from Thomas and Jennings, 2014).

Clinker mineral	Formula	Wt%	Mol%
Alite (C3S)	Ca_3SiO_5	61.40	58.74
Belite (C2S)	Ca_2SiO_4	16.21	20.56
Tricalcium aluminate (C3A)	$Ca_3Al_2O_6$	8.91	7.20
Ferrite (C4AF)	$Ca_4Al_2Fe_2O_{10}$	8.50	3.82
Gypsum	$CaSO_4 \cdot 2H_2O$	3.95	5.01
Periclase	MgO	0.79	4.29
Thenardite	Na_2SO_4	0.20	0.31
Arcanite	K_2SO_4	0.05	0.06

Simulations were performed by means of the geochemical code PHREEQC version 3.1.2 (Parkhurst and Appelo, 2013) using a modified version of the thermodynamic database PHREEQC_thermoddemv1.10_11dec2014.dat (http://thermoddem.brgm.fr/spip.php/rubrique14). The data of some cement solid phases (i.e., Alite, C3S, and Ferrite, C4AF) were obtained from the data0.ymp.R5 thermochemical database of the geochemical code EQ3/6 (Wolery and Jove-Colon, 2007).

2.3.3. Reactive Transport Modelling (RTM)

RTM of cement alteration was carried out by using the software package TOUGHREACT v2.1 (Xu et al., 2012) with the fluid property module ECO2N that reproduces the thermodynamics and thermophysical properties of H_2O-NaCl-CO_2 mixtures for temperatures from 10 to 110°C, pressures up to 600 bar, and salinities up to full halite saturation (Pruess and Spycher, 2007).

The items involved in RTM are: carbonate-rich host rocks, cement, casing, and the bi-phase fluid mixture flowing in the borehole, comprising a CO_2-rich gas phase and a liquid aqueous phase.

A CO_2-bearing layer was defined based on the information available for the CO_2 production wellbores in the study area, the local stratigraphic data, and the results of the geostatistical processing of CO_2 flux data from the three surveyed natural emission areas.

2. 3.3.1. From the conceptual model to the numerical model of the system of interest

The hypothetical wellbore considered in this study is an average production well with a damaged zone affecting casing and cement. The wellbore is assumed to attain a maximum depth of 100 m below ground level and to have a 9 $^{5/8}$ inch (24.4 cm) diameter. It is completed with a 7 inch (17.8 cm, external diameter) casing. Therefore, the average thickness of the cement sheath is 3.3 cm. It is also assumed that (i) bi-phase fluids made up of gaseous CO_2 and liquid H_2O are produced from a 20-m-thick fractured zone situated at 80 m depth and (ii) an 8-m-thick damaged zone is positioned at 53 m depth.

The 2D radial grid is represented by 200 vertical elements with a constant height of 0.5 m, from the surface to the maximum depth of 100 meters, whereas the width of the 72 horizontal elements increases progressively from 0.005 m, in the cement zone, up to 50 m, at the maximum radial distance considered in the model, 280 m (Figure 2.3). The small horizontal step near the wellbore was chosen to appreciate the reactive transport effects in the cement domain.

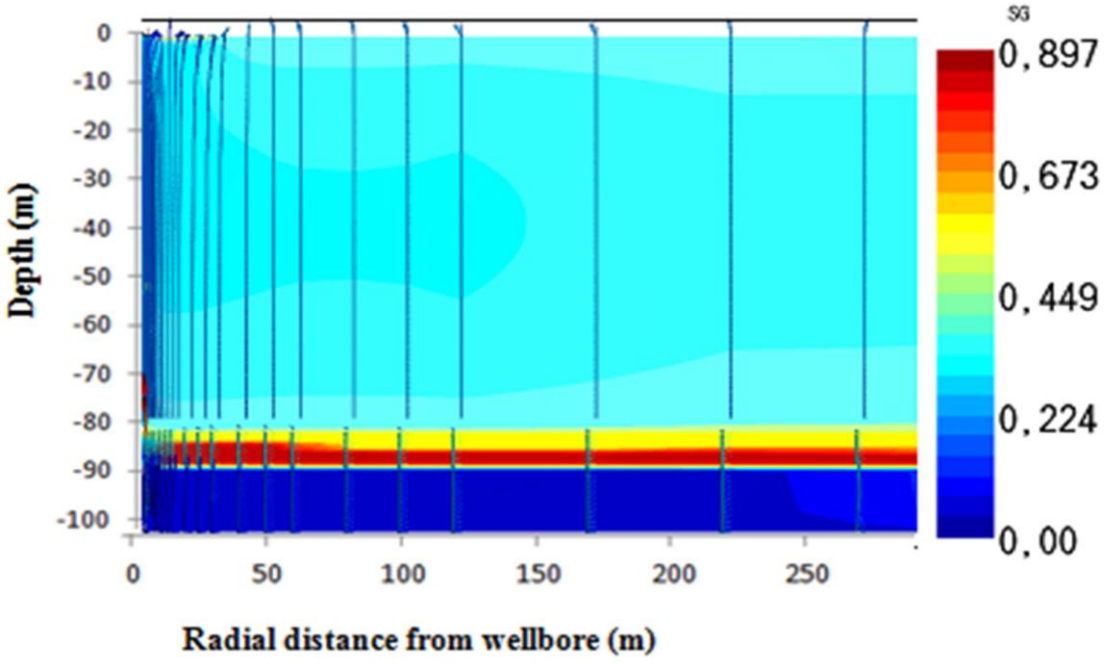

Figure 2.3. 2D radial model of the considered system showing the distribution of gas saturation (in Volume Fraction, in the right vertical axes) at time zero.

In the model, gaseous CO_2 flows mainly at the top of the fractured zone situated at 80 m depth, due to buoyancy effects, whereas liquid water flows at the bottom of this fractured zone. The well produces 2 t h^{-1} of CO_2(g) and 2 t h^{-1} of H_2O(l). The CO_2 production zone is recognized because of the high gas saturation values indicated in red and yellow colors in Figure 2.3. Consequently, cement alteration is expected to occur mainly at the CO_2/water interface in the fractured zone located at 80 m depth and in the damaged (leakage) zone positioned at 53 m depth.

2.3.3.2. Input data

Different material domains were defined for RTM calculations as follows (Table 2.2): (i) the production zone or ROCK, (ii) the cement or CEMENT, and (iii) the cap-rock overlying the production zone or BULK. The same mineralogical composition was assumed for both the production zone and the overlying cap-rock, which are considered to be impure limestones constituted by Calcite (40% by volume), Chlorite (20%), Illite (20%), Montmorillonite (18%) and Quartz (2%). Besides, the same initial porosity was taken for both the production zone and the overlying cap-rock assuming a typical value of carbonate rocks (Cantucci et al., 2009). Cement porosity and permeability were taken from Roy et al. (1993).

Table 2.2. Initial porosity and permeability for the three material domains considered in RTM of cement alteration, namely the production zone (ROCK), the cement (CEMENT) and the cap-rock (BULK).

Material	Porosity	Permeability (m^2)
ROCK	0.1	1.19E-12
CEMENT	0.2	3.08E-14
BULK	0.1	2.47E-16

A first calibration was carried out to assess the permeability of the cap-rock and the value of 2.47E-16 m^2 (corresponding to ~0.00025 D) was obtained on the basis of the measured CO_2 fluxes. A similar approach was adopted for the fractured zone containing water and CO_2, sustaining the extracted flow rates of 2 t h^{-1} of CO_2(g) and 2 t h^{-1} of H_2O(l), obtaining a permeability of 1.19E-12m^2.

Distinct permeability, porosity and thermal properties were assigned to each litostratigraphic unit considered in the RTM (Table 2.3). In particular, the Marne a *Posydonomia* unit was separated in marly limestone and marls/shales, corresponding to the productive part and the nonproductive part of the unit, respectively. Different values were adopted for the physical properties of the two sub-units.

Table 2.3. Physical properties of the litostratigraphic units considered in the RTM of cement alteration (from Cantucci et. al 2015). (*NP) Nonproductive part of the unit. (*P) Productive part of the unit.

Litostratigraphic Unit	Initial Porosity	Critical porosity	Permeability (m^2)	Thermal Conductivity (W/m°C)	Heat capacity (J/kg °C)
Travertine	0.06	N.D.	1.84E -16	4.08	920
Pliocene-Quaternary clays	0.14	N.D.	2.95E-17	2.08	1250
Santa Fiora	0.03	N.D.	7.65E-18	2.09	938
Scaglia Toscana (ST_1)	0.03	N.D.	7.65E-18	n/d	938
Scaglia Toscana (ST_2)	0.03	N.D.	7.65E-18	1.7	950
Marne a Posydonomia(*NP)	0.05	N.D.	2.04E-17	1.7	950
Marne a Posydonomia (*P)	0.1	0.044	1.02E-15	2.04	1040
Maiolica	0.01	0.055	2.48E-14	2.04	1040
Diaspri	0.05	0.046	2.04E-17	2.13	970
Calcare Selcifero	0.1	N.D.	2.34E-14	2.13	1026

The mineralogical composition of the cement domain is specified in Table 2.4, which is based on the results of the batch carbonation reaction simulated by PHREEQC for a reaction progress of 0.3, that is upon disappearance of Portlandite (see mineral assemblage evolution of Figure 2.5).

Table 2.4. Volume fraction of minerals present in the cement upon disappearance of Portlandite, as predicted by PHREEQC for batch cement carbonation.

Mineral	Volume fraction
Calcite	0.4445
CSH(1.6)	0.4544
Gibbsite	0.0181
Monosulfoaluminate	0.0198
Monocarboaluminate	0.0535
Ettringite	0.0036
Ferrhydrite	0.0062

2.3.3.3. Boundary conditions

The boundary conditions for representing the well in the RTM of cement alteration were computed using the wellbore simulator HOLA (Aunzo et al., 1991).

At the top of the BULK domain, corresponding to the uppermost horizontal cells of the grid (depths < 0.5 meters), pressure was set at 1 bar (atmospheric conditions) and water content was fixed for a rainfall of 2.22 m^3/year at an average input temperature of 15°C.

The dynamic wellbore pressure (under fluid extraction) varies from 24 bar at the production zone (Bottom Well Pressure) to 3 bar at the wellhead (Well Head Pressure).

A deep inflow of 2 t h^{-1} of CO_2(g) and 2 t h^{-1} of H_2O(l) was imposed at the same depth of the production zone (close to the bottom right in Figure 2.3). An enthalpy of 378 kJ/kg, corresponding to a temperature close to 90°C, for H_2O(l)-H_2O(g) equilibrium, was assumed for the inflowing water.

Two distinct compositions were assumed for the aqueous solution hosted in the soil and the aqueous solution hosted in the cement (Table 2.5). The second one was obtained through RPM of cement hydration before the onset of the carbonation process.

Table 2.5. Concentrations (mol/L) of relevant chemical components in the aqueous solutions hosted in the soil and in the cement.

Chemical component	Water in soil	Water in cement
H^+	1.68E-08	2.54E-14
Ca^{+2}	1.00E-09	9.50E-04
Mg^{+2}	1.00E-09	5.72E-12
Na^+	1.31E-01	3.66E-01
K^+	1.00E-09	3.58E-02
Fe^{+2}	1.00E-09	3.44E-34
Fe^{+3}	-----	1.31E-05
H_4SiO_4	1.00E-09	2.35E-14
HCO_3^-	1.00E-09	2.32E-13
SO_4^{-2}	1.00E-09	2.11E-07
Al^{+3}	1.00E-09	5.40E-05
Cl^-	1.31E-01	1.00E-02
O_2(aq)	1.00E-13	7.23E-07

2.3.3.3. Thermodynamic and kinetic data

The same thermodynamic database used for the batch reaction model (see section 2.3.2) was also utilized for the TOUGHREACT simulations, whereas kinetic data of cement phases and other relevant minerals were obtained from different sources (Table 2.6). Due to the considerable lack of knowledge on the kinetic parameters of cement minerals, several simplifications were necessary.

Table 2.6. Kinetic data of dissolution/precipitation reactions for relevant solid phases involved in TOUGHREACT simulations.

Minerals	Kinetic constant mole m^{-2} s^{-1}	Activation energy kJ $mole^{-1}$	Reference
Amorphous Silica	1.70E-13	68.7	Palandri and Kharaka (2004)
Calcite	1.60E-09	41.9	Svensson and Dreybrodt (1992)
CSH(0.8)	2.75E-12	-	Baur et al. (2004)
CSH(1.6)	2.75E-12	-	Baur et al. (2004)
CSH(1.2)	2.75E-12	-	Baur et al. (2004)
Ettringite	1.27E-12	-	Baur et al. (2004)
Ferrihydrite	7.00E-04	86.5	Larsen and Postma (2001)
Gibbsite	3.16E-12	61.2	Palandri and Kharaka (2004)
Gypsum	1.62E-03	-	Palandri and Kharaka (2004)
Hydrotalcite	1.45E-07	-	Carroll et al. (2011)
Magnesite	4.57E-10	23.5	Palandri and Kharaka (2004)
Monocarboaluminate	1.00E-11	-	Ipavek et al. (2010)
Monosulfate	6.31E-12	-	Baur et al. (2004)
Monosulfoaluminate	1.00E-11	-	Winnefeld and Lothenbach (2010)
Portlandite	6.45E-06	-	Halim et al. (2005)

The single dissolution rate of 2.75E-12, determined by Baur et al. (2004) for a CSH(1) phase (a structurally imperfect form of 1.4-nm tobermorite) with a Ca:Si ratio of 1, was assigned to all calcium-silicate-hydrates. This dissolution rate is about one order of magnitude lower than the average steady-state dissolution rate of CSH gel measured by Trapote-Barreira (2015), $1.02 \cdot 10^{-11} \pm 1.0 \cdot 10^{-12}$ mol m^{-2} s^{-1}, and the CSH(1) dissolution rate of $3.16 \cdot 10^{-11}$ mol m^{-2} s^{-1} determined by Schweizer (1999) at pH 12 under congruent dissolution conditions.

The rate adopted for monosulfate has to be considered with care, due experimental uncertainties (see discussion in Baur et al., 2004). The assumed rate of ettringite is the average of the four values reported by Baur et al. (2004), which vary from $7.08 \cdot 10^{-13}$ to $2.24 \cdot 10^{-12}$ mol m^{-2} s^{-1}.

The rate of hydrotalcite was computed from the conditional rate constants given by Carroll et al. (2011), $3.43 \cdot 10^{-9}$ mol g^{-1} s^{-1} on average, and the average specific surface area of this solid phase, 42.3 m^2/g (Miyata, 1980).

The rate of monocarboaluminate and monosulfoaluminate were taken from Ipavec et al. (2010) and Winnefeld and Lothenbach (2010), respectively, and corrected for consistency to be integrated in their reaction networks (Bullard et al., 2010). In addition, monocarboaluminate and

monosulfoaluminate kinetic constants were scaled up according to the gypsum kinetic constant assumed in this work to be consistent with it.

The reactive surface area of each solid phase was computed from its volume fraction (see section 2.3.3.2) and its specific surface area which was obtained by means of simple geometric calculations considering the particle size distribution of Valentini et al. (2014) for Portland cement.

2.4. Results

2.4.1. Results of the CO_2 soil flux survey

The log-probability plot of CO_2 soil flux for each of the three surveyed zones (Salcheto, Acqua Puzzola, and Terme di Montepulciano spa) show the presence of three individual log-normal populations, called A, B, and C, whose main statistical parameters are summarized in Table 2.7.

Table 2.7. Main statistical parameters of the individual populations A, B, and C obtained by partitioning the cumulative distribution of the CO_2 flux values for each of the three surveyed zones (Salcheto, Acqua Puzzola, and Terme di Montepulciano spa) of the study area. The permeability of the porous medium, *k*, was obtained from the median CO_2 flux using Equation (1).

Population	N. of stations	%	Mean mol m^{-2} d^{-1}	Median mol m^{-2} d^{-1}	95° percentile mol m^{-2} d^{-1}	Std. Dev. mol m^{-2} d^{-1}	Area m^2	*k* D
Salcheto zone								
A	16	34.0	593	285	2085	1080	106	0.31
B	13	27.7	6.53	4.66	18	6.41	1071	0.0050
C	18	38.3	0.441	0.358	1.04	0.318	-	0.00039
Acqua Puzzola zone								
A	10	24.4	611	464	1572	523	145	0.50
B	28	68.3	16.3	11.8	44.2	15.5	458	0.013
C	3	7.3	0.587	0.545	1.03	0.235	-	0.00059
Terme di Montepulciano spa zone								
A	16	42.1	622	566	1155	283	277	0.61
B	10	26.3	73	60.6	165	48.8	895	0.066
C	12	31.6	3.06	1.91	9.44	3.84	-	0.0021

Populations A and B are probably ascribable to gases of deep origin which can locally reach the surface due to the high or relatively high vertical permeability of the solid medium (see below), which is probably due to the presence of faults or fractures. In contrast, population C occurs in zones of low vertical permeability (see below) and is ascribable to the local background, which is

sustained by decay of organic matter and root respiration in soil as observed in several areas worldwide (e.g., Hernández-Rodríguez et al., 2016 and references therein).

Merging the results of the CO_2 soil flux survey carried out in the Sant'Albino area during this work with the outcomes of previous studies (Cardellini et al., 2004; Frondini et al., 2008), we estimate a total diffuse output of deep CO_2 of ~48.7 ± 8.1 t d^{-1} from an area of ~7360 m^2, corresponding to a specific CO_2 flux of ~150 ± 25 mol m^{-2} d^{-1} for the area of interest as a whole. The specific CO_2 fluxes are ~59 ± 11 mol m^{-2} d^{-1} for the Salcheto area, ~159 ± 28 mol m^{-2} d^{-1} for the Acqua Puzzola area, and 203 ± 25 mol m^{-2} d^{-1} for the area of the Terme di Montepulciano spa.

Assuming that the CO_2 production zone has a pressure p_B of 24 bar and is situated at 8000 cm depth and adopting a dynamic viscosity of 0.015 cP (Fenghour et al., 1998), vertical permeabilities of 0.31 to 0.61 D, 0.0050 to 0.066 D, and 0.00039 to 0.0021 D were computed by means of Equation (2.1) based on the median CO_2 flux values of populations A, B, and C, respectively (Table 2.7).

2.4.2. Results of RPM.

The solid phases produced during cement hydration as predicted by PHREEQC for a mixture made up of 9.42 moles of clinker and 55.6 moles of water are, in order of decreasing molar abundance: Portlandite [$Ca(OH)_2$], CSH(1.6) [$Ca_{1.60}SiO_{3.6}{\cdot}2.58H_2O$], Ca-monosulfoaluminate [$Ca_4Al_2(SO_4) \cdot 12H_2O$], Gibbsite [$Al(OH)_3$], Ferrihydrite [~$Fe(OH)_3$], and Hydrotalcite [$Mg_4Al_2O_7{\cdot}10H_2O$], as shown in Figure 2.4. The pH of the aqueous phase is close to 12.5 throughout the simulation.

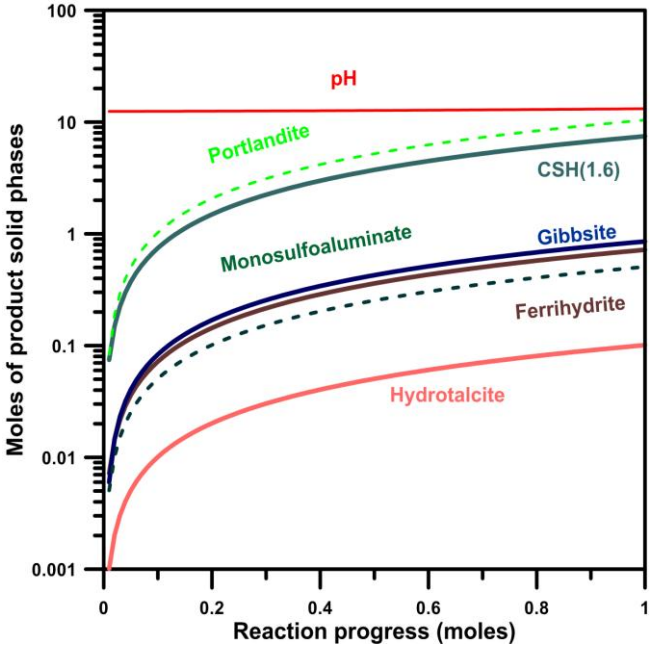

Figure 2.4. Molar amounts of cement solid phases formed during progressive cement hydration as predicted by PHREEQC for a mixture made up of 9.42 moles of clinker and 55.6 moles of water.

Progressive cement carbonation was simulated by adding 25.5 moles of CO_2 at 11 bar pressure to the mineral phases produced by cement hydration. PHREEQC predicts the formation of different solid phases during the carbonation process (Figure 2.5). Upon completion of this process, as indicated by the presence of excess (unreacted) CO_2(g), the product solid phases are, in order of decreasing molar abundance: Calcite, Amorphous Silica, Gibbsite, Ferrihydrite, Gypsum, and Magnesite.

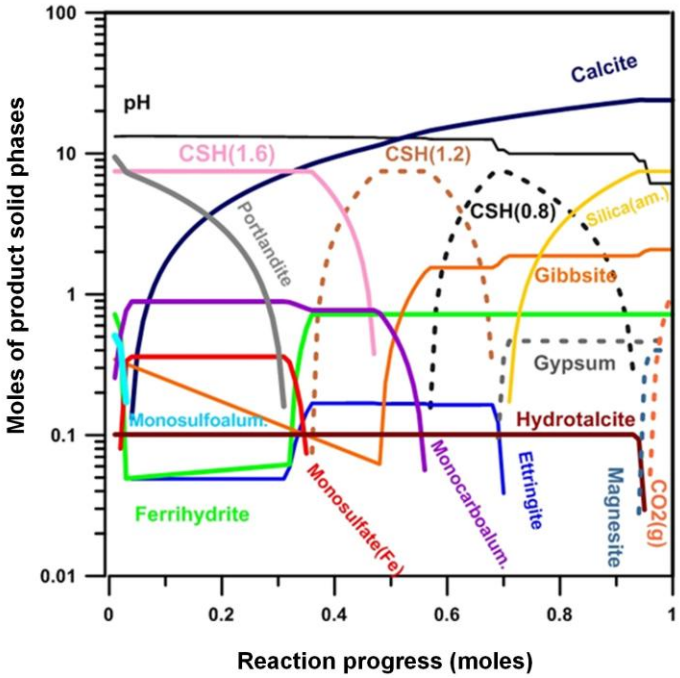

Figure 2.5. Molar amounts of product solid phases formed during progressive cement carbonation at 11 bar CO_2 partial pressure as predicted by PHREEQC.

The pH decreases progressively during the carbonation process, passing through a series of relatively constant values, which are dictated by different mineral assemblages acting as pH buffers. The final pH of the aqueous solution upon completion of the carbonation process is fixed at 6.13 by the Calcite/Magnesite buffer under a CO_2 partial pressure of ~11 bar (see below).

Portlandite is destroyed quickly and other Ca-bearing solid phases are formed. Ca-monosulfoaluminate is rapidly converted to Fe-monosulfate and ettringite [$Ca_6Al_2(SO_4)_3(OH)_{12}\cdot 26H_2O$], which have an ephemeral existence and produce gypsum, representing the stable sulfate mineral at the end of the carbonation process.

CSH(1.6) is transformed into CSH(1.2) [$Ca_{1.2}SiO_{3.2}\cdot 2.06H_2O$] first and into CSH(0.8) [$Ca_{0.8}SiO_{2.8}\cdot 1.54H_2O$] afterwards. All calcium-silicate-hydrates have an ephemeral existence and

are destroyed, producing amorphous silica and stable Ca-bearing solid phases, namely calcite and gypsum.

Among the Al-bearing phases, Ca-monocarboaluminate is dissolved and substituted by authigenic gibbsite, whereas hydrotalcite remains in the system over most of the carbonation but it is destroyed towards the end of the process to produce magnesite, which is part of the final mineral assemblage. The disappearance of hydrotalcite, at the reaction progress value of 0.974, is concurrent with the sharp increase in CO_2 partial pressure up to 10.9 bar at the end of the simulation (Figure 2.6).

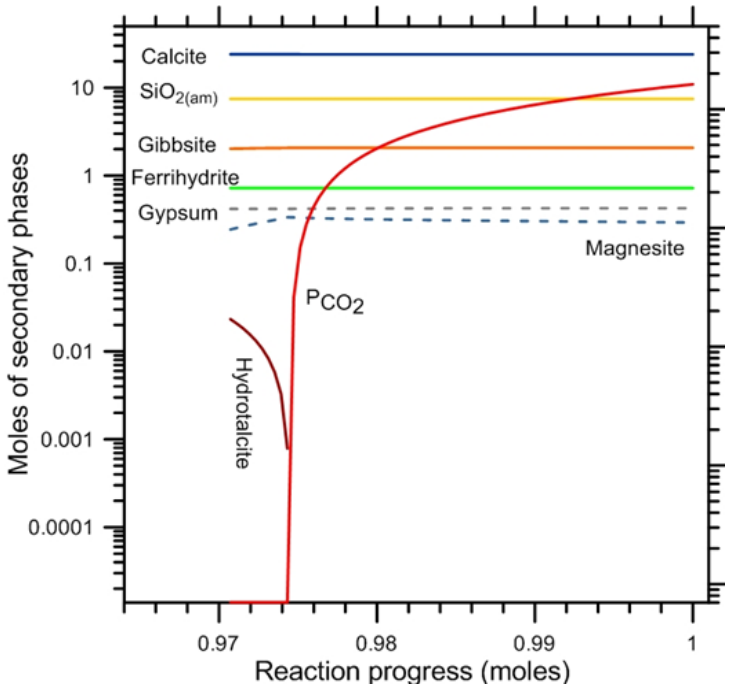

Figure 2.6. Zoomed view close to the end of the PHREEQC simulation of the molar amounts of product solid phases formed during progressive cement carbonation at 11 bar CO_2 partial pressure.

2.4.3. Results of RTM

The minerals of the rock formation (Calcite, Chlorite, Illite, Montmorillonite and Quartz) were equilibrated with the natural CO_2 abundance in soil and the formation water. Thus, no chemical changes occur in the soil during the RTM run.

The effects of CO_2-cement interaction, can be already appreciated after 1 day during the RTM in terms of changes in the abundance of solid phases, namely a limited decrease of hydrotalcite (Figure 2.7a) and the production of small amounts of magnesite (Figure 2.7b)

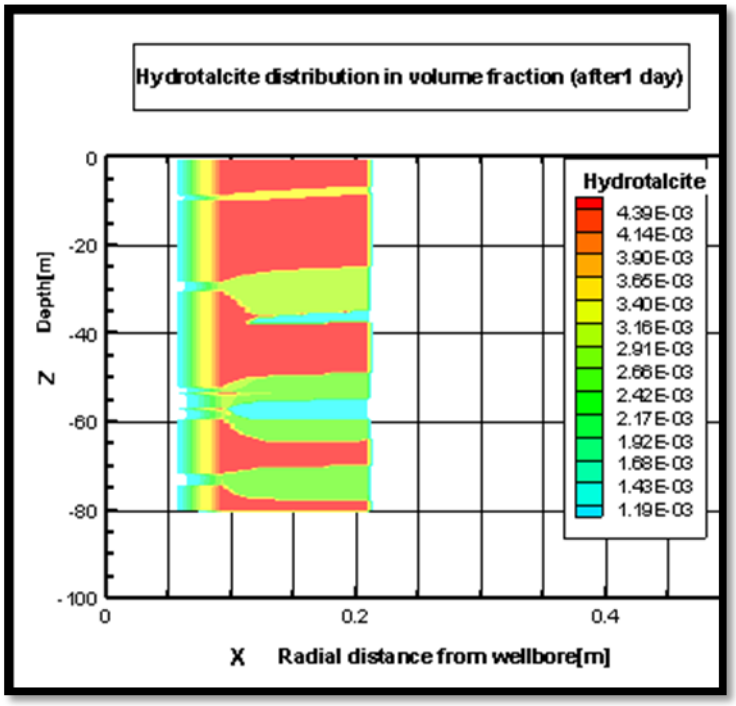

Figure 2.7a. 2D radial model of the system of interest showing the distribution of Hydrotalcite (in volume fraction of solids) in the cement domain, after 1 day of carbonation.

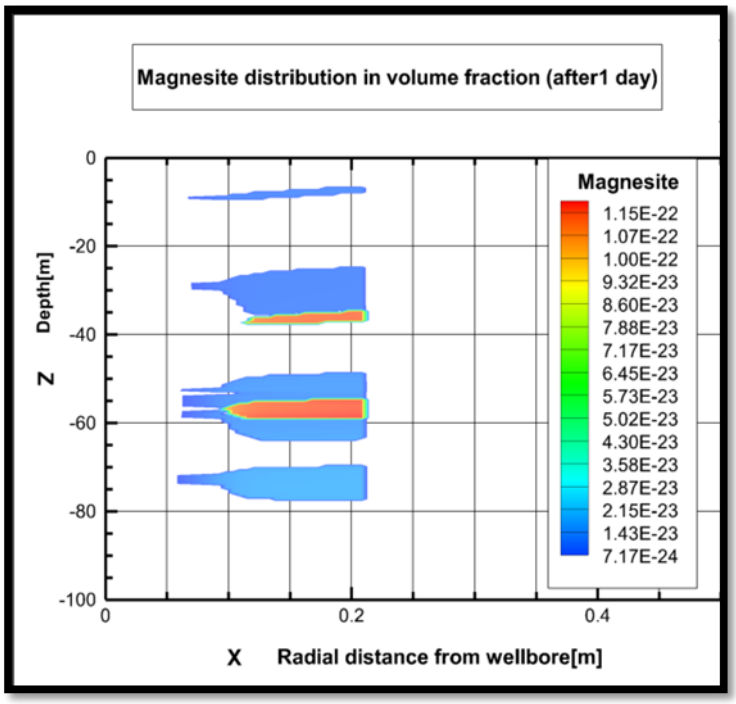

Figure 2.7b. 2D radial model of the considered system showing the distribution of Magnesite (in volume fraction of solids) in the cement domain, after 1 day of carbonation.

Two reactive fronts appears in the modelled domain due to cement-CO_2 interaction. The first reactive front is observed at 53 meters depth where the damaged zone affecting casing and cement is positioned, whereas the second reactive front appears above it, at 35 meters depth. Although magnesite starts to precipitate at the very beginning of the RTM run, the magnesite volume fraction remains very low throughout the simulation, suggesting the occurrence of coupled precipitation-dissolution of this solid phase, which has therefore ephemeral existence (Figure 2.8).

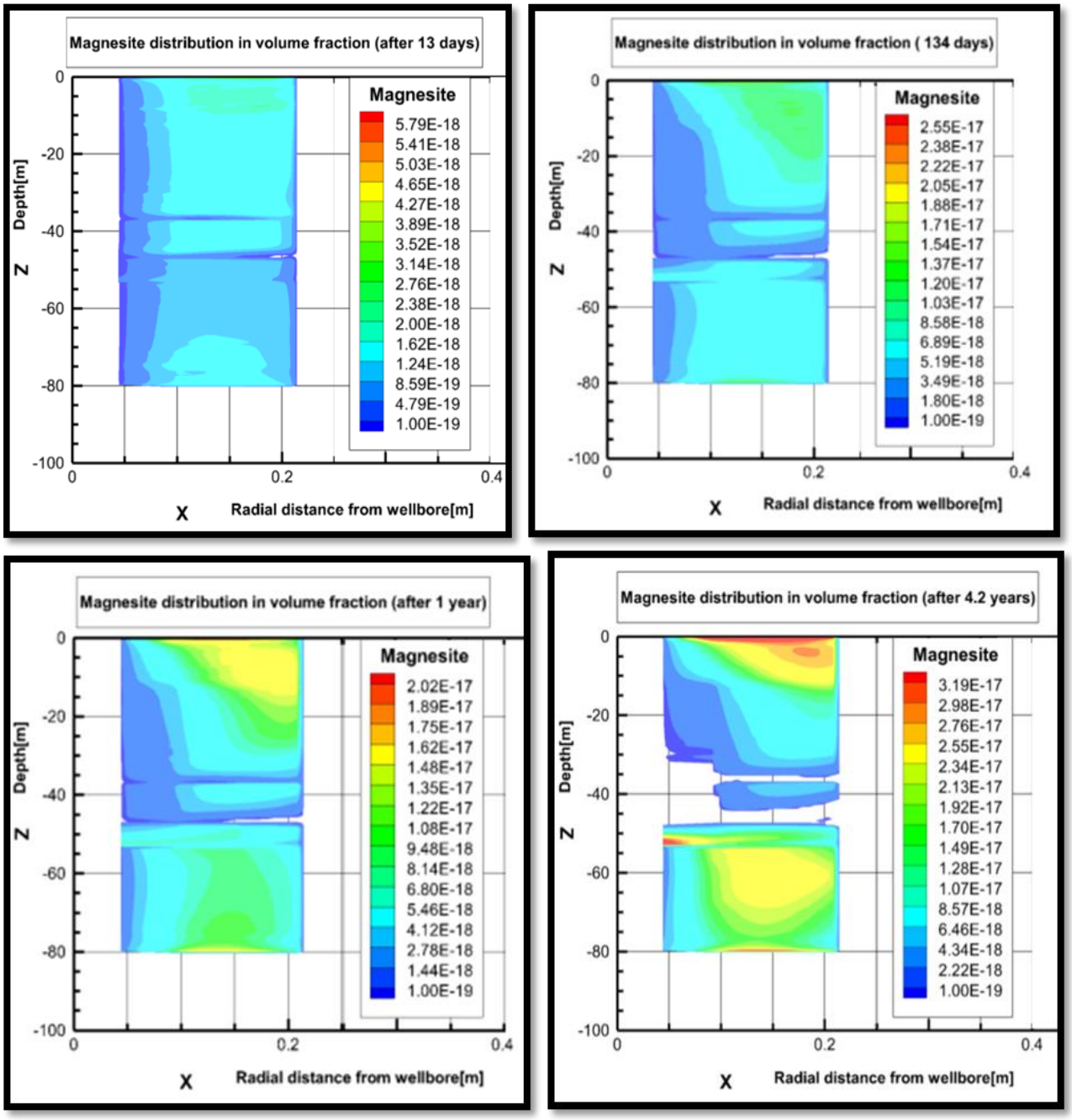

Figure 2.8. Magnesite distribution (in volume fraction of solids) at different times (13 days, 134 days, 1 year, 4.2 years) in the cement domain of the 2D radial model.

Mineral dissolution governed by CO_2 affects not only magnesite but also calcite, whose volume fraction in the cement domain experiences a considerable decrease after one year, with minima along the two reactive fronts at depths of 53 m and 35 m (Figure 2.9 right, Figure 2.10 right). This process causes a concurrent increase in porosity (Figure 2.9 left, Figure 2.10 left).

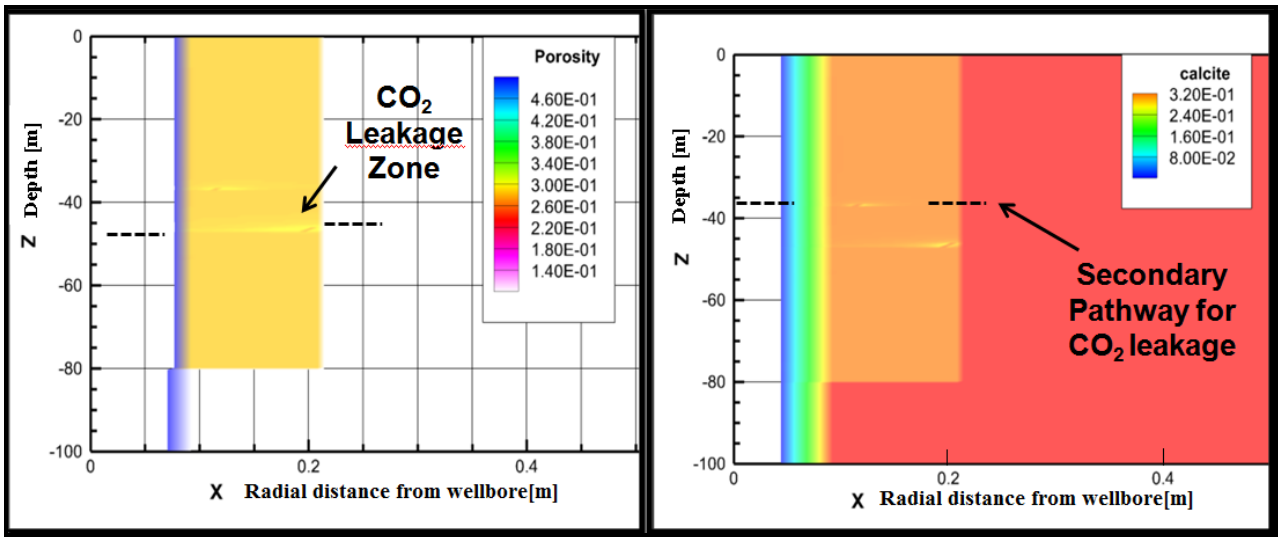

Figure 2.9. Porosity distribution (left) and Calcite distribution in volume fraction (right) in the cement domain of the 2D radial model after one year.

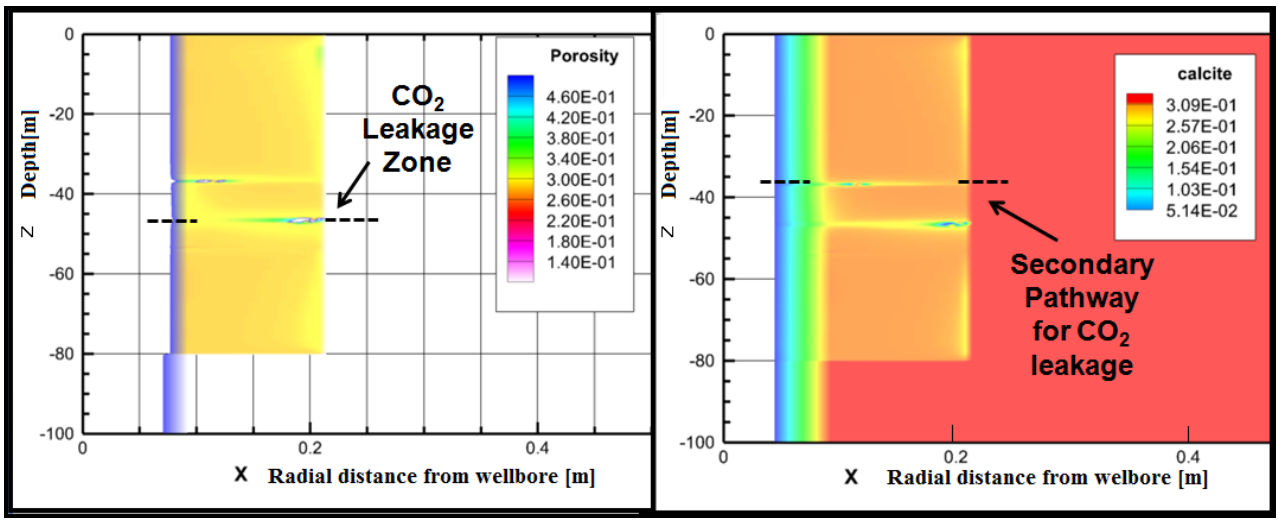

Figure. 2.10. Porosity distribution (left) and Calcite distribution in volume fraction (right) in the cement domain of the 2D radial model at the end of the simulation, that is after 4.2 years.

As expected high aqueous CO_2 molar fractions are present in the two reactive fronts throughout the RTM simulation as well as at its end, that is after 4.2 years (Figure 2.11).

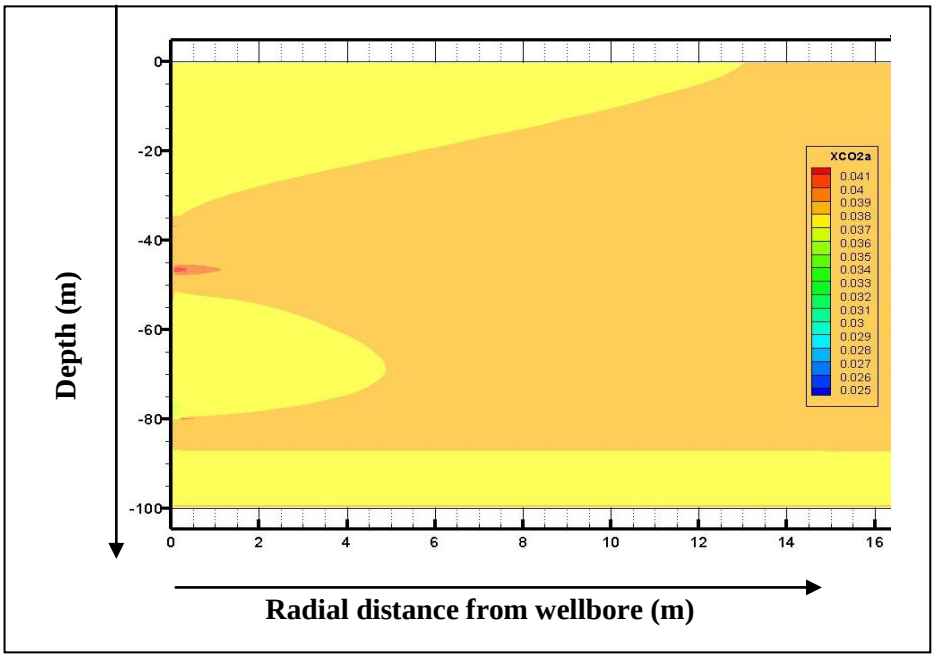

Figure 2.11. Molar fractions of the aqueous CO_2 in the cement domain of the 2D radial model after 4.2 year, shows the highest values at 53 m depth, where the gas leakage occurs first. The production zone of the reservoir is also well defined at ~ 80 m depth with high CO_2 molar values.

2.5. Discussion and conclusions

2.5.1 Permeability of porous materials

The calibration of the RTM involving the measured CO_2 fluxes leads to permeability values of ~0.00025 D for the cap-rock and ~1.20 D for the fractured zone sustaining the extracted flow rates of 2 t h^{-1} CO_2(g) and 2 t h^{-1} H_2O(l) (see section 2.3.3.2). The first value is somewhat lower than the range of values computed by means of Equation (2.1) from the median CO_2 flux values of population C, 0.00039 to 0.0021 D, whereas the second value is somewhat higher than the interval of values calculated inserting in Equation (2.1) the median CO_2 flux values of population A, 0.31 to 0.61 D (see section 2.4.1). The satisfactory agreement between the permeability values obtained by using the two distinct computational approaches is reassuring, though expected, since the measured CO_2 fluxes are involved in both approaches.

2.5.2. Limitations and uncertainties of RPM and RTM

RPM and RTM are affected by several limitations and uncertainties which are chiefly due to the poor knowledge of both: (i) the thermodynamic and kinetic properties of the solid phases involved in the geochemical modeling and (ii) the reactive surface areas of relevant minerals, as recognized by many authors (e.g. Lichtner, 1996).

For what concerns point (i), proxies are often used when the thermodynamic and kinetic properties are unknown for the phases of interest. For instance, magnesite was introduced in the RPM and RTM performed in this study because its thermodynamic properties are well constrained thanks to the recent study of Benezeth et al. (2011) and its kinetic properties are also well known thanks to the research of several authors (e.g., Chou et al., 1989; Pokrovsky and Schott, 1999a, 1999b; Arvidson and Mackenzie, 2000; Jordan et al., 2001; Higgins et al., 2002; Laçin et al., 2005; Pokrovsky et al., 2005; Saldi et al., 2009). However, magnesite precipitation at ambient temperature is limited by the very slow step advancement rates, limiting the step generation by spiral growth on the magnesite surface (Saldi et al., 2009). Consequently, hydrated magnesium carbonates either crystalline, such as hydromagnesite or nesquehonite or dypingite (e.g., Wang et al., 2008; Hopkinson et al., 2012) or amorphous (e.g., Orlando et al., 2012) readily precipitate at ambient temperatures instead of magnesite. Unfortunately, the involvement of these crystalline or amorphous hydrated magnesium carbonates in RPM and RTM is hindered by the poor knowledge of their thermodynamic and kinetic properties (e.g., Marini, 2006).

For what concerns point (ii), it must be underscored that the surface of contact between minerals and waters in natural aquifer systems may deviate significantly from the reactive surface area of mineral phases in kinetic geochemical models. This limit the transfer of geochemical modeling results to real systems. Moreover, the high uncertainties on reactive surface areas reflect in a correspondingly large error on time. In fact, there is an hyperbolic relation between the reactive surface area and time corresponding to an inverse linear dependence between the logarithm of the reactive surface area and the logarithm of time (see section 7.2.4 in Marini, 2006),

2.5.3. RPM of cement hydration and carbonation

The results obtained for the RPM of cement hydration (Figure 2.4) are reasonable. In fact, it is well known that the principal product phases formed during cement hydration are calcium-silicate-hydrates(CSH) and portlandite, usually constituting ~70 wt % (~53 mol %) and ~15-20% (~30 mol %) of the hydrated cement, respectively (e.g. Kutchko et al., 2007 and references therein). CSH phases are semi-amorphous gel-like substances acting as primary binding material. Portlandite

crystals nucleate in available capillary pore space during early hydration and grow quickly occupying available space between cement grains and early CSH deposits.

Cement carbonation is completed at the reaction progress value of 0.974 and is marked by Hydrotalcite-Magnesite-Gibbsite coexistence. This condition acts as a CO_2 buffer, as pointed out by the following reaction:

$$Mg_4Al_2O_7 \cdot 10H_2O + 4\ CO_2(g) = 4\ MgCO_3 + 2\ Al(OH)_3 + 7H_2O. \quad (2.3)$$

However, this buffer is unstable since it is destroyed by addition of gaseous CO_2 to the system which causes the conversion of hydrotalcite in magnesite plus gibbsite.

2.5.4. RTM of cement alteration

The RPM of cement carbonation ends upon total conversion of hydrotalcite in magnesite plus gibbsite. In contrast, the RTM of cement alteration takes into account not only cement carbonation, but also its further CO_2-promoted alteration, which causes the dissolution of carbonate minerals, namely calcite and magnesite. The occurrence of coupled precipitation-dissolution of magnesite explains the very low abundance of this ephemeral mineral throughout the simulation.

As long as cement carbonation occurs, TOUGHREACT predicts chemical and mineralogical changes in the cement domain substantially similar to those computed by PHREEQC, *mutatis mutandi*. The only exception concerns the CSH solid phases, which form in the batch reaction only. The absence of these minerals in RTM may be due to the small cell size adopted in RTM, as the cement thickness is less than 20 cm, with 5 mm of mesh size. Kinetic reasons can also explain the cement carbonation path predicted by TOUGHREACT, since the kinetic constant of calcite is higher than that of CSH phases by 3 orders of magnitude (Table 2.6), in spite of the considerable uncertainties on the dissolution/precipitation rates of CSH minerals and adopted approximations (see section 2.3.3.3). As a result, in the TOUGHREACT kinetic model, calcite is obtained directly from CSH(1.6) whereas the batch reaction model (which does not take into account reaction kinetics) predicts production of calcite through conversion of CSH(1.6) to CSH(1.2) followed by conversion of CSH(1.2) to CSH(0.8).

Both the alteration zone at 35 m depth and the advanced alteration in the cement domain close to the well, between the two alteration zones at 53 m and 35 m depths, might be caused by buoyancy effects, which are especially important close to the well casing as indicated by the CO_2 flow vector direction (not shown). Cement alteration beyond carbonation completion occurs in all these zones of the cement domain. The predicted increase in porosity is evidently due to calcite dissolution

since secondary amorphous silica is not (or not significantly) dissolved, due to the comparatively slow kinetics. These findings agree with the experimental and computational evidence of Abdoulghafour et al., (2016) and references therein, although the time intervals considered by these authors are much smaller than those of the RTM simulation of this work.

The obvious conclusion is that the advective flow of CO_2, such as that occurring along a damaged zone affecting casing and cement, has the potential, first, to bring cement carbonation to completion and, second, to promote further cement alteration through considerable dissolution of carbonate minerals. These CO_2-promoted reactions are relatively fast and may cause the alteration of important cement amounts in a relatively short time, in the order of some years. The ultimate consequence of these chemical reactions is, most likely, CO_2 leakage to the surface from either the production zone (in the considered natural analogue) or the reservoir (in a CO_2 storage scenario).

Acknowledgments

This research was supported by the CO_2 react Marie Curie Initial Trainig Network.

References

Abdoulghafour, H., Luquot, L., Gouze, P. (2013). Characterization of the mechanisms controlling the permeability changes of fractured cements flowed through by CO_2-rich brine. Environmental Science & Technology, 47(18), 10332-10338.

Abdoulghafour, H., Gouze, P., Luquot, L., Leprovost, R. (2016). Characterization and modeling of the alteration of fractured class-G Portland cement during flow of CO_2-rich brine. International Journal of Greenhouse Gas Control, 48, 155-170.

Arvidson, R.S., & Mackenzie, F.T. (2000). Temperature dependence of mineral precipitation rates along the CaCO3-MgCO3 join. Aquat. Geochem., 6, 249-256.

Aunzo, Z.P., Bjornsson, G., Bodvarsson., G.S. (1991). Wellbore Models GWELL, GWNACL, and HOLA. Lawrence Berkeley National Laboratory Report LBL-31428, Berkeley, CA.

Baur, I., Keller, P., Mavrocordatos, D., Wehrli, B., & Johnson, C.A. (2004). Dissolution-precipitation behaviour of ettringite, monosulfate, and calcium silicate hydrate. Cement and Concrete Research, 34(2), 341-348.

Bénézeth, P., Saldi, G.D., Dandurand, J.L., Schott, J. (2011). Experimental determination of the solubility product of magnesite at 50 to 200 °C. Chemical Geology, 286, 21-31.

Brunet, J.P.L., Li, L., Karpyn, Z.T., Kutchko, B.G., Strazisar, B., Bromhal, G. (2013). Dynamic evolution of cement compositional and transport properties under conditions relevant to geological carbon sequestration. Energy Fuels, 27(8), 4208-4220.

Bullard, J.W., Enjolras, E., George, W.L., Satterfield, S.G., Terrill, J.E. (2010). A parallel reaction-transport model applied to cement hydration and microstructure development. Modelling and Simulation in Materials Science and Engineering, 18(2), 025007.

Cantucci, B., Montegrossi, G., Vaselli, O., Tassi, F., Quattrocchi, F., Perkins, E.H. (2009). Geochemical modeling of CO_2 storage in deep reservoirs: the Weyburn Project (Canada) case study. Chemical Geology, 265(1), 181-197.

Cantucci, B., Montegrossi, G., Buttinelli, M., Vaselli, O., Scrocca, D., Quattrocchi, F. (2015). Geochemical Barriers in CO_2 Capture and Storage Feasibility Studies. Transport in Porous Media, 106(1), 107-143.

Cardellini C., Frondini F., Morgantini N., Chiodini G., Avino R., Caliro S., Granieri D., Russo M. (2004). Diffuse soil CO_2 degassing at Salcheto (Tuscany) and Lipary (Sicily): a probabilistic approach to mapping and quantification of gas release. Water-Rock Interaction, Wanty & Seal II (eds), 101-104.

Carey, J.W. (2013). Geochemistry of wellbore integrity in CO_2 sequestration: Portland cement-steel-brine-CO2 interactions. Reviews in Mineralogy and Geochemistry, 77(1), 505-539.

Carey, J.W, & Lichtner, P.C. (2007). Calcium silicate hydrate (CSH) solid solution model applied to cement degradation using the continuum reactive transport model FLOTRAN. In: Transport Properties and Concrete Quality: Materials Science of Concrete. Mobasher, B., Skalny, J. (Eds.) American Ceramic Society. Wiley, 73-106.

Carey, J.W., Wigand, M., Chipera, S., WoldeGabriel, G., Pawar, R., Lichtner, P., Wehner, S., Raines, M., Guthrie, G.D.Jr. (2007). Analysis and performance of oil well cement with 30 years of CO_2 exposure from the SACROC Unit, West Texas, USA. International Journal of Greenhouse Gas Control, 1, 75-85.

Carmignani, L., & Lazzarotto, A. (2004). Geological map of the tuscany region (scale 1: 250.000). Earth Science Department of the University of Siena, Center of GeoTechnology, Tuscany Region. *Litografia Artistica Cartografica*, Florence, Italy.

Carroll, S.A., McNab, W.W., Torres, S.C. (2011). Experimental study of cement-sandstone/shale-brine-CO_2 interactions. Geochemical transactions, 12(1), 1-19.

Collins, R.E. (1961). Flow of fluids through porous materials. PennWell Books. PennWell Publishing Company, Tulsa, Oklahoma, 270 pp.

Corvisier, J., Brunet, F., Fabbri, A., Bernard, S., Findling, N., Rimmelé, G., Barlet-Gouédard, V., Beyssac, O., Goffé, B. (2010). Raman mapping and numerical simulation of calcium carbonates distribution in experimentally carbonated Portland-cement cores. Eur. J. Mineral., 22, 63-74.

Crow, W., Carey, J.W., Gasda, S., Williams, D.B., Celia, M. (2010). Wellbore integrity analysis of a natural CO_2 producer. International Journal of Greenhouse Gas Control, 4(2), 186-197.

Chiaramonte, L., Zoback, M.D., Friedmann, J., Stamp, V. (2008). Seal integrity and feasibility of CO_2 sequestration in the Teapot Dome EOR pilot: geomechanical site characterization. Environmental Geology, 54(8), 1667-167.

Chiodini, G., Cioni, R., Guidi, M., Raco, B., Marini, L. (1998). Soil CO_2 flux measurements in volcanic and geothermal areas. Applied Geochemistry, 13, 543-552.

Chou, L., Garrels, R.M., Wollast, R. (1989). Comparative study of the kinetics and mechanisms of dissolution of carbonate minerals. Chemical Geology, 78, 269-282.

Deremble, L., Loizzo, M., Huet, B., Lecampion, B., Quesada, D. (2011). Stability of a leakage pathway in a cemented annulus. Energy Procedia, 4, 5283-5290.

Fabbri, A., Jacquemet, N., Seyedi, D.M. (2012). A chemo-poromechanical model of oilwell cement carbonation under CO_2 geological storage conditions. Cem. Concr. Res., 42, 8-19.

Fairbridge, R.W., Finkl Jr, C.W. (1979). The Encyclopedia of Soil Science Part 1. Physics, Chemistry, Biology, Fertility, and Technology. Dowden, Hutchinson & Ross, Inc. Stroudsburg, Pennsylvania.

Fenghour, A., Wakeham, W.A., Vesovic, V. (1998). The viscosity of carbon dioxide. J. Phys. Chem. Ref. Data, 27(1), 31-44.

Frondini, F., Caliro, S., Cardellini, C., Chiodini, G., Morgantini, N., Parello, F. (2008). Carbon dioxide degassing from Tuscany and northern Latium (Italy). Global and Planetary Change, 61(1), 89-102.

Geloni, C., Giorgis, T., Battistelli, A. (2011). Modeling of rocks and cement alteration due to CO_2 injection in an exploited gas reservoir. Transport in porous media, 90(1), 183-200.

Gherardi, F., Audigane, P., Gaucher, E.C. (2012). Predicting long-term geochemical alteration of wellbore cement in a generic geological CO_2 confinement site: tackling a difficult reactive transport modeling challenge. Journal of Hydrology, 420, 340-359.

Halim, C.E., Short, S.A., Scott, J.A., Amal, R., Low, G. (2005). Modelling the leaching of Pb, Cd, As, and Cr from cementitious waste using PHREEQC. Journal of Hazardous Materials, 125(1), 45-61.

Hernández-Rodríguez, A., Virgili, G., Continanza, D., Ferrante, L., Marini, L. (2016). Occurrence of a nearly constant air flux through the accumulation chamber during CO_2 flux measurements. Evidence from laboratory experiments and consequences. Journal of Volcanology and Geothermal Research (submitted).

Higgins, S.R., Jordan, G., Eggleston, C.M. (2002). Dissolution kinetics of magnesite in acidic aqueous solution: A hydrothermal atomic force microscopy study assessing step kinetics and dissolution flux. Geochimica et Cosmochimica Acta, 66, 3201-3210.

Hopkinson, L., Kristova, P., Rutt, K., Cressey, G. (2012). Phase transitions in the system MgO-CO_2-H_2O during CO_2 degassing of Mg-bearing solutions. Geochimica et Cosmochimica Acta, 76, 1–13.

Huet, B.M., Prevost, J.H., Scherer, G.W. (2010). Quantitative reactive transport modeling of Portland cement in CO_2-saturated water. International Juornal of Greenhouse Gas Control, 4, 561-574.

Ipavec, A., Gabrovšek, R., Vuk, T., Kaučič, V., Maček, J., Meden, A. (2011). Carboaluminate Phases Formation During the Hydration of Calcite-Containing Portland Cement. Journal of the American Ceramic Society, 94(4), 1238-1242.

Jacquemet, N., Pironon, J., Lagneau, V., Saint-Marc, J. (2012). Armouring of well cement in H_2S-CO_2 saturated brine by calcite coating-experiments and numerical modelling. Applied Geochemistry, 27, 782-795.

Jordan, G., Higgins, S.R., Eggleston, C.M., Knauss, K.G., Schmahl, W.W. (2001). Dissolution kinetics of magnesite in acidic aqueous solution, a hydrothermal atomic force microscopy (HAFM) study: Step orientation and kink dynamics. Geochimica et Cosmochimica Acta, 65, 4257-4266.

Kutchko, B.G., Strazisar, B. R., Dzombak, D.A., Lowry, G.V., Thaulow, N. (2007). Degradation of well cement by CO_2 under geologic sequestration conditions. Environmental Science & Technology, 41(13), 4787-4792.

Laçin, O., Dönmez, B., Demir, F. (2005) Dissolution kinetics of natural magnesite in acetic acid solutions. Int. J. Miner. Process., 75, 91-99.

Larsen, O., & Postma, D. (2001). Kinetics of reductive bulk dissolution of lepidocrocite, ferrihydrite, and goethite. Geochimica et Cosmochimica Acta, 65(9), 1367-1379.

Lichtner, P.C., (1996). Continuum formulation of multicomponent-multiphase reactive transport. In: Lichtner, P.C., Steefel, C.I., Oelkers, E.H. (Eds.). Reactive Transport in Porous Media. Reviews in Mineralogy, 34, 1–81.

Luquot, L., Abdoulghafour, H., Gouze, P. (2013). Hydro-dynamically controlled alteration of fractured Portland cements flowed by CO_2-rich brine. International Journal of Greenhouse Gas Control, 16, 167-179.

Marini, L. (2006). Geological Sequestration of Carbon Dioxide - Thermodynamics, Kinetics, and Reaction Path Modeling. Developments in Geochemistry, 11, 453 pp.

McNab, W.W., & Carroll, S.A. (2011). Wellbore integrity at the Krechba carbon storage site, In Salah, Algeria: 2. Reactive transport modeling of geochemical interactions near the cement-formation interface. Energy Procedia, 4, 5195-5202.

Miyata, S. (1980). Hydrotalcites in relation to composition. Clays Clay Miner, 28(1), 50-56.

Newell, D.L., & Carey, J.W. (2012). Experimental evaluation of wellbore integrity along the cement-rock boundary. Environmental Science & Technology, 47(1), 276-282.

Orlando, A., Lelli, M., Marini, L. (2012). Production of amorphous hydrated impure magnesium carbonate through ex-situ carbonation. Applied Geochemistry, 27, 2500-2510.

Palandri, J.L., & Kharaka, Y.K. (2004). A compilation of rate parameters of water-mineral interaction kinetics for application to geochemical modeling (No. OPEN-FILE-2004-1068). U. S. Geological Survey, Menlo Park, California.

Papadakis, V.G., Vayenas, C.G., Fardis, M.N. (1989). A reaction engineering approach to the problem of concrete carbonation. AIChE Journal 35 (10), 1639–1650.

Parkhurst, D.L., & Appelo, C.A.J. (2013). Description of input and examples for PHREEQC version 3-a computer program for speciation, batch-reaction, one-dimensional transport, and inverse geochemical calculations. US geological survey techniques and methods, book, 6, 497.

Pokrovsky, O.S., & Schott, J. (1999a). Processes at the magnesium-bearing carbonates/solution interface. II. Kinetics and mechanism of magnesite dissolution. Geochimica et Cosmochimica Acta, 63, 881-897.

Pokrovsky, O.S., & Schott, J. (1999b). Processes at the magnesium-bearing carbonates/solution interface. I. A surface speciation model for magnesite. Geochimica et Cosmochimica Acta, 63, 863-880.

Pokrovsky, O.S., Golubev, S.V., Schott, J. (2005). Dissolution kinetics of calcite, dolomite and magnesite at 25°C and 0 to 50 atm pCO_2. Chemical Geology, 217(3-4), 239-255.

Pruess, K., & Spycher, N. (2007). ECO2N–A fluid property module for the TOUGH2 code for studies of CO_2 storage in saline aquifers. Energy Conversion and Management, 48(6), 1761-1767.

Raoof, A., Nick, H., Wolterbeek, T., Spiers, C. (2012). Pore-scale modeling of reactive transport in wellbore cement under CO_2 storage conditions. International Journal of Greenhouse Gas Control, 11, 67-77.

Richardson, M.G. (1988). Carbonation of Reinforced Concrete: Its Causes and Management. Citis Ltd., Dublin, London and New York.

Roy, D.M., Brown, P.W., Shi, D., Scheetz, B.E., May, W. (1993). Concrete microstructure porosity and permeability (No. SHRP-C-628).

Saldi, G.D., Jordan, G., Schott, J., Oelkers, E.H. (2009). Magnesite growth rates as a function of temperature and saturation state. Geochimica et Cosmochimica Acta, 73, 5646-5657.

Schweizer, C., (1999). Calciumsilikathydrat-Mineralien. Lösungskinetik und ihr Einfluss auf das Auswaschverhalten von Substanzen aus einer Ablagerung mit Rückständen aus Müllverbrennungsanlagen, Ph.D. Thesis, Swiss Federal Institute of Technology (ETH), Zürich.

Sinclair, A.J. (1974). Selection of threshold values in geochemical data using probability graphs. J. Geochem. Explor., 3, 129-149.

Sinclair, A.J. (1976). Applications of probability graphs in mineral exploration. Spec. vol. 4, Association of Exploration Geochemists, 95 pp.

Sinclair, A.J., & Blackwell, G.H. (2002), Applied Mineral Inventory Estimation. Cambridge University Press, Cambridge, 381 pp.

Svensson, U., & Dreybrodt, W. (1992). Dissolution kinetics of natural calcite minerals in CO_2-water systems approaching calcite equilibrium. Chemical Geolology 100, 129–145.

Thomas, J., & Jennings, H. (2014). Manufacture and composition of Portland cement. http://iti.northwestern.edu/cement/monograph/Monograph3_2.html

Trapote Barreira, A. (2015). Dissolution kinetics of CSH gel and durability of mortar. PhD Thesis. Technical University of Catalonia.

Valentini, L., Parisatto, M., Russo, V., Ferrari, G., Bullard, J.W., Angel, R.J., Dalconi M.C., Artioli, G. (2014). Simulation of the hydration kinetics and elastic moduli of cement mortars by microstructural modelling. Cement and Concrete Composites, 52, 54-63.

Viswanathan, H.S., Pawar, R.J., Stauffer, P.H., Kaszuba, J.P., Carey, J.W., Olsen, S.C., Keating, G.N., Kavetski, D., Guthrie, G.D. (2008). Development of a hybrid process and system model for the assessment of wellbore leakage at a geologic CO_2 sequestration site. Environmental Science & Technology, 42(19), 7280-7286.

Wang, Y., Li, Z., Demopoulos, G.P. (2008). Controlled precipitation of nesquehonite ($MgCO_3 \cdot 3H_2O$) by the reaction of $MgCl_2$ with $(NH_4)_2CO_3$. J. Cryst. Growth, 310, 1220-1227.

Wertz, F., Gherardi, F., Blanc, P., Bader, A.G., Fabbri, A. (2013). Cement CO_2-alteration propagation at the well–caprock–reservoir interface and influence of diffusion. International Journal of Greenhouse Gas Control, 12, 9-17.

Wilson, J.C., Benbow, S.J., Metcalfe, R., Savage, D., Walker, C.S., Chittenden, N. (2011). Fully coupled modeling of long term cement well seal stability in the presence of CO_2. Energy Procedia, 4, 5162-5169.

Winnefeld, F., & Lothenbach, B. (2010). Hydration of calcium sulfoaluminate cements-experimental findings and thermodynamic modelling. Cement and Concrete Research, 40(8), 1239-1247.

Wolery, T.W., & Jove-Colon, C. (2007). Qualification of thermodynamic data for geochemical modeling of mineral-water interactions in dilute systems. Sandia National Laboratories Report ANL-WIS-GS-000003 REV 01.

Xu, T., Spycher, N., Sonnenthal, E., Zheng, L., Pruess, K. (2012). TOUGHREACT user's guide: A simulation program for non-isothermal multiphase reactive transport in variably saturated geologic media, version 2.0. Earth Sciences Division, Lawrence Berkeley National Laboratory, Berkeley, USA.

Zhang, M., Bachu, S. (2011). Review of integrity of existing wells in relation to CO_2 geological storage: What do we know? International Journal of Greenhouse Gas Control, 5(4), 826-840.

Chapter 3- EXPERIMENTAL ANALYSIS OF THE REACTION RATE OF HYDRATED CLASS G CEMENT POWDER AT P_{CO2} OF 1 TO 51 BAR AND AMBIENT TEMPERATURE

Abstract

The carbonation rate of G-class Portland cement was studied at room temperature and different P_{CO2} values, in the range 1 to 51 bar, through three types of laboratory experiments. Cement hydration (accompanied by limited carbonation) was carried out for 28 days at atmospheric conditions. Afterwards, cement carbonation was investigated using a micro-reactor by reacting, in separate runs, cement powder samples, under stirred conditions, and massive samples, under stagnant conditions, with pure CO_2(g) and MilliQ water. After the completion of each experiments, analyses were performed on both, the aqueous solution (IC, ICP-OES, acidimetric titration) and the solids (XRD, SEM, TGA/DTA).

In type 1 experiments cement powder was reacted at 11 bar P_{CO2}, for 1, 3, 6, 21, 67, 97 and 120 hours. Portlandite was present only in the hydrated cement paste and was converted to $CaCO_3$ in less than one hour.

In type 2 experiments cement powder was reacted for 6 hours at P_{CO2} of 1, 11, 31 and 51 bar. The extent of cement carbonation was similar at all P_{CO2} values.

The experiments of type 3 were performed with cement cube samples at 11 bar P_{CO2} for 6, 24 and 210 hours. The average carbonation depth attained 0.23 mm in 1 day and resulted to be linearly related to the square root of reaction time indicating that cement carbonation rate is controlled by diffusion (Fickian behavior).

Keywords*:* Cement Carbonation; Carbonation rate, Geological Carbon Storage.

3.1. Introduction

Portland cement clinker consists of four main solid phases: tricalcium silicate (Ca_3SiO_5, or C3S in cement chemistry notation), dicalcium silicate (Ca_2SiO_4, or C2S), tricalcium aluminate ($Ca_3Al_2O_6$, or C3A) and tetracalcium aluminoferrite ($Ca_4Al_2Fe_2O_{10}$, C4AF). Gypsum ($CaSO_4 \cdot 2H_2O$) is commonly added to the solid mixture during grinding (e.g., Taylor, H.F.W. (1997). Cement Chemistry, 2nd ed. Academic Press, New York. ISBN: 0-7277-2592-0.

The hydration of calcium silicates produces semi-amorphous, gel-like, calcium silicate hydrate (CSH) and crystalline portlandite [$Ca(OH)_2$]. CSH has Ca/Si ratio varying from 1.5 to 2.0 and variable amounts of water (Neville, 2004; Taylor, 1997). At ambient conditions, CSH accounts for about 65% of hydrated cement and is the main binding phase, whereas portlandite comprises 15-20% of hydrated cement (Neville, 2004). The hydration of C3S proceeds much faster than that of C2S, producing more than twice as much portlandite. The hydration of C3A is similar to that of C4AF, in which both compounds react with gypsum producing ettringite [$Ca_6Al_2O_6(SO_4)_3 \cdot 32H_2O$] (Nelson and Guillot, 2006). After gypsum depletion, ettringite reacts with C3A forming Ca-Al-monosulfate ($3Ca_4Al_2O_6SO_4 \cdot 12H_2O$; Nelson and Guillot, 2006).

At 25°C, the pH of pore fluids in hydrated Portland cement is expected to be either close to the pH of portlandite solubility, 12.37, based on simple speciation-saturation calculations carried out with EQ3/6, or somewhat higher, that is between 13 and 14, due to the presence of significant amounts of KOH and NaOH in Portland cement (Taylor 1997).

Cement carbonation consists of the reaction between the hydration products of Portland cement and aqueous CO_2, chiefly leading to the formation of $CaCO_3$ and amorphous silica (Richardson, 1988; Papadakis et al., 1989). Calcium carbonate is the main carbonation product and occurs as three distinct polymorphs (calcite, aragonite and vaterite) although calcite is the ultimate stable $CaCO_3$ form. First, portlandite reacts with aqueous CO_2:

$$Ca(OH)_2 + H_2CO_3 \rightarrow CaCO_3 + 2\ H_2O \qquad (3.1)$$

Reaction (3.1) lowers the pH of the cement pore fluids below 12 and triggers the incongruent dissolution of CSH (Chen et al. 2004):

$$Ca_xSiO_{2+x} \cdot xH_2O + yH_2CO_3 \rightarrow Ca_{x-y}SiO_{2+x-y} \cdot (x\text{-}y)H_2O + yCaCO_3 + 2yH_2O \qquad (3.2)$$

Reaction (3.2) causes the progressive decalcification of CSH whose Ca/Si ratio decreases from the initial value x to x-y, with $x > y$. Upon reaction completion, ($y = x$), CSH decomposes completely to amorphous silica and calcium carbonate according to the reaction:

$$Ca_xSiO_{2+x} \cdot xH_2O + xH_2CO_3 \rightarrow SiO_2 + xCaCO_3 + 2xH_2O \quad (3.3)$$

Other hydrated cement phases, such as ettringite and Ca-Al-Fe monosulfates, are decomposed by aqueous CO_2 similar to reactions (3.2) and (3.3), *mutatis mutandi*, with the formation of $CaCO_3$ and a gel-like, amorphous residue of Al, Fe(III), and/or silica oxyhydroxides.

The water produced in carbonation reactions hampers CO_2 diffusion through the pores of the cement paste, thus decreasing the carbonation rate, which is defined as the depth of carbonation[1] per exposure time (Richardson, 1988). Reardon et al. (1989) showed that (i) the rate of carbonation increases as water is removed from the cement paste pores allowing the inflow of CO_2, but (ii) carbonation proceeds very slowly under extreme drying, since water is needed to catalyze the carbonation reaction.

The rate of carbonation is influenced by several factors (e.g., cement types, additives, water/cement ratio, and curing conditions) controlling the chemical and physical properties of cement pastes (e.g., content of $Ca(OH)_2$, porosity and permeability). The rate of carbonation also depends on the conditions (temperature, P_{CO2}, and amount of water) under which the carbonation reaction takes place (Richardson, 1988).

In particular, among the previous laboratory experimental studies, we recall those performed by: (a) Duguid et al. (2004, 2005), Duguid (2008) and Duguid and Scherer (2010), in which different experimental settings were adopted, including P_{CO2} close to 1 bar or lower, and temperatures of 20 and 50°C; (b) Barlet-Gouédard et al. (2006, 2007, 2009) investigated the reaction between cement and supercritical CO_2 and CO_2-saturated brines at 90°C and P_{CO2} of 280 bar; (c) Kutchko et al. (2007, 2008) carried out laboratory experiments, in which cement samples were partially immersed in a 1% NaCl solution and pressurized with supercritical CO_2 at 50°C and 303 bar; (d) Kutchko et al. (2009) investigated fly ash/cement mixtures exposed to both supercritical CO_2 and CO_2-saturated solution (1% NaCl) at 50 °C and 150 bar; (e) Pratt et al. (2009) characterized cement samples exposed to wet supercritical CO_2 at 50°C and 100 bar; (f) Sweatman et al. (2009) reacted both pure cement and cement-sandstone mixtures with CO_2-saturated water and wet (with 40% humidity) supercritical CO_2 at 60°C and 138 bar; (g) Santra and Sweatman (2010) investigated the carbonation of both pure cement and cement-fly ash mixtures (16-50%) reacting both materials with CO_2 at 93°C and 138 bar.

[1] The depth of carbonation (or penetration depth) is defined as the distance from the surface of the cement sample to the boundary where no alteration occurs.

Core-flood, flow-through laboratory experiments were also performed to study cement carbonation as a result of CO_2 flow through pre-existing fractures or interfaces. Among the investigations of this type, we recall those carried out by: (1) Wigand et al (2009) at pore pressure of 199 bar and 54 °C, first, saturating an illite-rich shale and the Portland cement core with 1.65 M brine and, second, injecting supercritical CO_2 into the system adopting a pressure gradient of 7 bar; (2) Carey et al. (2010), at 40°C and 140 bar pore pressure by flowing a 1:1 mixture of supercritical CO_2 and 30,000 ppm NaCl-rich brine equilibrated with limestone.

Temperatures from 50 to 90°C and P_{CO2} from 100 to over 300 bar were adopted in most previous laboratory experimental studies, that cover the typical temperature-pressure range relevant for CO_2 geological storage. In addition, several investigations were performed at room temperature and atmospheric pressure. Taking this into account, we decided to study the carbonation of class G Portland cement at room temperature in the P_{CO2} interval from 1 to 51 bar to fill the existing gap of knowledge.

It must be noted that there are other good reasons to investigate cement carbonation in the range of P_{CO2} 1 to 51 bar. Based on the results of the Duan et al. (2006) code for a 0.1 *m* NaCl aqueous solution at 25°C, there is a considerable, almost linear increase of CO_2 molality with CO_2 partial pressure up to P_{CO2} values of ~50-60 bar and m_{CO2} values of ~1.2-1.3 (Figure 3.1).

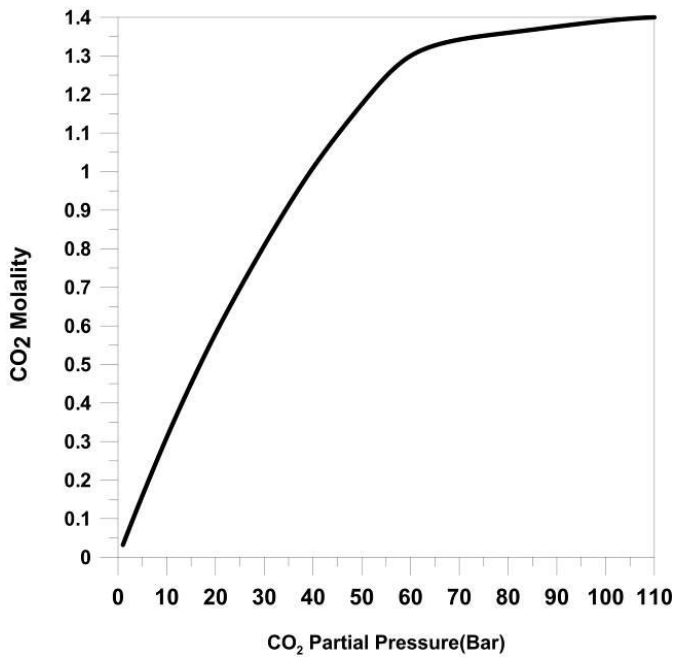

Figure 3.1. CO_2 molality as a function of CO_2 partial pressure at 25 °C and 0.1 *m* NaCl as computed by the Duan et al. (2006) code, that works in the T-P-X range 273-533 K, 0-2000 bar, and 0-4.5 *m* NaCl.

Under these conditions, deviations from ideality are limited for gaseous CO_2 and P_{CO2} does not differ significantly from the CO_2 fugacity, f_{CO2} (e.g., Marini, 2006). In contrast, the CO_2 molality does not increase appreciably with P_{CO2}, for P_{CO2} values higher than ~50-60 bar, due to the strong deviation from ideality in the gas phase. Since doubling the P_{CO2} from 55 to 110 bar leads to an increase in m_{CO2} of 12% only, the carbonation effects on cement at 110 bar are expected to be relatively similar to those for a P_{CO2} of 55 bar. In contrast, since doubling the P_{CO2} from 25 to 50 bar causes an increase in m_{CO2} of 68%, the carbonation effects at 50 bar should be more pronounced than those for a P_{CO2} of 25 bar. Consequently, it is important to investigate cement carbonation up to 50-60 bar, which is the range adopted in this work. Although experimental studies of cement carbonation are usually performed by using massive samples (see above), apart from that in the present work we also carried out carbonation experiments on cement powder samples, which are generally used in laboratory experiments aimed at investigating the dissolution/precipitation kinetics of minerals and rocks (e.g., Marini, 2006).

3.2. Experimental methods

3.2.1. Preparation of the hydrated cement paste, types of experiments and experimental schedule

The hydrated cement was prepared, on December 23rd, 2015, by mixing 1 kg of class G Portland clinker and 0.5 kg of water (water/clinker weight ratio of 0.5), and stored after the hydration process in a glass container with an air-tight plastic lid. The chemical composition of the class G Portland clinker used for all the experiments carried out in this investigation is given in Table 3.1, together with its mineralogical composition obtained from normative calculations (Bogue, 1955).

Table 3.1. Chemical and mineralogical composition of class G Portland clinker used for all the experiments performed in this work.

Chemical composition			Mineralogical composition			
Oxide	Wt%	Mol%	Mineral	Formula	Wt%	Mol%
CaO	65.31	69.72	C3S	Ca_3SiO_5	62.11	59.05
SiO_2	22.45	22.37	C2S	Ca_2SiO_4	16.31	20.56
Al_2O_3	3.45	2.03	C3A	$Ca_3Al_2O_6$	1.80	1.45
Fe_2O_3	4.32	1.62	C4AF	$Ca_4Al_2Fe_2O_{10}$	12.90	5.76
SO_3	2.77	2.07	Gypsum	$CaSO_4 \cdot 2H_2O$	4.25	5.36
MgO	1.1	1.63	Periclase	MgO	1.08	5.81
Na_2O	0.15	0.14	Thenardite	Na_2SO_4	0.34	0.52
K_2O	0.66	0.42	Arcanite	K_2SO_4	1.20	1.49

After 28 days curing at atmospheric pressure and room temperature conditions, on January 21st, 2016, part of the cement paste was cut in cubes of ~1 cm each side, whereas the other part of the cement paste was grinded and sieved. The powder size between 63 and 125 μm was selected for carbonation experiments and to determine the specific surface area by using the BET method. The cement cubes and the cement powder were stored in two separate glass containers with plastic air-tight lids. All the carbonation experiments were performed reacting the hydrated cement samples (either powders or cubes) with pure CO_2(g) and MilliQ water at room temperature for selected time intervals in a 25-mL-capacity micro-reactor (manufactured by Parr Instrument Company) equipped with an automatic magnetic stirrer. Three types of experiments were carried out.

In the experiments of type 1, the cement powder was reacted for different reaction times of 1, 3, 6, 21, 67, 97 and 120 hours, in separate runs, maintaining constant the P_{CO2} at 11 bar. The experiments of type 1 were performed from January 21st to February 25th, 2016, that is from 1 to 36 days after the end of the curing period.

In the experiments of type 2, the cement powder samples were reacted, under different P_{CO2} of 1, 11, 31 and 51 bar, in separate runs, keeping constant the reaction time at 6 hours. In the experiments of type 3, cement cube samples were employed, the reaction time was set at 6, 24 and 210 hours, in separate runs, whereas the P_{CO2} was maintained constant at 11 bar. The experiments of type 2 and, subsequently, those of type 3 were carried out from July 19th to August 31st, 2016, that is from 181 to 224 days after the end of the curing period.

Although the hydrated cement, cement cubes and powder were stored in glass containers with plastic air-tight lids, the hydrated cement paste was affected by dehydration and, to a limited extent, by carbonation driven by absorption of atmospheric CO_2.

3.2.2. Determination of surface characteristics of the hydrated cement powder

The hydrated cement samples sieved at 63-125 micron were characterized through N_2 sorption and desorption at 77 K after degassing at 100°C for 24 hours using an automated analyzer ASAP 2010 Micromeritics. The Brunauer-Emmett-Teller (BET) specific surface area, the C parameter, as well as the volumes of micropores (diameter < 2 nm), mesopores (diameter of 2-50 nm) and macropores (diameter >50 nm) were obtained following the approach recommended by Sing et al. (1985).

3.2.3. Carbonation experiments of types 1 and 2 with hydrated cement powder

Before starting each carbonation experiment, the hydrated cement powder was heated for 2 hours at 40°C in an oven to eliminate excess moisture. For each experiment of types 1 and 2, the micro-reactor was charged with 1 g of cement powder and 15 mL of MilliQ water. The micro-reactor was initially flushed with pure CO_2(g) to get rid of atmospheric air before setting the P_{CO2} at the selected value (see above). During the experiment the solution was continuously stirred at ~1000 rounds per minute.

At the end of each experiment, the aqueous solution was collected from the micro-reactor, filtered through membranes of pore size either 0.45μm, for experiments of type 1, or 0.2 μm, for the experiments of type 2, and stored in two 25 mL flasks, one containing 1 mL of concentrated HCl (30-37 wt%). The reacted cement powder was also collected and dried for two hours into an oven at 40°C before storage.

The aqueous solution and the reacted cement powder were analyzed by using different methods (see below).

3.2.3.1. Analysis of the aqueous solutions

The aqueous solutions of types 1 and 2 experiments were analyzed by ion chromatography for relevant cations (Ca^{2+}, Mg^{2+}, K^{+}, Na^{+}) and anions (Cl^{-}, F^{-}, SO_4^{-}, and Br^{-}). Alkalinity (~ HCO_3^{-}) was measured by acidimetric titration using methylorange as indicator. Dissolved Si, Al and Fe were determined by ICP-OES. Since the micro-reactor is not equipped with a pH electrode and the aqueous solution undergoes strong CO_2 loss once the micro-reactor is opened, the in-situ pH was assumed to be fixed by P_{CO2} and alkalinity. Temperature, P_{CO2}, the total concentration of main solutes, and alkalinity were used as input data for speciation and saturation index calculations. These were carried out by using the EQ3/6 code version 8.0 (Wolery and Jarek, 2003) and its most recent thermodynamic database; *data0.ymp.R5* (Wolery and Jove-Colon, 2007), which was updated by adding the solubility data of vaterite (Plummer and Busenberg, 1982) and Amorphous Calcium Carbonate, ACC (Ogino et al., 1987; Clarkson et al., 1992).

3.2.3.2. Analysis of the solid phases

The mineral species present in the cement before and after the carbonation experiments were characterized by X-ray powder diffraction (XRD), scanning electron microscopy (SEM) as well as thermogravimetric analysis (TGA) and differential thermal analysis (DTA), which were carried out from 30 to 1000°C for all the samples. TGA and DTA curves comprise three distinct parts, representing different types of reaction: (i) dehydration of hydrated phases, chiefly CSH (although

capillary pore water, interlayer water and adsorbed water are also involved in these reactions), up to 350°C; (ii) dehydration of portlandite in the temperature range 350-550°C; (iii) decarbonation of $CaCO_3$, mainly calcite, from 550 to 1000°C.

Hence, the weight percentage of H_2O released from CSH dehydration, H_2O_{CSH},wt%, the weight percentage of H_2O released from portlandite dehydration, H_2O_{CH},wt%, and the weight percentage of CO_2 released from calcite decarbonation, CO_{2Cc},wt%, are obtained from the deconvolution of the TGA and DTA curves. The weight percentages of portlandite and calcite, CH,wt% and Cc,wt%, respectively, are then obtained by means of the simple relations:

$$CH, wt\% = H_2O_{CH}, wt\% \cdot \frac{MW_{CH}}{MW_{H_2O}} \tag{3.4}$$

$$Cc, wt\% = CO_{2Cc}, wt\% \cdot \frac{MW_{Cc}}{MW_{CO_2}} \tag{3.5}$$

where MW_{CH}, MW_{Cc}, MW_{H2O} and MW_{CO2} represent the molecular weights of portlandite, calcite, H_2O and CO_2, respectively. Due to the variable stoichiometry of CSH (see above), a relation similar to Equations (3.4) and (3.5) cannot be used to compute the weight percentage of CSH, CSH,wt%. Hence this parameter is computed assuming that it is the complement to 100 of CH,wt% + Cc,wt%, using the relation:

$$CSH, wt\% = 100 - CH, wt\% - Cc, wt\%. \tag{3.6}$$

This assumption is certainly wrong, due to the presence of solid phases other than CSH, portlandite, and calcite in the cement upon its hydration (e.g., ettringite and Ca-Al-Fe monosulfates) and carbonation (e.g., Al, Fe(III), and/or silica oxyhydroxides). However, the error is acceptable due to the small amounts of these accessory solid phases. Knowing CSH,wt%, its stoichiometry formula $Ca_xSiO_{2+x} \cdot xH_2O$ is computed by trial and error through the following steps: (1) adoption of a value for the x parameter, (2) computation of the molecular weight of CSH, MW_{CSH}, for the adopted x value, (3) calculation of CSH,wt% by means of the simple relations:

$$CSH, wt\% = H_2O_{CSH}, wt\% \cdot \frac{MW_{CSH}}{MW_{H_2O}}. \tag{3.7}$$

The procedure is repeated until the CSH,wt% value computed by Equation (3.7) is equal to that previously obtained by Equation (3.6). The final x value and the corresponding CSH stoichiometry are retained.

3.2.4. Carbonation experiments with cubic samples of hydrated cement

Before starting each carbonation experiment, the cubic sample was heated in an oven for five days at 40°C (to remove the water used during the cutting process) and weighted on an analytical balance. In each experiment the micro-reactor was charged with one cubic sample and 5.5 mL of MilliQ water. The micro-reactor was initially flushed with pure $CO_{2(g)}$ to get rid of atmospheric air before setting the P_{CO2} value at 11 bar. Note that the cubic sample within the micro-reactor is completely immersed in water and is covered by a ~0.25-mm-thick layer of water, separating the gas phase, above, from the cement cube, below (Figure 3.2). This thin water layer is crossed by a diffusive O_2 flux controlling cement carbonation.

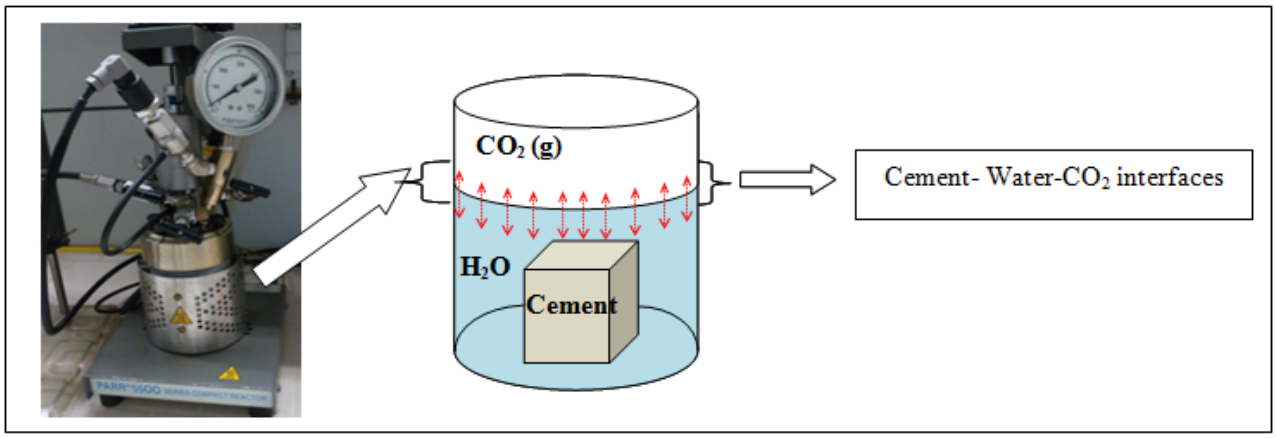

Figure 3.2. The Parr micro-reactor (left) and sketch showing the cement cube sample, water and CO_2 gas into the micro-reactor (right) during the carbonation experiments of cement cube samples.

At the end of each experiment, the cubic sample was heated in an oven at 40°C for 2 hours and weighted again on an analytical balance. The carbonation progress was assessed for each sample from: (1) the mass gain, that is the difference between the weight of the cement cube after and before the carbonation experiment, and (2) the carbonation depth, which was obtained by using the phenolphthalein method (according to the European Normative EN 14630:2006). It consists of cutting the cube perpendicular to the cement-water interface, keeping the same orientation as in the micro-reactor (Figure 3.2) and spraying a solution of phenolphthalein indicator onto the two surfaces resulting from the cut. The phenolphthalein solution is prepared dissolving 1 g of phenolphthalein in 70 mL ethyl alcohol and diluted to 100 mL with MilliQ water. The phenolphthalein indicator is colorless below pH 9 approximately and becomes red-purple above this pH value. Hence, a red-purple color is visible where the cement is not carbonated, whereas the cement has its typical grey color where it is affected by carbonation. The two zones are distinguished and the depth of the carbonated zone is measured.

3.3. Results

3.3.1. Results of the surface analysis for the hydrated cement powde samples.

The 63-125 µm fraction of the hydrated G class Portland cement powder were considered in this work, which experienced a 15.6% of water loss during the preliminary degassing at 100°C. Hence, all the obtained data are referred to the dry sample. The adsorption/desorption isotherms (Figure 3.3) show both the hysteresis loop (due to capillary condensation in mesopores) and the limiting uptake over a range of high relative pressures, which are typical of the Type IV class of Sing et al. (1985).

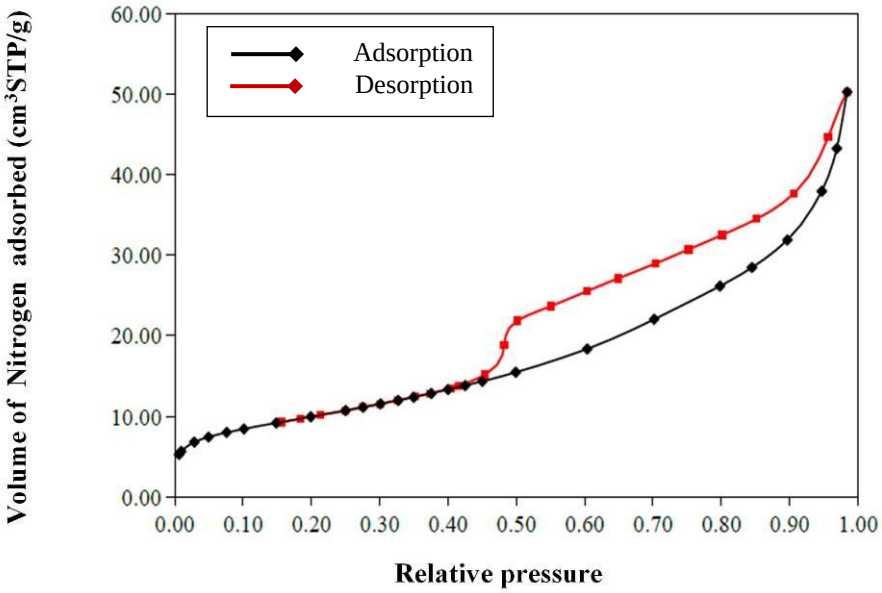

Figure 3.3. Adsorption/desorption isotherms for the 65-125 µm fraction of the hydrated G class Portland cement powder.

The initial part of this type of isotherm is attributed to monolayer-multilayer adsorption. The specific surface area obtained using the BET method is 35.7 m^2/g. The value of the C parameter, 114, suggests that monolayer-multilayer formation occurs and is not accompanied by micropore filling.

Porosity analysis indicates that: (i) the volume of micropores (pore size < 2 nm approximately) is < 0.01 cm^3/g, based on the t-plot method and (ii) the volume of mesopores (pore size 2-50 nm approximately) is 0.062 cm^3/g, based on the Barrett–Joyner–Halenda (BJH) method[2].

[2] The Barrett Joyner Halenda method is a procedure for calculating pore size distributions from experimental isotherms based on the Kelvin Equation for pore filling (Barrett, E.P., Joyner, L.G., & Halenda, P.P., 1951).

Adsorption/desorption hysteresis is of type H4 and is probably associated with narrow slit-like pores. The distribution curve of mesopore size shows maximum frequency close to 3.2 nm and maximum size of ~45 nm.

3.3.2. Results of carbonation experiments of types 1 and 2 with the hydrated cement powder

3.3.2.1. The solid phases in carbonation experiments of types 1 and 2

For the seven experiments of type 1, performed at P_{CO2} of 11 bar, XRD results (Figure 3.4a) reveals that portlandite is present in the initial hydrated cement powder (before the beginning of the run) whereas it is absent at the end of all the experiments, irrespective of their duration, either 1, 3, 6, 21, 67, 97 or 120 hours. Conversely, both calcite and vaterite are absent in the initial hydrated cement powder whereas they are both present at the end of all the runs, independent of the reaction time. Therefore, it seems likely that portlandite carbonation comes to completion, or nearly so, in less than 1 hour. The intensity of the calcite peaks increases gradually with the reaction time indicating the progressive increase in the mass of calcite produced through cement carbonation. The vaterite peaks are clearly recognizable, but their intensity does not change significantly with the experiment duration.

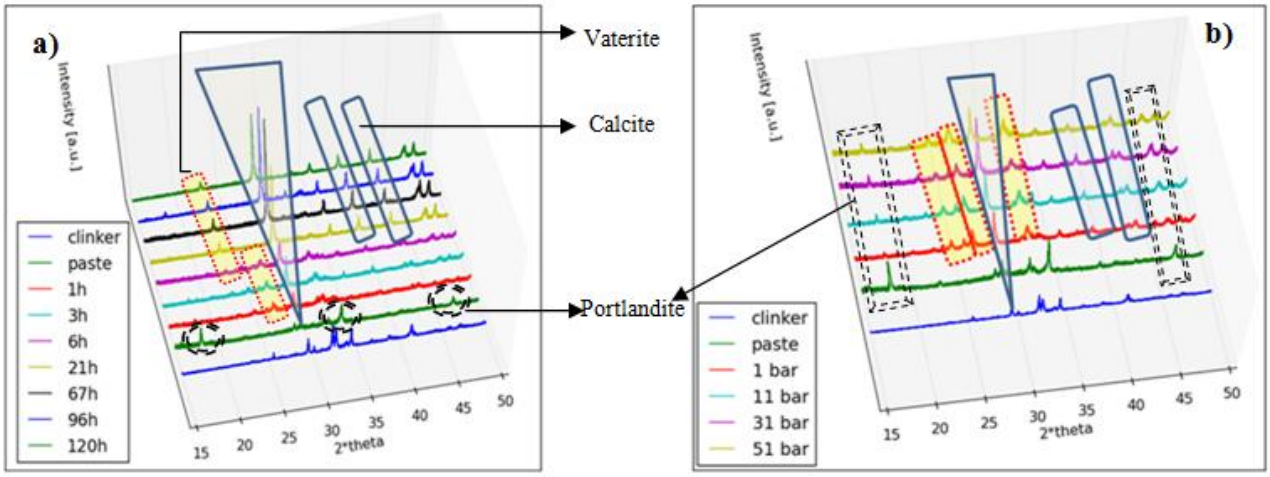

Figure 3.4. Diffractograms for (a) the seven experiments of type 1 at 11 bar P_{CO2} and different duration (as indicated), the clinker, and the initial hydrated cement paste and (b) the four experiments of type 2 performed at different P_{CO2} (as indicated), the clinker, and the initial hydrated cement paste. The first blue line and the second green line at the bottom of both diagrams are the clinker and the cement paste respectively.

For the four experiments of type 2, carried out at P_{CO2} of 1, 11, 31, and 51 bar and lasting 6 hours, XRD results (Figure 3.4b) show that portlandite is present not only in the initial hydrated cement powder but also at the end of the experimental runs, although in relatively small amounts. Comparatively small calcite and vaterite peaks are recognizable in the initial hydrated cement

indicating that both carbonate minerals are present, though in minor quantities. The height of the calcite peaks increases with P_{CO2} up to 31 bar, whereas shorter calcite peaks are observed at 51 bar. The height of vaterite peaks does not seem to change substantially with increasing P_{CO2}, although it is difficult to evaluate differences in vaterite peaks due to their comparatively small heights.

Typical rhombohedral calcite crystals are clearly evident in SEM images of carbonated samples (Figure 3.5), also showing less common spherical aggregates of small crystals, which are probably mixtures of vaterite and calcite.

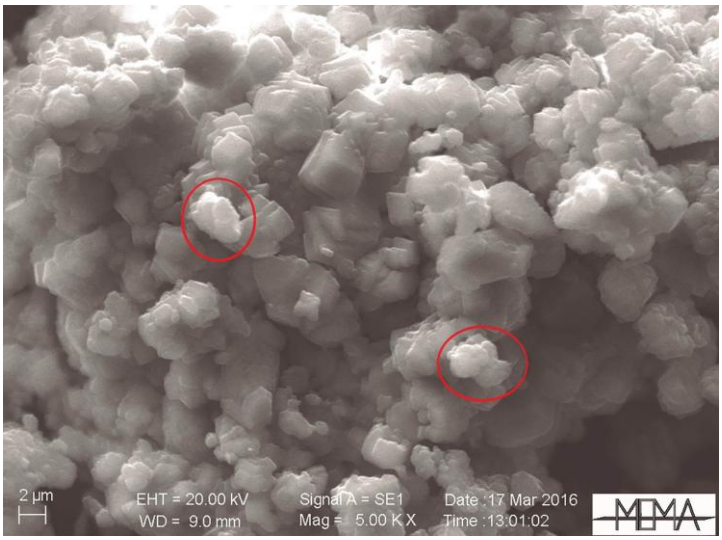

Figure 3.5. SEM image (secondary electrons) for the experiment of type 1 of 96 hours duration, showing both the typical rhombohedral calcite crystals and some spherical aggregates of small crystals (enclosed in the red ellipses), which are probably mixtures of vaterite and calcite.

The TGA/DTA results for the seven experiments of type 1 (Table 3.2) indicate that during cement carbonation at P_{CO2} of 11 bar and room temperature, the mass of calcite increases from the initial value of ~20 wt% in the hydrated cement to ~58 wt% in 3 hours, whereas the subsequent data (6-120 hours) show limited changes, with oscillations from ~56 to ~68 wt%. The mass of portlandite exhibits an opposite trend, with a marked decrease from the initial value of ~22 wt% in the hydrated cement to <1 wt% in 3 hours, whereas the following data experience relatively small variations from 0 to ~11 wt%. The mass of CSH decreases from the initial value of ~58 wt% in the hydrated cement to ~42 wt% in 3 hours, whereas the subsequent data vary from ~31 to ~40 wt%. The *x* value of CSH oscillates from 0.35 to 0.97, with corresponding changes in the molecular weight of CSH from 85.9 to 132.1 g/mol.

The TGA/DTA outcomes for the four experiments of type 2, carried out at P_{CO2} of 1, 11, 31, and 51 bar and lasting 6 hours, show very small differences, with mass of calcite ranging from 53.4 to 55.1

wt%, mass of portlandite varying from 10 to 14.1 wt% and mass of CSH oscillating from 32.5 to 34.9 wt%. However, these values are different from those of the initial hydrated cement, which comprises 75 wt% of CSH, 20 wt% of portlandite and 5 wt% of calcite. The *x* value of CSH in the carbonation experiments varies from 0.37 to 0.54, with corresponding changes in the molecular weight from 87.5 to 100.0 g/mol. However, the initial hydrated cement has a low *x* value of CSH, 0.29, and a correspondingly low molecular weight, 81.5 g/mol, due to occurrence of dehydration during storage.

Table 3.2. Results of TGA/DTA and related calculations (see section 3.2.3.2) for the initial hydrated cement, the seven experiments of type 1 and the four experiments of type 2: H_2O_{CSH},wt% is the weight percentage of H_2O released from dehydration of CSH; H_2O_{CH},wt%, is the weight percentage of H_2O released from dehydration of portlandite; CO_{2Cc},wt% is the weight percentage of CO_2 released from decarbonation of calcite; CSH,wt% is the weight percentage of CSH; CH,wt% is the weight percentage of portlandite; Cc,wt% is the weight percentage of calcite; *x* refers to the stoichiometry formula of CSH, $Ca_xSiO_{2+x} \cdot xH_2O$.

Exp. Type	Duration (h)	P_{CO2} (bar)	H_2O_{CSH},wt%	H_2O_{CH},wt%	CO_{2Cc},wt%	CH,wt%	Cc,wt%	CSH,wt%	*x*
-	0	-	10.63	5.38	8.57	22.1	19.5	58.4	0.53
1	1	11	6.98	2.66	19.89	10.9	45.2	43.8	0.72
1	3	11	5.67	0.19	25.35	0.8	57.7	41.6	0.97
1	6	11	5.5	0.14	26.19	0.6	59.6	39.9	0.95
1	21	11	4.51	2.55	25.56	10.5	58.1	31.4	0.88
1	67	11	6.92	0.01	29.06	0.0	66.1	33.9	0.38
1	96	11	7.67	1.88	24.49	7.7	55.7	36.6	0.35
1	120	11	5.15	0.01	29.72	0.0	67.6	32.4	0.72
-	0	-	16.58	4.88	2.18	20.1	5.0	75.0	0.29
2	6	1	6.29	2.43	24.22	10.0	55.1	34.9	0.54
2	6	11	6.55	3.26	23.81	13.4	54.1	32.4	0.39
2	6	31	6.33	3.28	24.08	13.5	54.8	31.7	0.41
2	6	51	6.7	3.42	23.49	14.1	53.4	32.5	0.37

3.3.2.2. The aqueous solution in the carbonation experiments of type 2.

Results for experiments of type 1 are not considered here due to their uncertainty interpretation, whereas the outcomes for all the chemical analyses of the aqueous solutions collected at the end of the four experiments of type 2 are presented in Table 3.3. These experiments, were carried out at P_{CO2} of 1, 11, 31, and 51 bar and resulted to have negative electrical charge unbalance of -6.2, -7.6, -17.7, and -1.7%, respectively. Alkalinity was therefore recomputed from the electrical charge balance in speciation-saturation calculations. These aqueous solutions are by far dominated by Ca and HCO_3. The pH decreases with increasing P_{CO2}, from 6.32 at 1 bar to 4.89 at 51 bar. Apart from

Amorphous Calcium Carbonate, ACC, for which oversaturation is recognized at all P_{CO2} values, the aqueous solutions of interest are oversaturated with carbonate minerals and ferrihydrite at low P_{CO2} values and undersaturated at high P_{CO2} values. The saturation conditions occur at ~26 bar for calcite, ~19 bar for aragonite, ~5 bar for vaterite, and ~28 bar for ferrihydrite. In principle, the saturation state with ferrihydrite and amorphous $Fe(OH)_3$ (for which speciation-saturation calculations predict undersaturation at all P_{CO2} values) is controlled not only by pH but also by the redox potential. In practice, since divalent Fe is unlikely to be present in the considered system, the redox potential was assumed to be fixed by equilibrium with atmospheric P_{O2}. Finally, ,the aqueous solution is at all the P_{CO2} values oversaturated with amorphous silica, which is expected to precipitate faster than other silica minerals, although SI-$SiO_{2,am}$ < SI-opal < SI-α-cristobalite < SI-chalcedony < SI-quartz.

Table 3.3. Chemical composition of the aqueous solutions at the end of the experiments of type 2 (duration 6 hours) performed at different P_{CO2} as indicated. Relevant results of speciation-saturation calculations are also shown. SI stands for saturation index.
(*) Analytical value; (**) Computed from the electrical charge balance.

P_{CO2}	Na	K	Mg	Ca	Alk(*)	Alk(**)	SO_4	F	Cl	Br
bar	mmol/kg				meq/kg		mmol/kg			
1	1.40	3.20	2.54	23.30	38.0	44.5	5.64	0.0661	0.407	0.0154
11	1.47	2.83	4.54	39.97	67.7	80.8	6.03	0.0846	0.339	0.0259
31	3.03	5.07	4.77	35.50	50.4	77.1	5.50	0.0788	0.401	0.0425
51	2.19	4.04	6.39	39.86	83.6	87.0	5.51	0.0852	0.592	0.0434

P_{CO2}	SiO_2	Fe	pH	Calcite	Aragonite	Vaterite	ACC	$SiO_{2,am}$	$Fe(OH)_{3,am}$	Ferrihydrite
bar	mmol/kg	µmol/kg		SI	SI	SI	SI	SI	SI	SI
1	2.35	0.139	6.32	0.857	0.713	0.291	-1.58	0.081	-0.878	1.08
11	2.71	0.133	5.51	0.420	0.276	-0.147	-2.02	0.143	-1.55	0.413
31	3.21	0.130	5.06	-0.095	-0.239	-0.661	-2.53	0.217	-2.01	-0.052
51	3.72	0.165	4.89	-0.187	-0.332	-0.754	-2.63	0.281	-2.10	-0.138

3.3.3. Results of the carbonation experiments of type 3 with cubic cement samples

3.3.3.1. Qualitative observations

Pores connected by a network of cracks as well as alteration rims around the pores are clearly recognizable, through simple macroscopic examination, on the surface of the massive, cubic-shaped samples reacted for 24 and 210 hours (Figure 3.6).

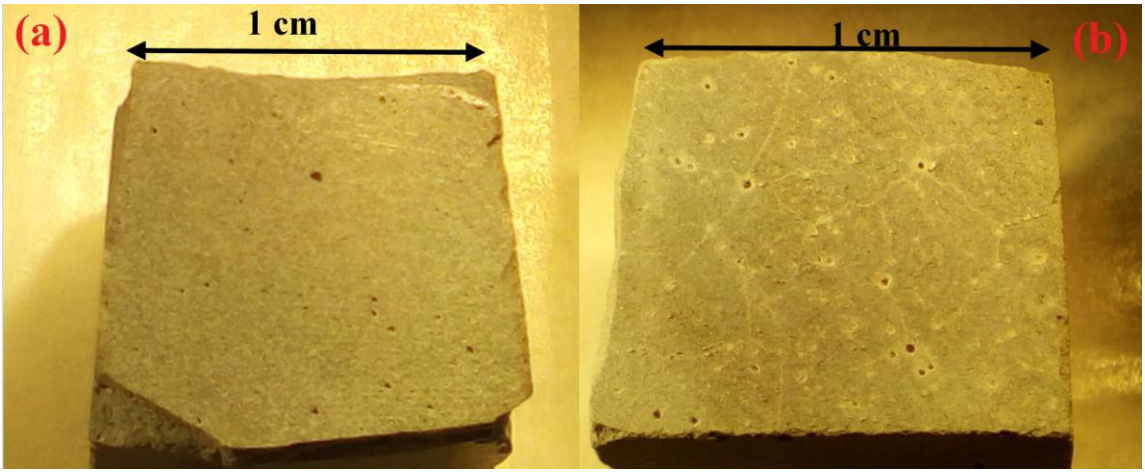

Figure 3.6. Different cubic cement samples, both carbonated at 11 bar P_{CO2} and room temperature (a) after 6 hours of reaction time, when some pores are observed, and (b) after 24 hours of carbonation, when both, cracks and more pores are observed.

Before the beginning of the carbonation experiments both types of features were not distinguishable neither by macroscopic analysis nor by use of the reflected light microscope. However, very small pores (10-100 µm in diameter) and rare tiny cracks were identifiable on SEM images. Tiny cracks are recognizable on the surface of the sample reacted for 6 hours by use of the reflected light microscope. Therefore, it can be concluded that cement alteration at 11 bar P_{CO2}, for reaction times of 24 and 210 hours, causes the formation of new pores and cracks and the enlargement of pre-existing features of these types, as well as the appearance of alteration rims around the pores. Cracks filled by carbonate minerals are present on the surface of the most carbonated sample, which was reacted for 210 hours (Figure 3.7). Minerals were identified as carbonates as they effervesce when treated with 10% HCl.

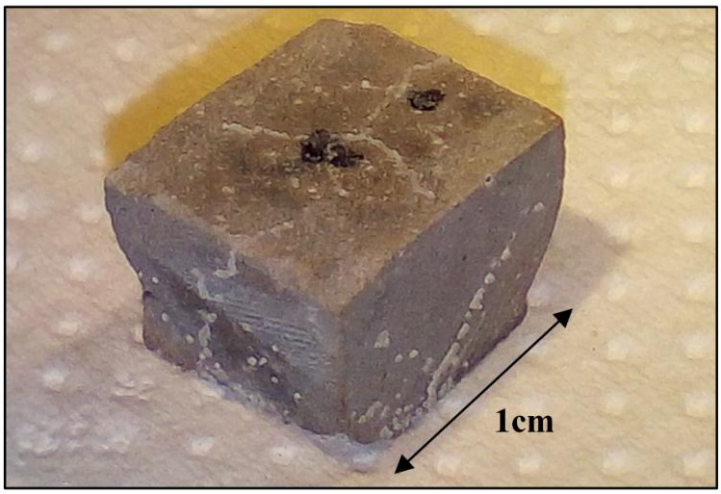

Figure 3.7. Carbonates material filling the cracks of carbonated cement samples after 210 hours at 11 bar of P_{CO2}.

3.3.3.2. Carbonation progress

The carbonation depth (phenolphthalein method) is recognizable in the three experiments performed at 11 bar P_{CO2} and room temperature (Figure 3.8). Precise measurements of the carbonation depth were carried out by using a reflected light microscope. Averaged results indicate an increasing carbonation progress with reaction time, especially between 24 and 210 hours, consistent with the mass gain (Table 3.4).

Table 3.4. Mass gain and carbonation depth (phenolphthalein method) for the cubic cement samples reacted at 11 bar P_{CO2} and room temperature in the experiments of type 3. The carbonation depth, *L*, is an average of several measurements on each sample.

Reaction time (hours)	Mass gain (%)	Carbonation depth, *L* (mm)
6	2.758	0.189
24	2.843	0.231
210	12.193	0.457

Figure 3.8. (below) Carbonation progress as indicated by the phenolphthalein method for reaction times of (A) 6 hours, (B) 24 hours and (C) 210 hours.

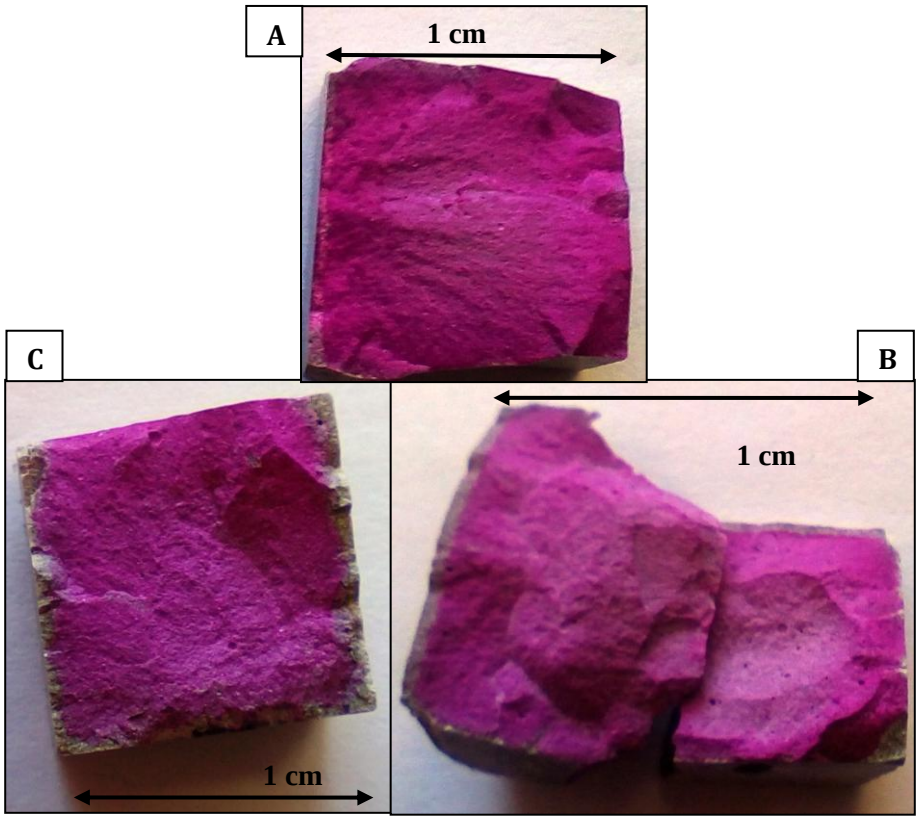

The obtained average value of the carbonation depth, L, for each cubic cement sample involved in experiments of type 3 are plotted against the square root of reaction time in days, t (Figure 3.9)

following the approach commonly used to interpret these data. This plot is used because a linear relation can be observed between L and $t^{1/2}$, that is:

$$L = \alpha \cdot t^{½}, \qquad (3.8)$$

if the rate of carbonation is controlled by Fick's second law of diffusion with a constant concentration boundary condition. In Equation (3.8), α is a constant related to the rate of diffusion of the ionic species through the cement frame that depends on the permeability, porosity, tortuosity, and chemical composition of the cement (e.g., Kutchko et al., 2008). Indeed, the rate of cement carbonation is expected to be limited by diffusion because the acid-base carbonation reactions proceed much faster than the diffusion of ionic species in the cement matrix (e.g., Kutchko et al., 2008 and references therein).

In the plot of carbonation depth against the square root of reaction time (Figure 3.9) the results obtained in this work for the cubic samples of class G Portland cement reacted in water at room temperature and 11 bar P_{CO2} distribute close to a linear trend, which is described by the following linear regression Equation (L in mm; t in day; $R^2 = 0.998$):

$$L = 0.111 \cdot t^{½} + 0.128. \qquad (3.9)$$

This suggests that the considered system has Fickian behavior and that the cement carbonation rate is controlled by diffusion.

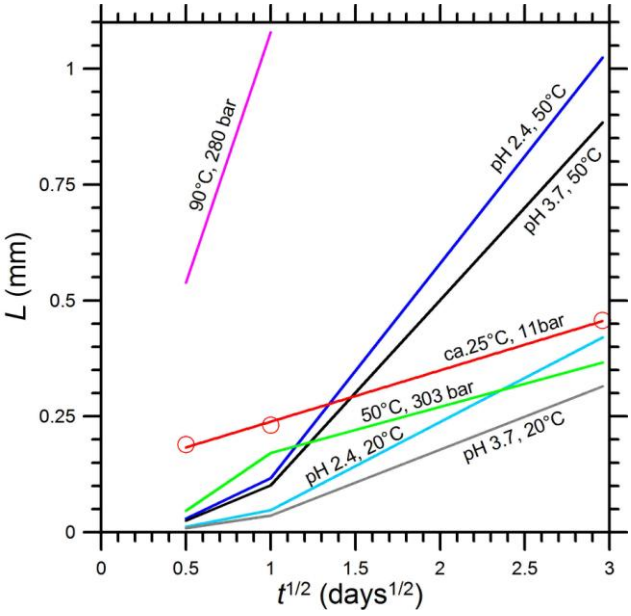

Figure 3.9. Plot of the carbonation depth vs. the square root of reaction time for the cubic samples of class G Portland cement reacted in water at room temperature and 11 bar P_{CO2} (this work, red circles and line). Also shown are the data obtained at different temperatures and pH or P_{CO2} values, as indicated, by Barlet-Gouedard et al. (2006, 2007; magenta line), Kutchko et al. (2008; green line) and Duguid and Scherer (2010); blue, black, sky blue and grey lines).

3.4. Discussion and conclusions

Pores and fractures - The slit-like mesopores highlighted by the surface analysis of the hydrated cement powder (see section 3.3.1) might play an important role in the carbonation of cement powder, assuming that these features were present also on the surface of the massive cubic cement samples. In fact, these relatively long cylindrical holes allow the deep penetration of the CO_2-rich aqueous phase and, consequently, determine the enlargement of pores, the appearance of alteration rims around the pores, and the formation of new pores and cracks, as observed in the experiments of type 3 (see section 3.3.3.1).

Portlandite - As consistently documented by both XRD and TGA/DTA results (see section 3.3.2.1), there was conflicting evidence on the fate of portlandite. In fact, portlandite disappeared completely in the seven carbonation experiments of type 1 at 11 bar P_{CO2}, irrespective of their duration, from 1 to 120 hours, whereas it was present, though in relatively small quantities, at the end of the 6-hours-long experimental runs of type 2, at 1 to 51 bar P_{CO2}. To explain these discrepancy, it must be recalled that the experiments of type 1 were performed 1 to 36 days after the end of the curing period, whereas the experiments of type 2 were carried out 181 to 224 days after the end of the curing period. This longer storage period preceding the type 2 experiments might have promoted the conversion of the outer parts of portlandite crystals into calcite (and vaterite) through absorption of atmospheric CO_2. If so, the armouring of portlandite crystals by $CaCO_3$ coatings would have prevented portlandite dissolution.

Calcite - In the seven carbonation experiments of type 1 at P_{CO2} of 11 bar, the intensity of the calcite peaks increased gradually with the reaction time, indicating a continuous progress of cement carbonation (see section 3.3.2.1). Similarly, the carbonation extent increased with reaction time in the three experiments carried out on massive cubic cement samples at 11 bar P_{CO2} and room temperature, as consistently indicated by the mass gain and carbonation depth (see section 3.3.3).

In the experimental runs of type 2, the height of the calcite peaks increased with P_{CO2} up to 31 bar, whereas shorter calcite peaks were recognizable at 51 bar P_{CO2}, suggesting that cement carbonation occurs up to 31 bar approximately, whereas decarbonation took place at higher P_{CO2} values. This finding agrees with the varying saturation index of calcite, which indicates attainment of saturation at ~26 bar P_{CO2}, oversaturation below this P_{CO2} value and undersaturation at higher P_{CO2} values (see section 3.3.2.2). The obvious implications is that calcite precipitation is thermodynamically possible below ~26 bar P_{CO2}, whereas calcite dissolution is thermodynamically possible above ~26 bar P_{CO2}.

These thermodynamic constraints have important implications also on the kinetics of cement carbonation (see below).

$CaCO_3$ polymorphs other than calcite - Several previous studies recognized that the formation of calcite in aqueous environments typically follows the Ostwald's step rule and often begins with the quick precipitation of amorphous calcium carbonate, ACC, from highly oversaturated solutions (Ogino et al., 1987; Clarkson et al., 1992; Kawano et al., 2002; Kitamura 2002; Kim et al., 2004; Andreassen, 2005) including lime pastes (Cizer et al., 2012). The ACC is transformed into a mixture of different crystalline $CaCO_3$ polymorphs within several minutes. Vaterite and calcite are formed at low temperatures, 14 to 30°C, aragonite and calcite at high temperature, 60 to 80°C, whereas all three polymorphs are produced at intermediate temperatures, 40 to 50°C. The metastable $CaCO_3$ polymorphs are transformed into stable calcite in ~200 min at 25°C. The polymorphic transformation of vaterite and aragonite to calcite occurs through dissolution of the metastable phase and growth of the stable phase, calcite. The rate-determining step of the transformation is the calcite growth. When the ion activity product of the initial supersaturated solution is lower than the solubility product of ACC at 25°C, only vaterite directly precipitates after some induction period.

Only vaterite and calcite were produced during our experiments whereas ACC and aragonite were not found (see section 3.3.2.2), probably due to undersaturation conditions and low experimental temperature, respectively. The height of XRD vaterite peaks did not seem to vary appreciably during the experiments of types 1 and 2, although it is difficult to appraise possible differences in vaterite peaks due to their relatively small heights (see section 3.3.2.1). Accepting that the vaterite mass did not change substantially during the experiments, it seems likely that vaterite was rapidly converted to calcite, due to coupled dissolution-precipitation. The occurrence of vaterite-calcite conversion is also indicate by SEM images of carbonated samples, showing the presence of spherical aggregates of small crystals, which are probably mixtures of vaterite and calcite, since vaterite often form polycrystalline spherulites (e.g., Ogino et al., 1987; Kawano et al., 2002; Andreassen, 2005; Nehrke, 2007).

Kinetics of cement carbonation - Let us now resume the examination of Figure 3.9, showing not only the data of this work but also the previous results obtained by other authors through carbonation experiments of Portland cement with CO_2-saturated water under different conditions, namely: (i) 90°C, 280 bar P_{CO2} (Barlet-Gouedard et al., 2006, 2007); (ii) 50°C, 303 bar (Kutchko et al., 2008); and (iii) pH 2.4, 50°C, pH 2.4, 20°C, pH 3.7, 50°C, and pH 3.7, 20°C (Duguid and

Scherer, 2010) at P_{CO2} close to 1 bar. Cement alteration experiments by supercritical CO_2 exposure are disregarded in this discussion. Incidentally, in contrast with our findings, Kutchko et al. (2008) observed a strong deviation from the Fickian behavior and used the Elovich Equation to model their kinetic data.

Since the available data on the rate of cement carbonation were obtained at different temperatures, they cannot be compared as such. In fact, reaction rate constants exhibit an exponential dependence on temperature, which is usually expressed by means of the Arrhenius Equation (Arrhenius, 1889). Assuming that the activation energy E_a is constant, the Arrhenius Equation can be simplified as follows for the purpose of this discussion:

$$\ln\left(\frac{dL}{dt}\right)_{298\&15} = \ln\left(\frac{dL}{dt}\right)_T + \frac{E_a}{R}\cdot\left(\frac{1}{T} - \frac{1}{298.15}\right), \qquad (3.10)$$

where R is the universal gas constant and T is the absolute temperature. Since the data of Duguid and Scherer (2010) refer to two distinct temperatures, 20 and 50°C, they were used to obtain the E_a/R term, which resulted to be 3036 K^{-1}. This value of the E_a/R term was then used to refer at 25°C (298.15 K) the carbonation depth rates determined at high temperatures.

The effect of CO_2 on the carbonation depth rates referred at 25°C can be investigated by means of the log-log plot of Figure 3.10, in which the carbonation depth rates for a reaction time of 1 day are plotted against the CO_2 partial pressure. As expected, the carbonation depth rate determined at 11 bar P_{CO2} in this work is about one order of magnitude higher than the two rates measured by Duguid and Scherer (2010) at P_{CO2} close to 1 bar. Considering only the rates determined by Duguid and Scherer (2010) and in this work, and assuming that there is a linear relation between the carbonation depth rate and P_{CO2}, the following Equation (carbonation depth rate in mm/day; P_{CO2} in bar; R^2 =0.997) is obtained:

$$\frac{dL}{dt} = 0.0189\cdot P_{CO_2} + 0.0231. \qquad (3.11)$$

Equation (3.11) is expected to hold true up to ~30 bar P_{CO2}, since the reverse (decarbonation) reaction is expected to occur at higher P_{CO2} values based on the indications obtained in this work (see above). Therefore, it does not come as a surprise that the carbonation depth rates measured by Barlet-Gouedard et al. (2006, 2007) at 280 bar P_{CO2} and by Kutchko et al. (2008) at 303 bar P_{CO2} are orders of magnitude lower than those predicted by Equation (3.11). In fact, in these high-P_{CO2} experiments, different reaction zones were observed, including a porous silica-rich zone dominated by dissolution (e.g., Kutchko et al., 2007).

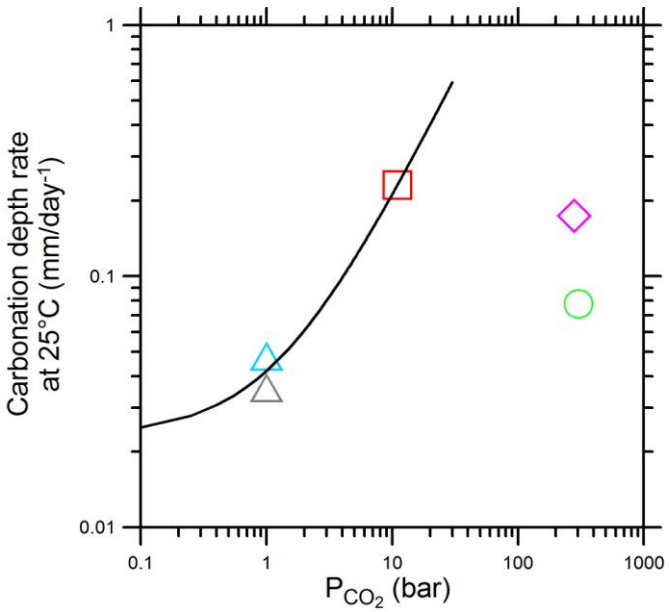

Figure 3.10. Log-log plot of the carbonation depth rate (for a reaction time of 1 day) vs. the CO_2 partial pressure showing the data obtained in this work for the cubic samples of class G Portland cement reacted in water at room temperature and 11 bar P_{CO2} as well as the data from previous studies (Kutchko et al. (2008); Barlet-Gouedard et al. (2006, 2007); Kutchko et al. (2008); Duguid and Scherer (2010) referred at the temperature of 25°C. Colours of symbols are the same as in Figure 3.9.

Acknowledgements

This research was supported by the CO_2 REACT Marie Curie Initial Training network. We are indebted to all the people who helped out to carry out the analytical work, namely: Marco Agnelli, Daniele Borrini, Francesco Capecchiacci, Jacopo Cabassi, Fabio Marmottini, Mario Paolieri, Elena Pecchione, Franco Tassi, Maurizio Ulivi, and Stefania Venturi.

References.

Andreassen, J.P. (2005). Formation mechanism and morphology in precipitation of vaterite—nano-aggregation or crystal growth? Journal of crystal growth, 274(1), 256-264.

Arrhenius, S. (1889). Ober die reacktionsgeschwindigkeit bei der inversion von rohrzucker durch sauren. Z. Physik. Chem., 4, 226-248.

Barlet-Gouédard, V., Rimmelé, G., Goffé, B., Porcherie, O. (2006). Mitigation strategies for the risk of CO_2 migration through wellbores. In: IADC/SPE 98924, IADC/SPE Drilling Conference, Miami, FL, U.S.A., February 21-23, 2006.

Barlet-Gouédard, V., Rimmelé, G., Goffé, B., Porcherie, O. (2007). Well technologies for CO_2 geological storage: CO_2-resistant cement. Oil & Gas Science and Technology-Rev IFP, 62 (3), 1-12.

Barlet-Gouédard, V., Rimmelé, G., Porcherie, O., Quisel, N., Desroches, J. (2009). A solution against well cement degradation under CO_2 geological storage environment. International Journal of Greenhouse Gas Control, 3 (2), 206-216.

Barrett, E.P., Joyner, L.G., & Halenda, P.P. (1951). The determination of pore volume and area distributions in porous substances. I. Computations from nitrogen isotherms. Journal of the American Chemical society, 73(1), 373-380.

Bogue R.H. (1955) Chemistry of Portland Cement. 2nd Edition. Reinhold, New York, NY, USA, 793 pp.

Carey, J.W., Svec, R., Grigg, R., Zhang, J., Crow, W. (2010) Experimental investigation of wellbore integrity and CO_2-brine flow along the casing-cement microannulus. International Journal of Greenhouse Gas Control, 4 (2), 272-282.

Chen J.J., Thomas J.J., Taylor H.F.W., Jennings H.M. (2004). Solubility and structure of calcium silicate hydrate. Cem. Concr. Res., 34,1499-1519.

Cizer, Ö., Rodriguez-Navarro, C., Ruiz-Agudo, E., Elsen, J., Van Gemert, D., Van Balen, K. (2012). Phase and morphology evolution of calcium carbonate precipitated by carbonation of hydrated lime. Journal of Materials Science, 47(16), 6151-6165.

Clarkson, J.R., Price, T.J., Adams, C.J. (1992). Role of metastable phases in the spontaneous precipitation of calcium carbonate. Journal of the Chemical Society, Faraday Transactions, 88(2), 243-249.

Duan, Z., Sun, R., Zhu, C., Chou, I.M. (2006). An improved model for the calculation of CO_2 solubility in aqueous solutions containing Na^+, K^+, Ca^{2+}, Mg^{2+}, Cl^-, and SO_4^{2-}. Marine Chemistry, 98(2), 131-139.

Duguid, A. (2008). An estimate of the time to degrade the cement sheath in a well exposed to carbonated brine. In: Proceedings of the 9th Annual Conference on Greenhouse Gas Control Technologies, Washington, DC, U.S.A., November 16-20.

Duguid, A. & Scherer, G.W. (2010). Degradation of oilwell cement due to exposure to carbonated brine. International Journal of Greenhouse Gas Control, 4 (3), 546-560.

Duguid, A., Radonjic, M., Bruant, R., Mandecki, T., Scherer, G., Celia, M. (2004). The effect of CO_2 sequestration on oil well cements. In: Proceedings of the 7th Annual Conference on Greenhouse Gas Control Technologies, Vancouver, Canada, September 5-9.

Duguid, A., Radonjic, M., Scherer, G. (2005). Degradation of well cement exposed to carbonated brine. In: Proceedings of the 4th Annual Conference on Carbon Capture and Sequestration, Alexandria, VA, U.S.A., May 2–5.

Kawano, J., Shimobayashi, N., Kitamura, M., Shinoda, K., Aikawa, N. (2002). Formation process of calcium carbonate from highly supersaturated solution. Journal of crystal growth, 237, 419-423.

Kim, W.S., Hirasawa, I., Kim, W.S. (2004). Polymorphic change of calcium carbonate during reaction crystallization in a batch reactor. Industrial & engineering chemistry research, 43(11), 2650-2657.

Kitamura, M. (2002). Controlling factor of polymorphism in crystallization process. Journal of Crystal Growth, 237, 2205-2214.

Kutchko, B.G., Strazisar, B.R., Dzomback, D.A., Lowry, G.W., Thaulow, N. (2007). Degradation of well cement by CO_2 under geologic sequestration conditions. Environmental Science & Technology, 41 (12), 4787-4792.

Kutchko, B.G., Strazisar, B.R., Lowry, G.V., Dzombak, D.A., Thaulow, N. (2008). Rate of CO_2 attack on hydrated Class H well cement under geologic sequestration conditions. Environmental Science & Technology, 42, 6237-6242.

Kutchko, B.G., Strazisar, B.R., Huerta, N., Lowry, G.V., Dzombak, D.A., Thaulow, N. (2009). CO_2 reaction with hydrated Class H well cement under geologic sequestration conditions: effects of fly ash admixtures. Environmental Science & Technology, 43, 3947-3952.

Marini, L. (2006). Geological Sequestration of Carbon Dioxide - Thermodynamics, Kinetics, and Reaction Path Modeling. Developments in Geochemistry, 11, 453 pp.

Nelson, E.B & Guillot, D. (2006). Well Cementing, 2nd ed. Schlumberger, Sugar Land, TX, U.S.A.

Nehrke, G. (2007). Calcite precipitation from aqueous solution: transformation from vaterite and role of solution stoichiometry. Geologica Ultraiectina, Vol. 273. Utrecht University, 133 pp.

Neville, A.M. (1995). Properties of Concrete, 4th ed. Pearson Education Limited, Essex, England.

Ogino, T., Suzuki, T., Sawada, K. (1987). The formation and transformation mechanism of calcium carbonate in water. Geochimica et Cosmochimica Acta, 51(10), 2757-2767.

Papadakis, V.G., Vayenas, C.G., Fardis, M.N. (1989). A reaction engineering approach to the problem of concrete carbonation. AIChE Journal 35 (10), 1639-1650.

Plummer, L.N.& Busenberg, E. (1982). The solubilities of calcite, aragonite and vaterite in CO_2-H_2O solutions between 0 and 90°C, and an evaluation of the aqueous model for the system $CaCO_3$-CO_2-H2O. Geochimica et Cosmochimica Acta, 46(6), 1011-1040.

Pratt, A., Talman, S., Zhang, M., Thibeau, Y. (2009). Characterization of Portland cement reacted with supercritical CO_2. In: Present at the 8th Annual Conference on Carbon Capture and Sequestration, Pittsburgh, PA, U.S.A., May 4-7, 2009.

Reardon, E.J., James, B.R., Abouchar, J. (1989). High pressure carbonation of cementitious grout. Cement & Concrete Research, 19, 385-399.

Richardson, M.G. (1988). Carbonation of Reinforced Concrete: Its Causes and Management. Citis Ltd., Dublin, London and New York

Santra, A. & Sweatman, R. (2010). Chemical and mechanical integrity of cement under CCS environment. In: Present at the 9th Annual Conference on Carbon Capture and Sequestration, Pittsburgh, PA, U.S.A., May 10-13, 2010.

Sing, K.S.W., Everett, D.H., Haul, R.A.W., Moscou, L., Pierotti, R.A, Rouquerol, J., Siemieniewska, T., (1985). Reporting physisorption data for gas/solid systems with special reference to the determination of surface area and porosity (Recommendations 1984). Pure and applied chemistry, 57(4), 603-619.

Sweatman, R.E., Santra, A.K., Kulakofsky, D. S., Calvert, D.G. (2009). Effective zonal isolation for CO2 sequestration wells. In: SPE Paper 126226, SPE International Conference on CO_2 Capture, Storage, and Utilization, San Diego, CA, U.S.A., November 2-4, 2009.

Taylor, H.F.W. (1997). Cement Chemistry, 2nd ed. Academic Press, New York. ISBN: 0-7277-2592-0.

Wigand, M., Kaszuba, J.P., Carey, J.W., Hollis, W.K. (2009). Geochemical effects of CO_2 sequestration on fractured wellbore cement at the cement/caprock interface. Chemical Geology, 265 (1-2), 122-133.

Wolery, T.W. & Jarek, R.L. (2003) Software user's manual. EQ3/6, Version 8.0. Sandia National Laboratories, U.S. Dept. of Energy Report.

Wolery, T.J &. Jove-Colon, C.F. (2007) Qualification of thermodynamic data for geochemical modeling of mineral-water interactions in dilute systems. Sandia National Laboratories Report ANL-WIS-GS-000003 REV 01.

Chapter 4- OCCURRENCE OF A NEARLY CONSTANT AIR FLUX THROUGH THE ACCUMULATION CHAMBER DURING CO_2 FLUX MEASUREMENTS. EVIDENCE FROM LABORATORY EXPERIMENTS AND CONSEQUENCES.

Abstract

Different types of laboratory experiments were carried out during this study. In particular, in type A experiments a standard gas mixture was continuously injected, at constant flux, into the accumulation chamber, mimicking the soil CO_2 flux measurements performed in field surveys. In type B experiments, a standard gas mixture was initially injected into the accumulation chamber for a short lapse of time, to achieve a relatively high CO_2 concentration inside the accumulation chamber; then the injection of the standard gas mixture was stopped and the CO_2 concentration inside the chamber was monitored for a sufficient interval of time. In both types of experiments, the accumulation chamber appears to be flushed by a considerable flux of atmospheric air, which is virtually constant in each experiment but is different from experiment to experiment. The type C experiments, which are a modified version of those of type B, including the use of a plaster to seal the chamber-desk interface, to verify the absence of gas leakage in the system.

We underscore that the occurrence of this air flux through the accumulation chamber (i) has no effect on the determination of the soil CO_2 flux on the basis of the initial slope (at time zero) of the CO_2 concentration-time curve, but (ii) it complicates the evaluation of the two components of the soil CO_2 flux, namely the CO_2 molar fraction of soil gas and the flux of the soil gas mixture.

Atmospheric air enters and leaves the accumulation chamber chiefly through the interface between the chamber rim and the surface onto which the chamber rests whereas the pressure compensation device is considered a less likely pathway for atmospheric air.

The air flux appears to be controlled by the membrane pump flowrate in type B experiments, in which there was only a gas flow driven by the membrane pump, from the accumulation chamber to the CO_2 analyzer and back again into the chamber, whereas no gas flow entered the chamber from below.

In type A experiments, there was both a gas flow entering the chamber from below and a gas flow driven by the membrane pump. Consequently, the gas exchanges between the chamber and the atmosphere are probably more complex than in the experiments of type B, leading to a relation

between the air flux and the gas flow entering the chamber from below, when it is relatively high (1.67 to 6.67 $cm^3\ s^{-1}$).

A possible way to obtain the two components of the soil CO_2 flux is presented although it must be improved. The implications related to the knowledge of both the CO_2 molar fraction of soil gas and the flux of the soil gas mixture are discussed.

Keywords: carbon dioxide; flux; soil gas; degassing; accumulation chamber; geological carbon storage.

4.1. Introduction

Since the early 1990's, the soil CO_2 flux, F_{CO_2}, has been measured, mapped, and monitored in several sites worldwide for geothermal exploration, volcanic surveillance, surface monitoring of CO_2 geological sequestration sites and other geo-scientific purposes (e.g., Baubron et al., 1990, 1991; Allard et al., 1991; Chiodini et al., 1998, 2001, 2007, 2008; Hernández et al., 1998, 2001; Carapezza and Federico, 2000; Lewicki and Brantley, 2000; Werner et al., 2014; Bergfeld et al., 2001; Brombach et al, 2001; Salazar et al., 2001; Carapezza and Granieri, 2004; Frondini et al., 2004, 2009; Notsu et al., 2005; Fridriksson et al., 2006; Werner and Cardellini, 2006; Padrón et al., 2008a; Carapezza et al., 2009; Evans et al. 2009; Toutain et al., 2009; Mazot et al., 2011; Rissmann et al., 2012; Parks et al., 2013; Dionis et al., 2015; Hutchison et al., 2015; Jolie et al., 2015; Lee et al., 2016; Robertson et al., 2016). These F_{CO_2} studies have been performed adopting the accumulation chamber method, where an inverted chamber is positioned on the ground, the CO_2 concentration inside the chamber is monitored, and the initial slope (at time zero) of the CO_2 concentration-time curve is used to compute the F_{CO_2} (Chiodini et al., 1998).

The method has some limitations and uncertainties. For instance, the F_{CO_2} from soil is affected by changes in atmospheric pressure and other meteorological parameters, such as soil temperature and moisture, wind speed, and rain (e.g., Edwards, 1975; Hanson et al., 1993; Chiodini et al., 1998; Rogie et al., 2001; Salazar et al., 2001; Granieri et al., 2003, 2010; Brusca et al, 2004; Lewicki et al, 2007; Padrón et al., 2008b; Viveiros et al., 2008, 2009; Perez et al., 2012; Lewicki and Hilley, 2014; Padilla et al., 2014; Werner et al., 2014). Consequently, surveys of F_{CO_2} from soil have to be carried out under dry and stable weather conditions to avoid the detrimental effects caused by variations of meteorological parameters.

The use of the accumulation chamber may change the soil gas flow from its natural undisturbed state by altering the gas pressure inside the chamber, varying the pressure and concentration gradients in the underlying soil, diverting the soil gas flow around the chamber, altering locally soil physical properties (e.g., by inserting a "collar" into the soil to position the chamber), and determining an increase of water vapor within the chamber (Norman et al., 1992; Healy et al., 1996; Evans et al. 2001; Gerlach et al. 2001; Welles et al. 2001). These effects have been quantified through controlled laboratory tests, showing that measured F_{CO_2} values are 0–25% lower than the imposed F_{CO_2} values, in the range 200 - 12,000 g m^{-2} day^{-1} (Evans et al. 2001). However, these uncertainties can be mitigated imposing known F_{CO_2} values and calibrating the system accordingly (Chiodini et al., 1998).

All in all, taking suitable precautions and accepting some minor uncertainties, the accumulation chamber method can be effectively used to determine the soil F_{CO_2} values from 0.2 to over 10,000 g m^{-2} day^{-1}, i.e., from the low values sustained by decay of organic substances to the high values of steaming grounds (Chiodini et al., 1998), as also supported by the results of comparative studies (e.g., Norman et al., 1992, 1997; Lewicki et al., 2005; Lewicki and Hilley, 2014).

In spite of the impressive number of studies carried out in the last 25 years, the behaviour of the accumulation chamber has not been fully understood yet and the potentialities of the accumulation chamber method have not been fully exploited yet. For instance, the accumulation chamber CO_2 time series can be used, in principle, to obtain not only the F_{CO_2} value but also its two components, namely the CO_2 molar fraction of soil gas, $X_{CO_2,G}$, and the flux of the soil gas mixture, F_G. Note that only two of the three variables F_{CO_2}, F_G, and $X_{CO_2,G}$ are independent, as they are linked by the simple relation:

$$F_{CO_2} = F_G \cdot X_{CO_2,G}. \qquad (4.1)$$

This study intends to discuss (1) the results of suitable laboratory experiments aimed at improving the understanding of the behaviour of the accumulation chamber, (2) a possible way to obtain the two components of F_{CO_2}, i.e., F_G and $X_{CO_2,G}$, from the CO_2 time series acquired by means of the accumulation chamber method, and (3) the implications related to the knowledge of the two components of F_{CO_2}.

4.2. Methods

4.2.1. The laboratory experiments

In this work, all the laboratory experiments were performed using West Systems portable CO_2 fluxmeters comprising the following main components (Figure 4.1):

(a) A West Systems™ accumulation chamber of type A, equipped with both a 80 rpm fan, to ensure the homogenization of the gas mixture inside the chamber, and a pressure compensation device, to maintain pressure equilibrium between inside the chamber and the surrounding air outside the chamber, avoiding the pressurization of the chamber that would alter the gas flow from soil (see above).

(b) A non dispersive infrared spectrometer as CO_2 analyzer, either a LICOR LI-820™ or a Vaisala CARBOCAP® CO_2 sensor GMP343. The CO_2 analyzer performs the continuous determination of CO_2 concentration inside the accumulation chamber. The main technical specifications of the LICOR LI-820™ are: measurement range 0-20,000 ppmv; root mean square noise <1 ppmv at 370 ppmv with 1 s signal filtering; accuracy 3% of reading. The main technical specifications of the Vaisala GMP343™ are: measurement range 0-20,000 ppmv; noise at 370 ppm CO_2 ± 3 ppmv CO_2; accuracy ± (5 ppmv + 2% of reading).

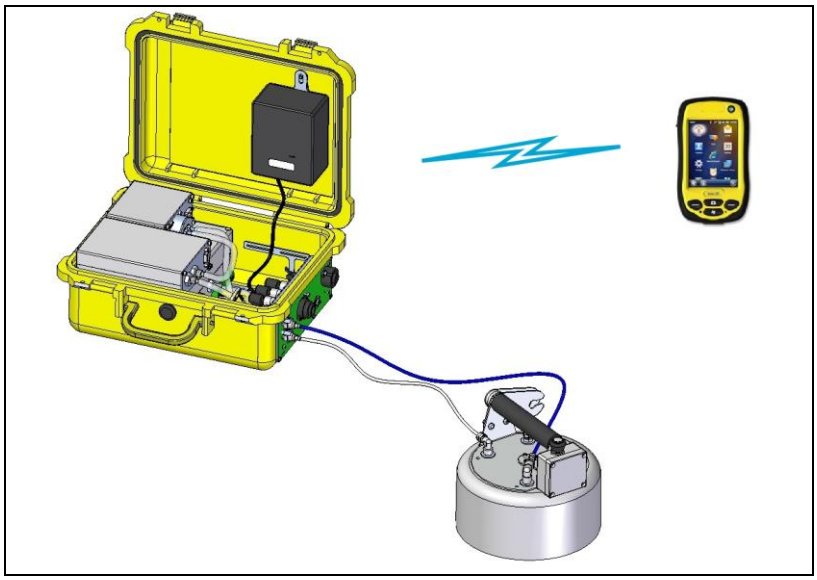

Figure 4.1. The West Systems portable CO_2 flux meter (from the Handbook of the West Systems CO_2 fluxmeter).

(c) A membrane pump ensuring the continuous transfer of the gas from the accumulation chamber to the CO_2 analyzer and back again into the chamber through the inlet and outlet tubes. The used fluxmeters were equipped with one of the following three pumps KNF NMP830, KNF NF30, and KNF NMS020. The flowrate of each pump was measured with an accuracy close to 1% by using a

Gilian Gilibrator-2 NIOSH Primary Standard Air Flow Calibrator, obtaining the following values: 47.5 cm^3 s^{-1} for KNF NMP830, 35.5 cm^3 s^{-1} for KNF NF30, and 24.2 cm^3 s^{-1} for KNF NMS020.

(d) A palmtop computer for data acquisition with the frequency of one record per second. Acquired data include: time, CO_2 concentration, pressure and temperature in the measuring cell of the CO_2 analyzer, ambient temperature and barometric pressure. The palmtop communicates with the CO_2 analyzer through either a wired or a wireless connection.

Further details are given by the handbook of the West Systems CO_2 fluxmeter which can be downloaded through the link http://www.westsystems.com/doc/HandBook_LI820_7_0.pdf. The flux meter, comprising the accumulation chamber, the inlet and outlet tubes, the cell of the CO_2 analyzer and filters, has a net total volume of 3063 cm^3, whereas the accumulation chamber has a basal area of 314 cm^2.

In the adopted experimental set up (Figure 4.2), the accumulation chamber is positioned with the open side over a desk, either inserting its rim into a collar, to minimize the possible input of atmospheric air (see below), or without any collar. The desk is equipped with a gas injection point which conveys the standard gas mixture, at the selected flux, from the cylinder to the accumulation chamber. The gas flux is controlled by using an electronically stabilized mass flow controller Alicat Scientific MC-2LPM-D™ with accuracy ± 0.2% of full scale, working range from 0.17 to 33.33 cm^3 s^{-1} and repeatability ± 0.2 %. The used gas mixtures have the following compositions (percentages by volume): (a) 2 % CO_2, 1% CH_4, 97% N_2; (b) 9 % CO_2, 91% N_2 and (c) 50 % CO_2, 50 % CH_4.

Three types of experiments were performed, called A, B, and C. In type A experiments, the standard gas mixture was continuously injected into the accumulation chamber keeping the gas flux constant at the selected value. These experiments mimic the F_{CO_2} measurements performed in field surveys. In type B experiments: (1) first, the standard gas mixture was injected into the accumulation chamber for a short interval of time, typically 100-120 s, to achieve a CO_2 concentration inside the accumulation chamber of ~7000 ppmv; (2) second, the injection of the standard gas mixture is stopped and the CO_2 concentration inside the chamber is monitored for a long interval of time, typically 1900-2100 s. These experiments are used to understand if the accumulation chamber is flushed or not by atmospheric air and to quantify the air flux if any. The type C experiments are similar to those of type B. The only difference is the use of plaster to seal both the chamber - desk interface and the pressure compensation device. These experiments are utilized to verify the absence of gas leaks in the whole system.

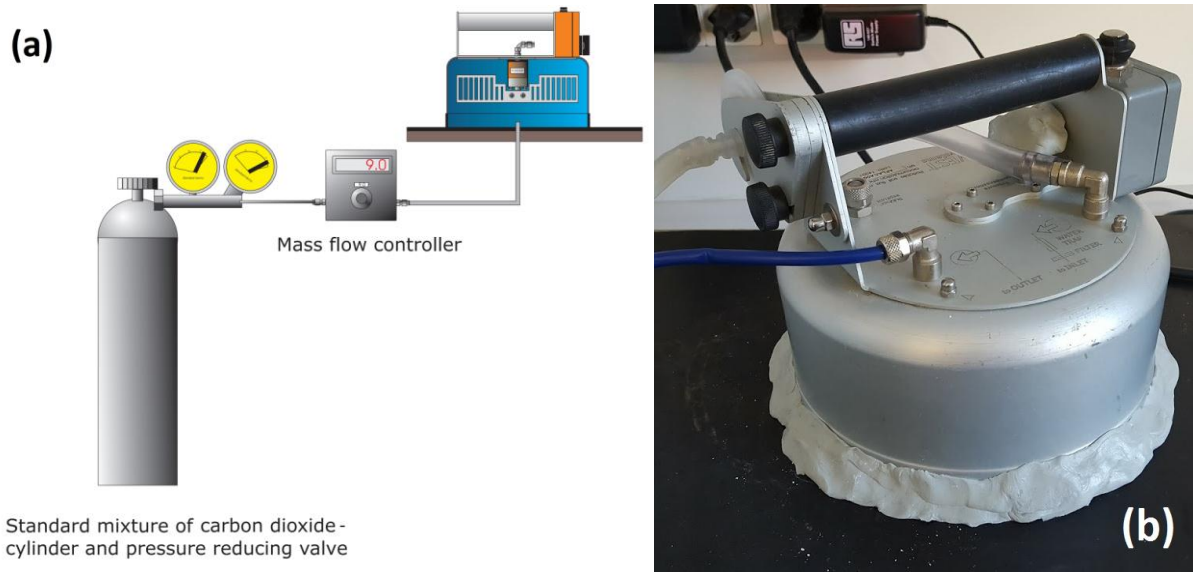

Figure 4.2. (a) Experimental set up for experiments of type A and B, adopted in the West Systems laboratory (from the Handbook of the West Systems CO_2 fluxmeter, modified). Note that the accumulation chamber is positioned on the desk over the gas injection point either with the collar or without it. (b) Accumulation chamber during the experiments of type C, in which plaster was used to seal both the chamber - desk interface and the pressure compensation device.

4.2.2. Methods of interpretation of CO_2 time series

To interpret the CO_2 time series acquired during the different types of laboratory experiments of all types, the accumulation chamber is assumed to behave as a perfectly-mixed single box model. Two different mass balance approaches can be used, as detailed below. In this work, simple mass balances involving the total soil-chamber-atmosphere CO_2 mass exchanges are preferred to Equations in which the diffusive and advective components of the soil gas flux are considered separately (e.g., Welles et al., 2001) due to the ambiguities in the characterization and separation of these two distinct components.

Approach (1) is based on the hypothesis that the accumulation chamber is not flushed by atmospheric air. It means that the flux of the standard gas mixture entering the accumulation chamber is balanced, at any time, by the flux of gas mixture leaving it through either the space between the chamber rim and the desk or the security valve or both. This hypothesis was adopted by Chiodini et al. (1998).

Approach (2) is based on the assumption that the gas mixture leaving the accumulation chamber comprises the standard gas mixture flux plus a flux of atmospheric air. In other terms, the accumulation chamber is considered to be flushed not only by a continuous flux of the standard gas

mixture but also by a continuous flux of atmospheric air. The need to invoke this second approach will become apparent in the following discussion.

4.2.2.1. Methods of interpretation of CO_2 time series: Approach (1)

The CO_2 time series in approach (1) is described by the following Equation[3] :

$$X_{CO_2,t+dt} \cdot V = X_{CO_2,t} \cdot V + X_{CO_2,G} \cdot F_G \cdot dt - X_{CO_2,t} \cdot F_{out} \cdot dt \qquad (4.2)$$

where:

t (s) stands for time,

V (cm^3) is the volume of the flux meter comprising the accumulation chamber, the inlet and outlet tubes, the cell of the CO_2 analyzer and the filters,

$X_{CO_2,t+dt}$ and $X_{CO_2,t}$ (mol/mol) designate the CO_2 molar fraction in the accumulation chamber at time $t+dt$ and at time t, respectively,

$X_{CO_2,G}$ (mol/mol) represents the CO_2 molar fraction of the standard gas mixture,

F_G and F_{out} ($cm^3\ s^{-1}$) stand for the flow rates of the standard gas mixture entering and leaving the accumulation chamber, respectively, which are assumed to be equal, that is:

$$F_G = F_{out}. \qquad (4.3)$$

Dividing both sides of Equation (4.2) by V and considering that $X_{CO_2,t+dt} - X_{CO_2,t} = dX_{CO_2}$, Equation (4.2) can be rearranged as follows:

$$\frac{dX_{CO_2}}{dt} = \frac{F_G \cdot X_{CO_2,G}}{V} - \frac{F_G}{V} X_{CO_2,t}. \qquad (4.4)$$

Note that in the plot of dX_{CO_2}/dt vs. X_{CO_2}, Equation (4.4) defines a straight line of slope $-F_G/V$ and intercept $F_G \cdot X_{CO_2,G}/V$.

4.2.2.2. Methods of interpretation of CO2 time series: Approach (2)

The main difference with respect to the previous approach is that in this case, the air entrance is taken into consideration. Therefore, Equation (4.2) has to be modified as follows:

[3] Note that Equation (4.2) corresponds to Equation (3) of Chiodini et al. (1998), although CO_2 fluxes are expressed in $cm^3\ s^{-1}$ in this work and in $cm^3\ s^{-1}\ cm^{-2}$ (or $cm\ s^{-1}$) in Chiodini et al. (1998). The conversion factor is the basal area of the accumulation chamber, 314 cm^2. The $cm^3\ s^{-1}$ was adopted as measurement unit of the gas flow because the section related through the flux of atmospheric air flushing the system is unknown (see below).

$$X_{CO_2,t+dt} \cdot V = X_{CO_2,t} \cdot V + X_{CO_2,G} \cdot F_G \cdot dt + X_{CO_2,A} \cdot F_A \cdot dt - X_{CO_2,t} \cdot (F_G + F_A) \cdot dt \quad (4.5)$$

where

$X_{CO_2,A}$ (mol/mol) represents the CO_2 molar fraction of atmospheric air,

F_A ($cm^3\ s^{-1}$) is the flow rate of atmospheric air entering the accumulation chamber.

Equation (4.5) assumes that, at any time, the sum of the standard gas mixture flux and atmospheric air flux is equal to gas flux leaving the accumulation chamber. Again, dividing both sides of Equation (4.5) by V and considering that $X_{CO_2,t+dt} - X_{CO_2,t} = dX_{CO_2}$, the final Equation is rewritten as follows:

$$\frac{dX_{CO_2}}{dt} = \frac{F_G \cdot X_{CO_2,G} + F_A \cdot X_{CO_2,A}}{V} - \frac{F_G + F_A}{V} X_{CO_2,t} \cdot \quad (4.6)$$

In the plot of dX_{CO_2}/dt vs. X_{CO_2}, Equation (4.6) defines a straight line of slope $-(F_G + F_A)/V$ and intercept $(F_G \cdot X_{CO_2,G} + F_A \cdot X_{CO_2,A})/V$. This plot is used to compute F_G and $X_{CO_2,G}$, as discussed in section 4.4.1.

4.3. Results.

Considering that in both types of experiments A and B, the accumulation chamber seems to be flushed by an atmospheric air flux but it does not occur for experiments of type C (due to the use of a plaster to seal the chamber-desk interface) we consider to report first the outcomes of experiments of type C and then the others.

4.3.1. The type C experiments

For all the type C experiments, the CO_2 concentration-time curve includes:

(1) a quick build up determined by the input of CO_2 into the accumulation chamber, followed by

(2) a flat part due to the almost constant CO_2 content upon ending the CO_2 input into the accumulation chamber (Figure 4.3).

Since plaster is not totally impermeable to gases, the CO_2 concentration-time curve deviates from the ideal condition of constant CO_2 content in the chamber, upon discontinuance of the CO_2 input into it. The decrease in CO_2 concentration with time, although very small, depends on the flowrate of the membrane pumps, F_P, with values of

(a) $-1.1 \cdot 10^{-7}$ to $-2.6 \cdot 10^{-7}$ s^{-1} for runs 2 and 4, in which a membrane pump with flowrate of 24.2 $cm^3\ s^{-1}$ was deployed, and

(b) $-3.4 \cdot 10^{-7}$ to $-5.0 \cdot 10^{-7}$ s^{-1} for runs 1 and 3, in which a membrane pump with flowrate of 47.5 $cm^3\ s^{-1}$ was used.

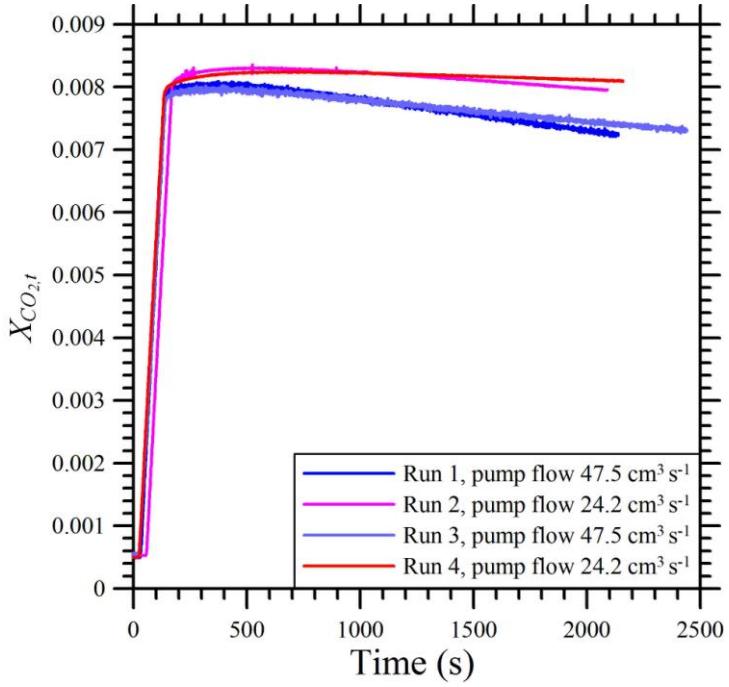

Figure 4.3. Plot of the measured CO_2 concentration inside the accumulation chamber versus time for four experiments of type C, in which plaster was used to seal both the chamber - desk interface and the pressure compensation device.

The average difference between the atmospheric pressure and the pressure in the cell of the LICOR LI-820™ CO_2 analyzer, ΔP^*, was 43.4 mbar in run 1, 19.2 mbar in run 2, 43.9 mbar in run 3 and 18.9 mbar in run 4.

4.3.2. The type B experiments

The CO_2 concentration-time curve of all the type B experiments comprises (1) a fast build up caused by the injection of CO_2 into the accumulation chamber, followed by (2) a relatively slow drawdown, upon cessation of the CO_2 injection into the accumulation chamber (Figure 4.4). The buildup curve does not give any information of interest. In contrast, the form of the drawdown curve, with a negative slope decreasing with time, suggests that the accumulation chamber is continuously flushed by atmospheric air. In fact, in the absence of such atmospheric air flush, the CO_2 concentration inside the accumulation chamber would be expected to remain constant or nearly so at the maximum value achieved due to CO_2 injection into the chamber, as it is observed in the experiments of type C (see section 4.3.1).

In addition to this important qualitative information on the behavior of the accumulation chamber, the drawdown curve was used to evaluate the flux of atmospheric air flushing the chamber assuming that it is constant and adopting the trial and error method. The sought solution

corresponds to the minimum of the average absolute deviation (AAD) between measured $X_{CO_2,t}$ values and corresponding $X_{CO_2,t}$ values computed by means of Equation (4.5).

Both the measured CO_2 concentrations and the corresponding calculated CO_2 values are plotted against time for the two experimental runs of type B 152131 and 161126 in Figure 4.4. Run 152131 (Figure 4.4a) was performed inserting the rim of the accumulation chamber into a collar, to minimize the input of atmospheric air, whereas run 161126 (Figure 4.4b) was carried out placing the accumulation chamber directly on the desk over the gas injection point without using any collar.

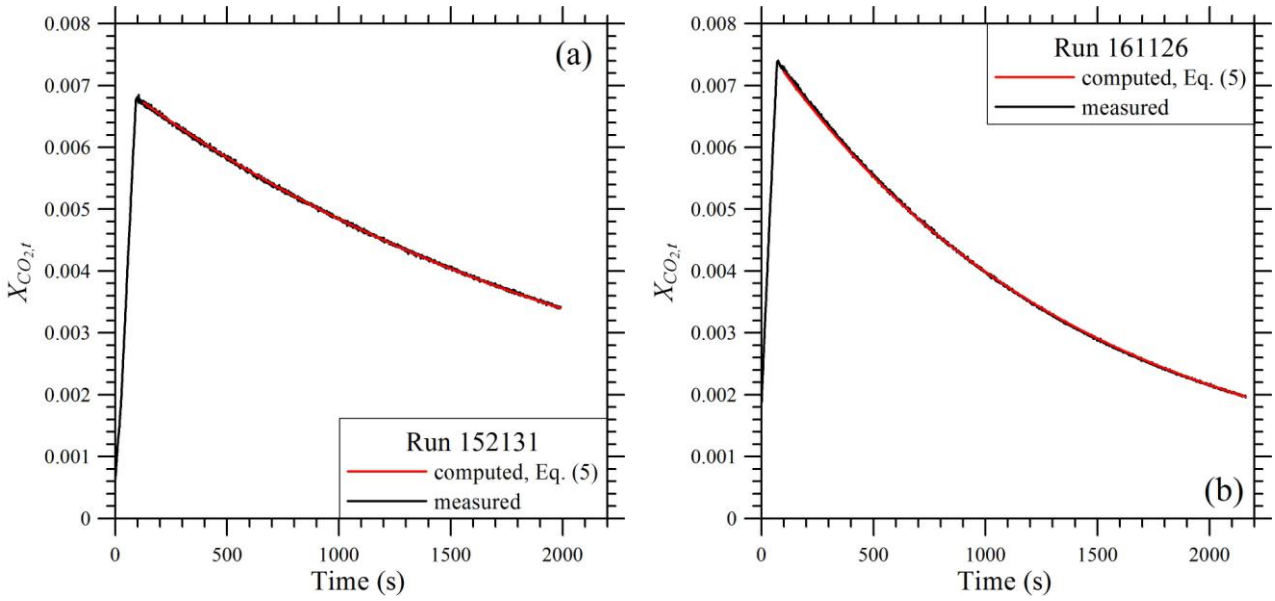

Figure 4.4. Plot of the measured and computed CO_2 concentration inside the accumulation chamber versus time for two experimental runs of type B 152131 and 161126. Run 152131 (a) was performed inserting the rim of the accumulation chamber into a collar whereas run 161126 (b) was carried out placing the accumulation chamber directly on the desk over the gas injection point without any collar.

For both runs there is a perfect match between the measured drawdown curve and the calculated counterpart, with an AAD of 0.26% and a maximum absolute deviation (MAD) of 1.2% in the run with the collar and with an AAD of 0.38% and a MAD of 1.5%, in the run without the collar. The main results of the experimental runs of type B, including those depicted in Figure 4.4, are reported in Table 4.1, showing that there is a very good correspondence between the measured drawdown curves and the calculated counterparts, with AAD values of 0.14 to 1.54%. Since that the $X_{CO_2,t}$ values computed using Equation (4.5) reproduce with acceptable accuracy the corresponding measured $X_{CO_2,t}$ values, the starting hypothesis is satisfied, i.e., the flux of atmospheric air flushing the accumulation chamber during the experiments of type B can be considered to be virtually constant.

Table 4.1 also shows that F_A represents 1.4 to 2.8 % of F_P in the experiments with the collar, whereas F_A constitutes 2.2 to 4.7 % of F_P in most experimental runs without the collar, apart from run 144401, with F_A equal to 1.4% of F_P, and run 122850, with F_A equal to 6.6% of F_P. The lower F_A/F_P ratios of the experiments with the collar are not surprising, since the collar acts as a partial seal, reducing the flow of air entering the accumulation chamber.

Table 4.1. Main characteristics of some experimental runs of type B. The experiments with the code in bold are displayed in Figure 4.4.

Code	F_P ($cm^3\ s^{-1}$)	F_A ($cm^3\ s^{-1}$)	**Collar**	**Duration** (s)	**AAD (%)**	**100·(F_A/F_P)** in (%)
152131	47.5	1.310	Yes	1991	0.26	2.8
105250	47.5	0.768	Yes	2369	0.75	1.6
115215	24.2	0.381	Yes	2064	0.30	1.6
145200	47.5	1.030	Yes	2508	0.69	2.2
153741	24.2	0.581	Yes	2355	0.65	2.4
95957	35.5	0.482	Yes	2623	0.14	1.4
113154	35.5	0.958	Yes	2247	0.99	2.7
140400	35.5	0.982	Yes	2278	0.80	2.8
161126	47.5	2.210	No	2161	0.38	4.7
122850	47.5	3.130	No	2352	1.54	6.6
141406	24.2	0.789	No	2173	0.49	3.3
164527	47.5	1.270	No	2832	1.12	2.7
173700	24.2	1.010	No	1518	0.78	4.2
105130	35.5	0.927	No	2249	1.15	2.6
121233	35.5	0.789	No	2106	1.07	2.2
144401	35.5	0.513	No	2333	0.78	1.4

4.3.3. The X_{CO_2} - time curve of type A experiments

Plots of CO_2 concentration versus time are shown for the four selected experiments of type A No. 103212 (Figure 4.5a), 154723 (Figure 4.5b), 112311 (Figure 4.5c), and 141306 (Figure 4.5d), all with F_G in the range 1.67 to 6.67 $cm^3\ s^{-1}$. In these plots, the measured CO_2 time series (black line) are compared with the corresponding CO_2 time series calculated using: (i) Equation (4.2), i.e., assuming that the accumulation chamber is not flushed by atmospheric air (blue curve) and (ii) Equation (4.5), i.e., assuming that the accumulation chamber is flushed by a constant flux of atmospheric air (red curve). Again, since the flux of atmospheric air through the chamber was unknown, this was obtained by the trial and error method until the AAD between measured and computed data attains the minimum value. These CO_2-time plots show that the data calculated using Equation (4.2) overestimate significantly the measured CO_2 time series, whereas the data computed

using Equation (4.5) closely approximate the measured CO_2 time series. Note that the agreement between the measured data and those computed for a constant flux of atmospheric air is very good for the three type A experiments 103212, 154723, and 112311, of duration ranging betwen ~600 and ~1800 s (Figure 4.5a, b, and c, respectively). In contrast, the agreement between the measured data and those computed for a constant flux of atmospheric air is less satisfactory for the type A experiment 141306 of longer duration, ~7000 s (Figure 4.5d).

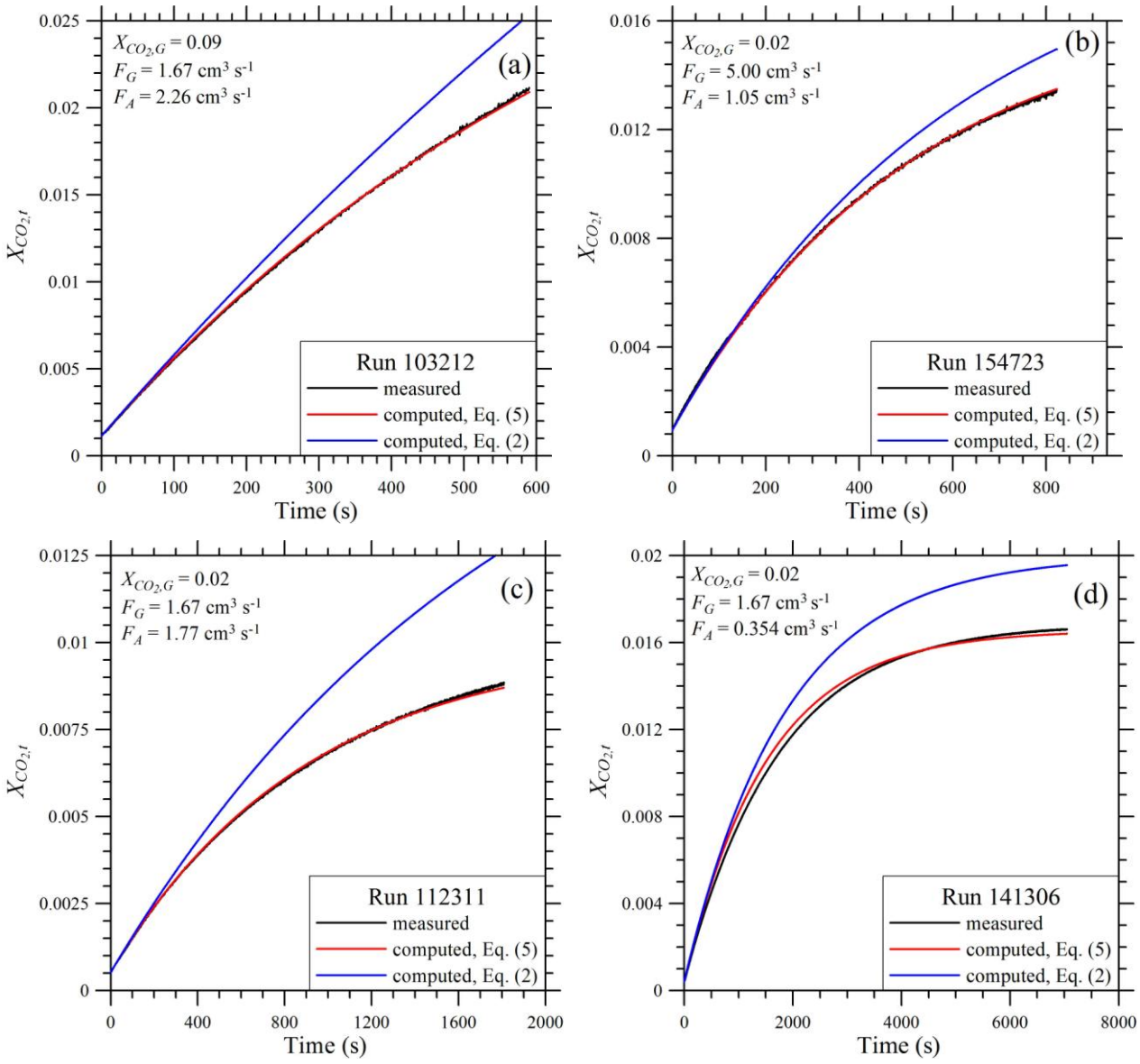

Figure 4.5. Plot of CO_2 concentration in the accumulation chamber versus time for four selected experiments of type A showing the measured CO_2 time series (black line), the CO_2 time series calculated using Equation (4.2), i.e., assuming that the accumulation chamber is not flushed by atmospheric air (blue curve), and the CO_2 time series calculated using Equation (4.5), i.e., assuming that the accumulation chamber is flushed by a constant flux of atmospheric air (red curve).

For this experimental run, the appearance of a crossover between the measured data line and the computed curve (for a constant flux of atmospheric air) might be due to the moderate decrease of the atmospheric air flux with time, an effect which is evidently detectable only in experiments of long duration at these F_G values.

The main characteristics of some experimental runs of type A, with F_G in the range 1.67 to 6.67 cm^3 s^{-1}, including those displayed in Figure 4.5, are reported in Table 4.2, showing that: (i) the AAD between measured and computed data is low, varying between 0.64 and 3.37%; (ii) F_A decrease progressively with increasing F_G (Figure 4.6), apart from the long-duration experiment 141306, and (iii) consequently, the $F_A/(F_A+F_G)$ ratio decreases gradually from 0.52-0.60 at F_G of 1.67 cm^3 s^{-1} to 0.08 at F_G of 6.67 cm^3 s^{-1}.

Table 4.2. Main characteristics of some experimental runs of type A with F_G of 1.67-6.67 cm^3 s^{-1}. The experiments with code in bold are displayed in Figure 4.5.

Code	X_{CO_2}	F_G (cm^3 s^{-1})	F_A (cm^3 s^{-1})	**Collar**	**Duration** (s)	**AAD** (%)	$F_A/(F_A+F_G)$ in %
103212	0.09	1.67	2.26	Yes	590	0.84	0.58
141142	0.09	1.67	2.20	No	560	1.54	0.57
112311	0.02	1.67	1.77	Yes	1809	0.64	0.52
104636	0.09	1.67	2.54	Yes	714	2.37	0.60
141306	0.02	1.67	0.354	Yes	7049	2.69	0.18
113108	0.02	3.33	1.25	No	1481	2.14	0.27
154723	0.02	5.00	1.05	No	822	1.09	0.17
155254	0.09	5.00	1.00	No	160	1.82	0.17
121322	0.02	6.67	0.550	Yes	1982	3.37	0.08

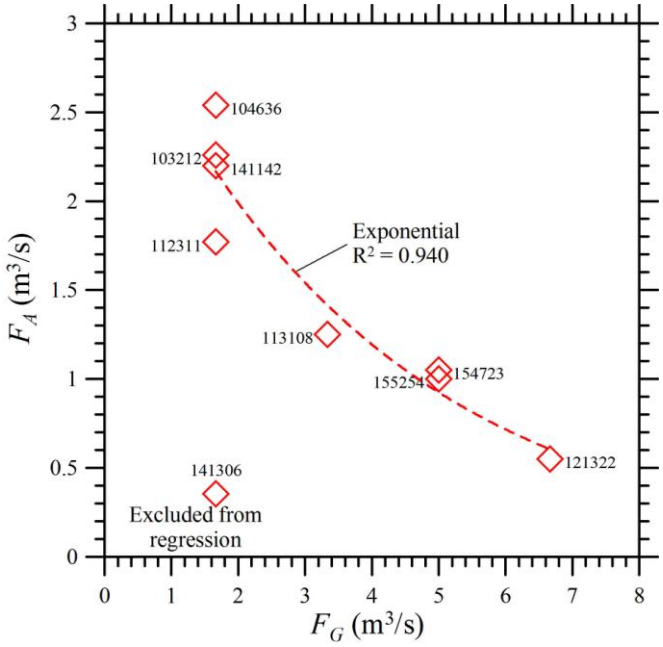

Figure 4.6. Plot of F_A vs. F_G for some experiments of type A, with F_G in the range 1.67 to 6.67 cm^3 s^{-1}. The exponential model was adopted to fit the F_A and F_G values since the squared regression coefficients is higher than for other models.

Type A experiments with F_G in the range 0.0833 to 0.833 cm^3 s^{-1} have higher AAD between measured and computed data, exhibit a crossover between the measured data line and the computed curve (for a constant flux of atmospheric air), have high F_A values, in the range 5 to 10 cm^3 s^{-1}, and, therefore, high $F_A/(F_A+F_G)$ ratios, from 0.85 to 0.99. Since the results for the type A experiments with F_G in the range 0.0833 to 0.833 cm^3 s^{-1} are affected by relatively high uncertainties, whose origins are not properly understood, they are not considered in the following discussion.

4.4. Discussion and conclusions

In all the laboratory experiments carried out during this work, of both type B and type A, with F_G in the range 1.67 to 6.67 cm^3 s^{-1}, the accumulation chamber appears to be flushed by a considerable flux of atmospheric air. F_A is virtually constant in each type B experiment as well as in each type A experiment of duration lower than 1800-2000 s, but F_A is different from experiment to experiment.

The occurrence of this considerable air flux through the chamber raises some questions, the first and most important is **does this air flux affect the determination of the F_{CO_2} from soil?** To answer this question, it must be noted that Equation (4.6), which incorporates the air flux through the chamber, reduces to;

$$F_{CO_2} = \frac{dX_{CO_2}}{dt} \cdot V \qquad (4.7)$$

at the initial conditions, i.e., at time zero. Equation (4.7) corresponds to Equation (7) of Chiodini et al. (1998) which is used to evaluate the F_{CO_2} from soil on the basis of the initial slope (at time zero) of the CO_2 concentration-time curve. The only difference between these two equations is the physical dimension (and consequently the measurement unit) of F_{CO_2}, which is [volume · time^{-1} · area^{-1}] in Chiodini et al. (1998) and [volume · time^{-1}] in this work. Leaving aside this difference, the important thing to be noted is that F_A does not appear in Equation (4.7) and, therefore, the flux of air through the accumulation chamber has no effect on the determination of the F_{CO_2} from soil.

A second question is **which are the entry and exit points through which air enters and leaves the chamber?** Before answering this question it must be recalled that maintenance of pressure equilibrium between inside the chamber and the surrounding air outside the chamber is a necessary requirement so that the measured F_{CO_2} and its two component terms (F_G and $X_{CO_2,G}$) can be truly representative of the natural values (e.g., Xu et al., 2006). For this reason, the chamber is equipped with a pressure compensation device. For the same reason, an effective seal cannot be emplaced between the chamber and either the soil surface in field deployment or the desk surface in laboratory tests[4]. Only a collar can be used to minimize the inflow of atmospheric air during the measurements, as done in some experiments of type A and B (see above). Therefore, it can be assumed that atmospheric air may enter and leave the accumulation chamber through both the interface between the chamber rim and the surface onto which the chamber rests and the pressure compensation device. The second pathway is considered less likely than the first one unless the pressure inside the chamber attains a value significantly higher than the external atmospheric pressure.

A third question is **what controls F_A?** To answer this question let us consider the plot of F_A vs. F_P for the type B experiments (Figure 4.7), in which there was only a gas flow driven by the membrane pump, from the accumulation chamber to the CO_2 analyzer and back again into the chamber, whereas no gas flow entered the chamber from below. Figure 4.7 shows that the spread of points is limited for the type B experiments with the collar, whose F_A and F_P data fit the following linear regression Equation through the origin ($R^2 = 0.944$):

$$F_A = 0.0219 \cdot F_P. \qquad (4.8).$$

[4] The only exception is represented by the experiments of type C, whose purpose is to verify the absence of gas leaks in the system.

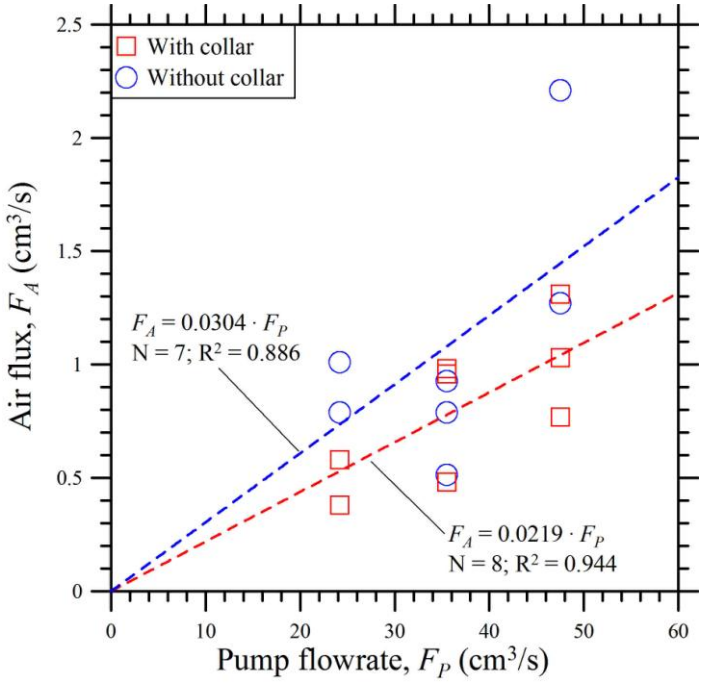

Figure 4.7. Plot of the the air flux, F_A, vs. the membrane pump flowrate, F_P for the experiments of type B with the collar and without it (see legend). Experiment 122850 is not plotted due to its high F_A, 3.13 cm^3 s^{-1}, and its high AAD, 1.54% (Table 1).

In contrast, the type B experiments without the collar show a remarkable spread of points, also considering that experiment 122850 was not plotted in Figure 4.7 due to the high F_A, 3.13 cm^3 s^{-1}, and the high AAD, 1.54% (Table 4.1). The F_A and F_P values for the type B experiments without the collar fit the following linear regression Equation through the origin (R^2 = 0.886)

$$F_A = 0.0304 \cdot F_P \qquad (4.9)$$

Equation (4.8) has a slope lower than that of Equation (4.9) since the collar acts to some extent as a seal, reducing the flux of air through the chamber, as already noted above. The notable spread of points and the comparatively low squared regression coefficient, are probably due to the variable section, from one experiment to another, through which air enters the chamber, reflecting the irregularities of the desk surface onto which the chamber is positioned. In contrast, the use of the collar seems to decrease the variability of the section through which air entered the chamber. Irrespective of the somewhat erratic results of the experimental runs without the collar, there is no doubt that the membrane pump flowrate, F_P, controls the air flux, F_A, in all the type B experiments.

In type A experiments with F_G in the range 1.67 to 6.67 cm^3 s^{-1} and duration lower than 1800-2000 s, F_A appears to be strictly related to F_G as already recalled above (Figure 4.6). It must be noted that in type A experiments there was both a gas flow entering the chamber from below and a gas flow driven by the membrane pump. Consequently, the gas exchanges between the chamber and the

atmosphere are probably more complex than in the the experiments of type B. In spite of these complexities, in type A experiments, F_A is neither a random effect nor a noise, but it was due to the unavoidable gas exchanges between the chamber and the atmosphere. These gas exchanges must be taken into account properly to try to estimate F_G and $X_{CO_2,G}$ on the basis of the measured CO_2 time series.

4.4.1. A possible way to obtain F_G and $X_{CO_2,G}$

Let us now use the results of some type A experiments to discuss a possible way to obtain F_G and $X_{CO_2,G}$, assuming that both variables are unknown and that the accumulation chamber is flushed by an unknown, constant flux of air, F_A, during the experimental run. Since type A experiments mimicked the field measurements, only the data acquired during the first 300 s were taken into account. First, we prepared the plot of dX_{CO_2}/dt vs. X_{CO_2}, in which the mean dX_{CO_2}/dt and X_{CO_2} values, calculated averaging the data acquired in time intervals of 10 s, were plotted instead of the original data to reduce the scatter of points (Figure 4.8). Second, dX_{CO_2}/dt was fitted against X_{CO_2} adopting a linear model corresponding to Equation (4.6).

As already recalled in section 4.2.2.2, the obtained straight line has intercept $\left(F_G \cdot X_{CO_2,G} + F_A \cdot X_{CO_2,A}\right)/V$. Since the product $F_G \cdot X_{CO_2,G}$ is equal to F_{CO_2} (see Equation 4.1), the intercept can be rewritten as $\left(F_{CO_2} + F_A \cdot X_{CO_2,A}\right)/V$. Following the approach of Chiodini et al. (1998), F_{CO_2} is obtained from the initial slope (at time zero) of the CO_2 concentration-time curve and F_A was calculated from the intercept of Equation (4.6), since V and $X_{CO_2,A}$ are known. Knowing F_A, then F_G was computed from the slope of Equation (4.6), which is equal to $-\left(F_G + F_A\right)/V$.

The procedure is straightforward, but the obtained $X_{CO_2,G}$ and F_G, values are somewhat at variance from the corresponding known, imposed values. Therefore, we used the procedure outlined above to compute, by trial and error, the CO_2 flux values, $F^*_{CO_2}$, which are needed to reproduce the known $X_{CO_2,G}$ values.

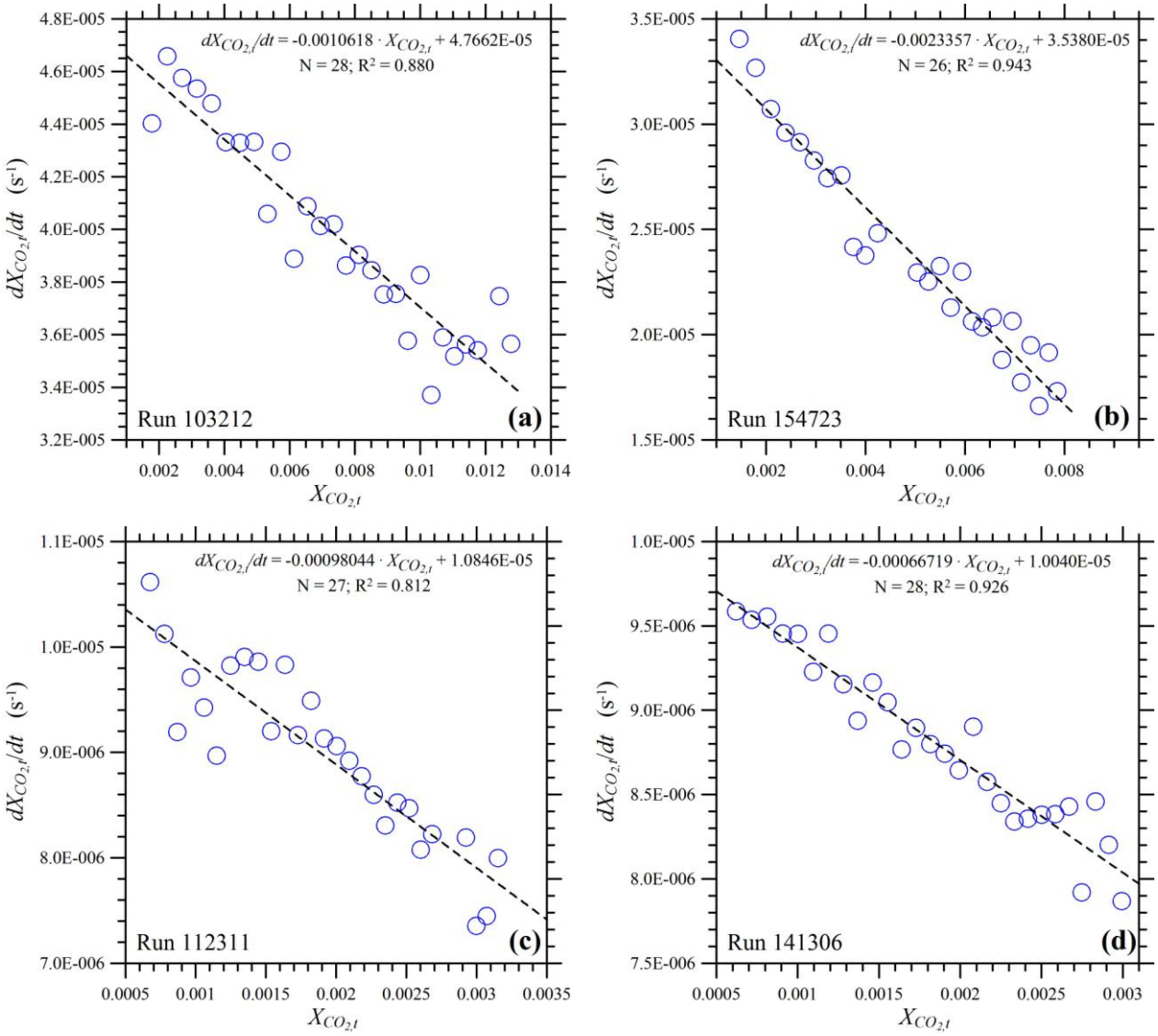

Figure 4.8. Plot of dX_{CO_2}/dt vs. X_{CO_2} for the four selected experiments of type A shown in Figure 4.5.

For the four runs reported in Table 4.3, the absolute percentual deviations of the $F^*_{CO_2}$ values from the corresponding F_{CO_2} values were 0.35, 0.21, 0.88 and 0.12%, which are lower than the uncertainty on the F_{CO_2} values determined from the initial slope (at time zero) of the CO_2 concentration-time curve. Table 4.3 also show that increasing and decreasing the $F^*_{CO_2}$ values by 1‰ cause absolute percentual deviations of 3 to 18% in $X_{CO_2,G}$ and 4 to 16% in F_G for the four considered runs, indicating that the precision on F_{CO_2} must be in the order of 1‰ or even better to reproduce $X_{CO_2,G}$ and F_G with an acceptable approximation by using the procedure described in this section. Since we cannot expect to achieve this precision (and accuracy) on the F_{CO_2} measurement,

the determination of the $X_{CO_2,G}$ and F_G values from the accumulation chamber CO_2 time series, a different procedure has to be found.

Table 4.3. Known and computed $X_{CO_2,G}$, F_G, F_A, and F_{CO_2} values for the experimental runs of type A shown in Figure 4.5.

Code	$X_{CO_2,G}$ (1)	F_G (1)	F_A (2)	F_{CO_2} (3)	$F^*_{CO_2}$ (4)	$X_{CO_2,G}$ (5)	F_G (5)	F_A (5)
		$cm^3 s^{-1}$	$cm^3 s^{-1}$	$cm^3 s^{-1}$	$cm^3 s^{-1}$		$cm^3 s^{-1}$	$cm^3 s^{-1}$
103212	0.09	1.67	2.26	0.14698	0.14647	0.0899	1.629	1.655
"	"	"	"	"	0.14632	0.1065	1.374	1.910
"	"	"	"	"	0.14661	0.0778	1.884	1.400
154723	0.02	5.00	1.05	0.10818	0.10841	0.0200	5.415	1.809
"	"	"	"	"	0.10830	0.0207	5.223	2.001
"	"	"	"	"	0.10852	0.0194	5.607	1.617
112311	0.02	1.67	1.77	0.032527	0.032817	0.0200	1.641	1.392
"	"	"	"	"	0.032784	0.0208	1.578	1.454
"	"	"	"	"	0.032850	0.0193	1.703	1.329
141306	0.02	1.67	0.354	0.030865	0.030828	0.0200	1.540	0.5233
"	"	"	"	"	0.030797	0.0210	1.468	0.5955
"	"	"	"	"	0.030859	0.0191	1.613	0.4510

(1) Known, imposed value;
(2) computed using Equation (4.5), assuming that the accumulation chamber is flushed by a constant flux of atmospheric air;
(3) computed from the initial slope (at time zero) of the CO_2 concentration-time curve;
(4) first of three lines: F_{CO_2} values adopted to reproduce the known $X_{CO_2,G}$ using the procedure outlined in section 4.4.1; second of three lines: F_{CO_2} - 1‰; third of three lines: F_{CO_2} + 1‰;
(5) computed from the plot of dX_{CO_2}/dt vs. X_{CO_2}, using the procedure outlined in section 4.4.1 and adopting the $F^*_{CO_2}$ value.

4.4.2. Implications

Assuming that $X_{CO_2,G}$ and F_G values can be obtained from the accumulation chamber CO_2 time series by means of a suitable procedure, it is worth to underscore two related implications.

One implication results from the availability of three variables, namely F_{CO_2}, F_G, and $X_{CO_2,G}$, only two of which are independent, instead of a single variable, F_{CO_2}. Through the bivariate statistics and geostatistics of these variables we expect to improve the knowledge of the natural systems of interest. For instance, it should be possible to understand if high F_{CO_2} values are controlled by either (i) high F_G values or (ii) high $X_{CO_2,G}$ values or (iii) high values of both variables and,

conversely, if low F_{CO_2} values are due to either (a) low F_G values or (b) low $X_{CO_2,G}$ or (c) low values of both parameters.

The other implication is the proper interpretation of isotopic data, which has been the subject of several recent papers (e.g., Chiodini et al., 2008; Parks et al., 2013; Dionis et al., 2015; Lee et al., 2016; Robertson et al., 2016; Hutchison et al., 2016). To discuss this point, let us assume that two gas samples are collected at each measurement point from the accumulation chamber, as done by Chiodini et al. (2008). The first sample (sample A) is collected after a few seconds to allow homogenisation of the gas mixture inside the chamber, whereas the second sample (sample B) is collected some time later, at higher CO_2 concentration. Both samples are then analyzed for the $\delta^{13}C_{CO_2}$ value. The X_{CO_2} and $\delta^{13}C_{CO_2}$ value of the two samples constrain the mixing line between soil gas and air, which is a straight line in the plot of $\delta^{13}C_{CO_2}$ vs. the inverse of X_{CO_2} (Faure, 1986), as schematically shown in Figure 4.9. This plot also shows that it is possible to reconstruct the $\delta^{13}C_{CO_2}$ value of soil gas, $\delta^{13}C_{CO_2,G}$, but only if $X_{CO_2,G}$ is known. This is why the CO_2 concentration of soil gas is of utmost importance for the proper interpretation of the $\delta^{13}C_{CO_2}$ values of soil gas – air mixtures collected inside the accumulation chamber.

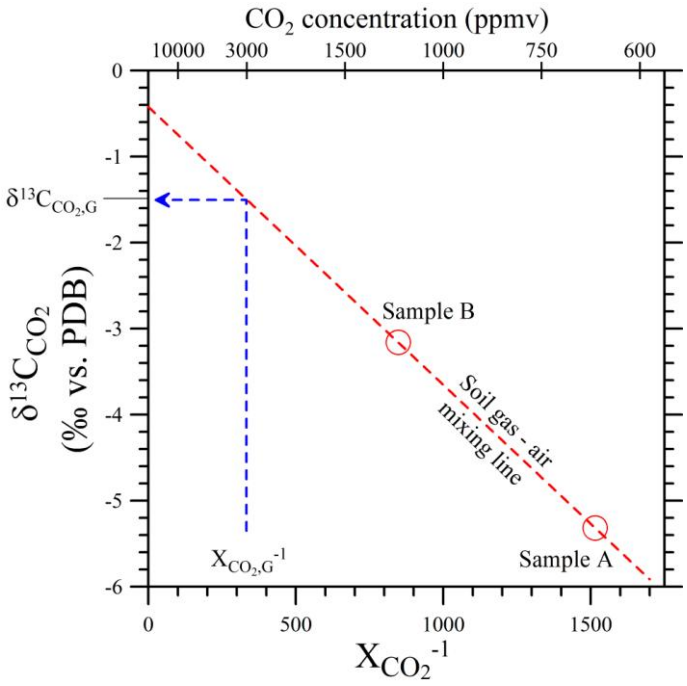

Figure 4.9. Plot of the $\delta^{13}C$ value of CO_2 vs. the inverse of the CO_2 molar fraction for two soil gas – air mixtures collected inside the accumulation chamber, samples A and B, which constrain the soil gas – air mixing line (red dashed line). The inverse of the CO_2 molar fraction of soil gas allows one to estimate the ^{13}C value of CO_2 of soil gas, following the blue dashed line with arrow.

Acknowledgements **-** This research was supported by the CO_2 REACT Marie Curie Initial Training Network (http://www.see.leeds.ac.uk/co2react/).

References

Allard P., Carbonnelle J., Dajlevic D., Le Bronec J., Morel P., Robe M.C., Maurenas J.M., Faivre-Pierret R., Martin D., Sabroux J.C., Zettwoog P. (1991). Eruptive and diffuse emissions of CO_2 from Mount Etna. Nature, 351, 387-391.

Baubron J.C., Allard P., Toutain J.P. (1990). Diffuse volcanic emissions of carbon dioxide from Vulcano Island, Italy. Nature, 344, 51-53.

Baubron J.C., Allard P., Sabroux J.C., Tedesco D., Toutain, J.P. (1991). Soil gas emanations as precursory indicators of volcanic eruptions. J. Geol. Soc. London, 148, 571-576.

Bergfeld D., Goff F., Janik C.J. (2001). Elevated carbon dioxide flux at the Dixie Valley geothermal field, Nevada; relations between surface phenomena and the geothermal reservoir. Chemical Geology, 177, 43-66.

Brombach T., Hunziker J.C., Chiodini G., Cardellini C., Marini L. (2001). Soil diffuse degassing and thermal energy fluxes from the southern Lakki plain, Nisyros (Greece). Geophys. Res. Lett., 28, 69-72.

Brusca L., Inguaggiato S., Longo M., Madonia P., Maugeri R. (2004). The 2002–2003 eruption of Stromboli (Italy): Evaluation of the volcanic activity by means of continuous monitoring of soil temperature, CO_2 flux, and meteorological parameters. Geochem. Geophys. Geosyst., 5, Q12001, doi:10.1029/2004GC000732.

Carapezza M.L. & Federico C. (2000). The contribution of fluid geochemistry to the volcano monitoring of Stromboli. Journal of Volcanology and Geothermal Research, 95, 227-245.

Carapezza M.L. & Granieri D. (2004). CO_2 soil flux at Vulcano (Italy): comparison between active and passive methods. Applied Geochemistry, 19, 73-88.

Carapezza M.L., Ricci T., Ranaldi M., Tarchini L. (2009). Active degassing structures of Stromboli and variations in diffuse CO_2 output related to the volcanic activity. Journal of Volcanology and Geothermal Research, 182, 231-245.

Chiodini G., Cioni R., Guidi M., Raco B., Marini L. (1998). Soil CO_2 flux measurements in volcanic and geothermal areas. Applied. Geochemistry., 13, 543-552.

Chiodini G., Frondini F., Cardellini C., Granieri D., Marini L., Ventura G. (2001). CO_2 degassing and energy release at Solfatara volcano, Campi Flegrei, Italy. J. Geophys. Res., 106(B8), 16213-16221.

Chiodini G., Baldini A., Barberi F., Carapezza M.L., Cardellini C., Frondini F., Granieri D., Ranaldi M. (2007). Carbon dioxide degassing at Latera caldera (Italy): evidence of geothermal reservoir and evaluation of its potential energy. J. Geophys. Res., 112, B12204, doi:10.1029/2006JB004896.

Chiodini G., Caliro S., Cardellini C., Avino R., Granieri D., Schmidt A. (2008). Carbon isotopic composition of soil CO2 efflux, a powerful method to discriminate different sources feeding soil CO2 degassing in volcanic-hydrothermal areas. Earth Planet. Sci. Lett., 274, 372-379.

Dionis S.M., Melián G., Rodríguez F., Hernández P.A., Padrón E., Pérez N.M., Barrancos J., Padilla G.ermán, Sumino H., Fernandes P., Bandomo Z., Silva S., Pereira J.M., Semedo H. (2015). Diffuse volcanic gas emission and thermal energy release from the summit crater of Pico do Fogo, Cape Verde. Bull. Volcanol., 77, 1-13.

Edwards N.T. (1975). Effects of temperature and moisture on carbon dioxide evolution in a mixed deciduous forest floor. Soil Sci. Soc. Am. Proc., 39, 361–365.

Evans W.C., Sorey M.L., Kennedy B.M., Stonestrom D.A., Rogie J.D., Shuster D.L. (2001). High CO_2 emissions through porous media: Transport mechanisms and implications for flux measurement and fractionation, Chemical Geology, 177, 15 – 29.

Evans W.C., Bergfeld D., McGimsey R.G., Hunt A.G. (2009). Diffuse gas emissions at the Ukinrek Maars, Alaska: Implications for magmatic degassing and volcanic monitoring. Applied Geochemistry, 24, 527-535.

Faure G. (1986). Principles of isotope geology. 2nd edition. Wiley, New York, 589 pp.

Fridriksson T., Kristjánsson B.R., Ármannsson H., Margrétardóttir E., Ólafsdóttir S., Chiodini G. (2006). CO_2 emissions and heat flow through soil, fumaroles, and steam heated mud pools at the Reykjanes geothermal area, SW Iceland. Applied Geochemistry., 21, 1551-1569.

Frondini F., Chiodini G., Caliro S., Cardellini C., Granieri D., Ventura G. (2004). Diffuse CO_2 degassing at Vesuvio, Italy. Bull. Volcanol., 66, 642–651.

Frondini F., Caliro S., Cardellini C., Chiodini G., Morgantini N. (2009). Carbon dioxide degassing and thermal energy release in the Monte Amiata volcanic-geothermal area (Italy). Applied Geochemistry, 24, 860-875.

Gerlach T., Doukas M., McGee K., Kessler R. (2001). Soil efflux and total emission rates of magmatic CO2 at the Horseshoe Lake tree kill, Mammoth Mountain, California. Chemical Geology, 177, 101–116.

Granieri, D., Chiodini, G., Marzocchi, W., Avino, R. (2003). Continuous monitoring of CO_2 soil diffuse degassing at Phlegraean Fields (Italy): influence of environmental and volcanic parameters. Earth Plan. Sci. Lett. 212, 167–179.

Granieri D., Avino R., Chiodini G. (2010). Carbon dioxide diffuse emission from the soil: ten years of observations at Vesuvio and Campi Flegrei (Pozzuoli), and linkages with volcanic activity. Bull. Volcanol., 72, 103–118.

Hanson P.J., Wullschleger S.D., Bohlman S.A., Todd D.E. (1993). Seasonal and topographic patterns of forest floor CO2 efflux from an upland oak forest. Tree Physiol., 13, 1-15.

Healy R.W., Striegl R.G., Russell T.F., Hutchinson G.L., Livingston G.P. (1996). Numerical evaluation of static-chamber measurements of soil-atmosphere gas exchange: identification of physical processes. Soil Sci. Soc. Am. J., 60, 740-747.

Hernández P.A., Pérez N.M., Salazar J.M., Nakai S., Notsu K., Wakita H. (1998). Diffuse emissions of carbon dioxide, methane, and hellium-3 from Teide volcano, Tenerife, Canary Islands, Geophys. Res. Lett., 25, 3311–3314, doi:10.1029/98GL02561.

Hernández P.A., Salazar J.M., Shimoike Y., Mori T., Notsu K., Pérez N. (2001). Diffuse emission of CO2 from Miyakejima volcano, Japan. Chemical Geology, 177, 175-185.

Hutchison W., Mather T.A., Pyle D.M., Biggs J., Yirgu G. (2015). Structural controls on fluid pathways in an active rift system: a case study of the Aluto volcanic complex. Geosphere 11, 542–562.

Hutchison W., Biggs J., Mather T.A., Pyle D.M., Lewi E., Yirgu G., Caliro S., Chiodini G., Clor L.E., Fischer T.P. (2016). Causes of unrest at silicic calderas in the East African Rift: New constraints from InSAR and soil-gas chemistry at Aluto volcano, Ethiopia. Geochem. Geophys. Geosyst., 17, 3008– 3030, doi:10.1002/2016GC006395.

Jolie E., Klinkmueller M., Moeck I. (2015). Diffuse surface emanations as indicator of structural permeability in fault-controlled geothermal systems. Journal of Volcanology and Geothermal Research, 290, 97-113.

Lee H., Muirhead J.D., Fischer T.P., Ebinger C.J., Kattenhorn S.A., Sharp Z.D., Kianji G. (2016). Massive and prolonged deep carbon emissions associated with continental rifting. Nature Geoscience. DOI: 10.1038/NGEO2622.

Lewicki J.L. & Brantley S.L. (2000). CO_2 degassing along the San Andreas fault, Parkfield, California. Geophys. Res. Lett. 27, 5–8.

Lewicki J.L., Bergfeld D., Cardellini C., Chiodini G., Granieri D., Varley N., Werner C. (2005). Comparative soil CO_2 flux measurements and geostatistical estimation methods on Masaya volcano, Nicaragua. Bull. Volcanol., 68, 76-90.

Lewicki J.L., Hilley G.E., Tosha T., Aoyagi R., Yamamoto K., Benson S.M. (2007). Dynamic coupling of volcanic CO_2 flow and wind at the Horseshoe Lake tree kill, Mammoth Mountain, California. Geophys. Res. Lett., 34, L03401, doi:10.1029/2006GL028848.

Lewicki J.L., & Hilley G.E (2014). Multi-scale observations of the variability of magmatic CO_2 emissions, Mammoth Mountain, CA, USA. Journal of Volcanology and Geothermal Research 284 (2014) 1–15.

Mazot A., Rouwet D., Taran Y., Inguaggiato S., Varley N. (2011). CO_2 and He degassing at El Chichón volcano, Chiapas, Mexico: gas flux, origin and relationship with local and regional tectonics. Bull. Volcanol., 73, 423-441.

Norman J.M., Garcia R., Verma S.B. (1992). Soil surface CO_2 fluxes and the carbon budget of a grassland. J. Geophys. Res., 97, 18845-18853.

Norman J.M., Kucharik C.J., Gower S.T., Baldocchi D.D., Crill P.M., Rayment M., Savage K., Strieglfi R.G. (1997). A comparison of six methods for measuring soil-surface carbon dioxide fluxes. J. Geophys. Res.,102, 28-771.

Notsu K., Sugiyama K., Hosoe M., Uemura A., Shimoike Y., Tsunomori F., Sumino H., Yamamoto J., Mori T., Hernández P.A. (2005). Diffuse CO_2 efflux from Iwojima volcano, Izu-Ogasawara arc, Japan. Journal of Volcanology and Geothermal Research, 139, 147-161.

Padilla G.D., Hernández P.A., Pérez N.M., Pereda E., Padrón E., Melián G., Herrera M. (2014). Anomalous diffuse CO_2 emissions at the Masaya Volcano (Nicaragua) related to seismic-volcanic unrest. Pure and Appl. Geophys., 171, 1791-1804.

Padrón E., Hernández P.A., Toulkeridis T., Pérez N.M., Marrero R., Melián G., Virgili G., Notsu K. (2008a). Diffuse CO_2 emission rate from Pululahua and the lake-filled Cuicocha calderas, Ecuador. Journal of Volcanology and Geothermal Research, 176, 163-169.

Padrón E., Melián G., Marrero R., Nolasco D., Barrancos J., Padilla G., Hernández P.A., Pérez N.M. (2008b). Changes in the diffuse CO_2 emission and relation to seismic activity in and around El Hierro, Canary Islands, Pure Appl. Geophys., 165, 95–114, doi:10.1007/s00024-007-0281-9.

Parks M.M., Caliro S., Chiodini G., Pyle D.M., Mather T.A., Berlo K., Edmonds M., Biggs J., Nomikou P., Raptakis C. (2013). Distinguishing contributions to diffuse CO_2 emissions in volcanic areas from magmatic degassing and thermal decarbonation using soil gas 222Rn–δ13C systematics: Application to Santorini volcano, Greece. Earth Planet. Sci. Lett., 377, 180-190.

Pérez N.M., Padill, G.D., Padrón E., Hernández P.A, Melián G.V., Barrancos J., Dionis S., Nolasco D., Rodríguez F., Calvo D., Hernández I. (2012). Precursory diffuse CO_2 and H_2S emission signatures of the 2011–2012. El Hierro submarine eruption, Canary Islands.

Rissmann C., Christenson B., Werner C., Leybourne M., Cole J., Gravley D. (2012). Surface heat flow and CO_2 emissions within the Ohaaki hydrothermal field, Taupo Volcanic Zone, New Zealand. Applied Geochemistry, 27, 223-239.

Rogie J.D., Kerrick D.M., Sorey M.L., Chiodini G., Galloway D.L. (2001). Dynamics of carbon dioxide emission at Mammoth Mountain, California. Earth Planet. Sci. Lett., 188, 535-541.

Robertson E., Biggs J., Edmonds M., Clor L., Fischer T.P., Vye-Brown C., Kianji G., Koros W., Kandie R. (2016). Diffuse degassing at Longonot volcano, Kenya: Implications for CO_2 flux in continental rifts. Journal of Volcanology and Geothermal Research. http://dx.doi.org/10.1016/j.jvolgeores.2016.06.016 (in press).

Salazar J.M., Hernández P.A., Pérez N.M., Melián G., Álvarez J., Segura F., Notsu K. (2001). Diffuse emission of carbon dioxide from Cerro Negro volcano, Nicaragua, Central America. Geophys. Res. Lett., 28, 4275-4278.

Toutain J.P., Sortino F., Baubron J.C., Richon P., Sumarti S., Nonell A. (2009). Structure and CO_2 budget of Merapi volcano during inter-eruptive periods. Bull. Volcanol., 71, 815-826.

Viveiros F., Ferreira T., Vieira J.C., Silva C., Gaspar, J.L. (2008). Environmental influences on soil CO_2 degassing at Furnas and Fogo volcanoes (São Miguel Island, Azores archipelago). Journal of Volcanology and Geothermal Research, 177, 883-893.

Viveiros F., Ferreira T., Silva C., Gaspar J.L. (2009). Meteorological factors controlling soil gases and indoor CO_2 concentration: a permanent risk in degassing areas. Sci. Total Environ., 407, 1362–1372.

Welles J.M., Demetriades-Shah T.H., McDermitt D.K. (2001). Considerations for measuring ground CO_2 effluxes with chambers. Chemical Geology, 177, 3-13.

Werner C. & Cardellini C. (2006) Comparison of carbon dioxide emissions with fluid upflow, chemistry, and geologic structures at the Rotorua geothermal system, New Zealand. Geothermics, 35, 221-238.

Werner C., Bergfeld D., Farrar C.D., Doukas M.P., Kelly P.J., Kern C. (2014). Decadal-scale variability of diffuse CO_2 emissions and seismicity revealed from long-term monitoring (1995–2013) at Mammoth Mountain, California, USA. Journal of Volcanology Geothermal Research, 289, 51-63.

Xu L., Furtaw M.D., Madsen R.A., Garcia R.L., Anderson D.J., McDermitt D.K. (2006). On maintaining pressure equilibrium between a soil CO_2 flux chamber and the ambient air. J. Geophys. Res., 111, D08S10, doi:10.1029/2005JD006435.

CHAPTER 5- CONCLUSIONS

The present PhD Thesis consists of four chapters, a general introduction as well as three additional chapters where the results of the research studies are reported. Each of these chapters stand as an independent manuscript, two that have already been submitted to international scientific journals and one that is ready to be submitted. The main conclusions are summarized hereunder.

The first part of the thesis (chapter 2: A study on wellbore cement carbonation by CO_2 leakage in a natural analogue for the geological CO_2 storage) focuses on a hypothetical average production well with a damaged leaking zone, affecting casing and cement, in the natural analogue for the geological storage of CO_2 of Sant'Albino, Southern Tuscany. The results of reaction path modeling and reactive transport modeling of cement alteration driven by CO_2-rich fluids demonstrate that CO_2 causes a comparatively rapid cement alteration (within few years), first characterized by complete carbonation and later by dissolution of carbonate minerals. This reaction sequence may ultimately lead to a CO_2 leakage to the surface in CO_2 sequestration sites.

The second part of the thesis (chapter 3: Experimental analysis of the reaction rate of hydrated G-class cement at P_{CO2} of 1 to 51 bar and ambient temperature) presents and discusses the results of several experiments carried out to investigate the carbonation rate of cement powder and cement cube samples in contact with an aqueous solution, at 1 to 51 bar CO_2. Solid reaction products and aqueous solution chemistry were thoroughly characterized adopting different analytical techniques. The main results reports that (i) cement powder carbonation is very fast (few hours to days) and (ii) the carbonation rate of cement cube samples is diffusion-controlled. These experimental outcomes support the results of geochemical modeling performed in part I.

The third part of the thesis (chapter 4: Occurrence of a nearly constant air flux through the accumulation chamber during CO_2 flux measurements. Evidence from laboratory experiments and consequences) focuses on the results of laboratory tests carried out with an accumulation chamber either (i) injecting a known gas mixture at known constant flow, thus mimicking the soil CO_2 flux measurements performed in field surveys or (ii) stopping the injection of the gas mixture after a given time. In both test types the chamber seems to be flushed by atmospheric air. Such an air flux does not affect the measurement of the soil CO_2 flux, F_{CO2},. However, it influences the determination of CO_2 molar fraction of soil gas, X_{CO2}, and total soil gas flux, F_G. These are the two components of the soil CO_2 flux, which are linked through the simple relation $F_{CO2} = X_{CO2} \cdot F_G$. The knowledge, not only of F_{CO2} but also of the X_{CO2} and the F_G has important practical consequences,

for instance, for monitoring the possible CO_2 leakage at the CO_2 storage sites. Minor improvements have to be made in order to obtain a reliable and easy applicable method to determine X_{CO2} and F_G.

ANNEX 1- ***Relazione sulle attività svolte nel corso del dottorato (*** *Summary of research studies, seminars and congresses attendance, pubblications****).***

UNIVERSITÀ DEGLI STUDI FIRENZE
DST DIPARTIMENTO DI SCIENZE DELLA TERRA

Dottorato di Ricerca in Scienze della Terra

Relazione sulle attività svolte nel corso del dottorato

First Name: ANA

Last name: HERNANDEZ RODRIGUEZ

Ciclo XXIX

Thesis title: Study of CO_2 leakage from gas reservoirs through the further development of a gas flux device and the role of CO_2 on cap rock integrity and cement/casing degradation by Reaction-Path- and Reactive-Transport-Modeling.

Tutor: PROF. Orlando Vaselli.

Co-Tutors: Luigi Marini, Giordano Montegrossi, Bruno Huet, Giorgio Virgili.

GOALS OF THE RESEARCH

My PhD Thesis is focused on three different aspects related to geological CO_2 storage. First, on the assessment of one of the major risks posed by the geological sequestration of CO_2; the leakage of CO_2-rich gases from the deep reservoirs in which they have been disposed. This risk can be mitigated monitoring the flux of CO_2 from deep reservoirs where CO_2 is injected, by means of the accumulation chamber method, (see chapter 4). Second, the study of wellbore cement alteration and well integrity by using Reaction Path and Reactive Transport Modeling (see chapter 2). The third topic was the experimental determination of cement alteration by means of laboratory experiments, these studies are reported in chapter 3

1ST YEAR (2013-2014)

Research studies (summary); I focused on the study of a natural analogue for the geological CO_2 storage at Sant'Albino, Southern Tuscany, which is affected by intense CO_2 degassing and where a thermal spa and a CO_2 production plant are present. During this period I measured and mapped the diffuse CO_2 fluxes from soil to monitor the gas leakage in this area. Reaction Path and Reactive Transport Modeling of cement hydration and carbonation of cement alteration were used to investigate the processes occurring near a hypothetical average production well with a damaged leaking zone, affecting casing and cement.

Seminars/Workshops/Congress:

- "The use of the geochemical code Phreeqc" and "Introdution to write a paper". *Kick off-meeting of CO_2-REACT*, Fuerteventura, Spain: 7-14 th, February, 2014
- Giornata della Geochimica Italiana, Florence. May 8 th, 2014.
- Workshop Geobasi Project: the Regional Geochimical Database, 27th of May, 2014. First application for the management and data analysis of surface waters and groundwaters
- Workshop Prospects and solutions for the development of geothermal district heating in Italy and Europe, 25th of June , 2014.
- Media training workshop. Communicating science to the media. 24th August Reykjavik, Iceland.
- The International Carbon Conference, Iceland. August 25-29 th , 2014.
- GIS per le applicazioni geologiche e ambientali. University of Florence (Italy), September 10-12th, 2014.
- Research project management and communication skills. *Mid-term review CO_2-REACT project*. Seefeld, Austria.

2ND YEAR (2014-2015)

Research studies (summary): During this period I performed hydration and carbonation experiments for Portland cement G-class. One part of the study was carried out at the University of Florence and the other part was carried out at Lafarge-Holcim Research based on Lyon-France,

where I spent a month of the entire secondment as a PhD student. During this period at Lafarge I was studying and understanding hydration and carbonation in cements and different techniques for studying these processes, in the laboratory and/or in the field. Then, I performed first cement hydration experiments for 28 days at atmospheric conditions. Afterwards, I carried out cement carbonation experiments using a micro-reactor by reacting, in separate runs, cement powder samples, under stirred conditions with pure CO_2(g) and MilliQ water. The reaction time and the CO_2 partial pressure were varied to constrain the reaction kinetics of the carbonation process and to investigate the evolution of primary and secondary solid phases. After the completion of each experiments, mineralogical analyses (X-ray Powder Diffraction and Scanning Electron Microscope) were carried out to this purpose. Water analyses were also performed by ion chromatography, ICP-OES and acidimetric titration at the end of each experimental run, to investigate the chemical effects of cement carbonation on the aqueous solution. The carbonation degree was calculated from the results of Thermo-Gravimetric Analysis (TGA).

Seminars/ Workshops/ Congress;

- Congress; *4th CO2 REACT Project. Network Meeting Tuscany*. Career management course. Demonstration on how to use a Gas Flux Meter, West Systems (Pontedera, Italy). 8-12sd March, 2015.
- Course: Hydrogeochemical transport modeling with PHREEQC version 3. Given by Dr. C.A.J. Appelo Hydrochemical Consultant, Amsterdam. 30th March- 02 April, 2015
- Workshop: Innovation in Tuscany on dredging sediment processing. Livorno. West Systems- Progetto Life SEKRET. 14th April 2015.
- Workshop: PhD Day Florence. University of Florence. Poster presentation. 27th May, 2015.
- Course: Pore Scale geochemical processes. Mineralogical society of America. Goldschmidt Conference, Prague. 15-16th August, 2015.
- Godschmidt International Conference 2015. Prague. 16-21st August, 2015.
- TOUGH2 SHORT COURSE. Lawrence Berkeley National Laboratory. Berkeley, California. 28-30th September, 2015.
- TOUGH SYMPOSIUM 2015, Lawrence Berkeley National Laboratory. Berkeley, California. 23-25th September, 2015.
- Course; Introduzione all'utilizzo di Matlab. University of Pisa. 26th -29th October, 2015.

3RD YEAR (2015-2016)

Research studies (summary): I completed the carbonation experiments for a G-class Portland cement powder samples explained above together with the performance of new cement carbonation experiments in massive samples. For the new carbonation experiments, I used the same hydration cement made for the previous studies. The experiments were performed in a micro-reactor with pure CO_2(g) and MilliQ but with massive samples, under stagnant conditions at room temperature. In this case the pressure was maintained and the reaction time was changed in different runs. The carbonation progress was assessed for each sample from: (1) the mass gain, that is the difference between the weight of the cement cube after and before the carbonation experiment, and (2) the carbonation depth, which was obtained by using the phenolphthalein method.

Part of the experiments were carried out either at the University of Florence or at Lafarge-Holcim research center where I completed also the three-month secondment period for my PhD.

Last months, I performed gas laboratory experiments to improve the present understanding of the accumulation chamber method. These studies concerns the measuring of diffuse CO_2 fluxes from soil to monitor the gas leakage in gas reservoirs or CO_2 injection sites.

Seminars/Workshops/Congress:

- Tecniche di misura di flussi di gas dal suolo ed applicazioni. Professor; Orlando Vaselli. University of Florence. 10-11st March, 2016.
- *CO_2-React network meeting on Industrial Applications of Water-Rock Interactions*. 13-17th March, 2016.
- Participation at the EGU Conference . Vienna, Austria. 17-22nd April, 2016.
- Attendance to the *CO_2-React last meeting*. Training in Career Management Skills. 18-23 rd September 2016.
- Attendance to the Water Rock Interaction Conference. Evora, Portugal. 16-21St October 2016.

LIST OF ABSTRACTS and PUBBLICATIONS

- Hernández A., Montegrossi G., Vaselli O., Virgili G., Minardi I., Marini L. (2014) Use of Reaction Path Modeling to investigate wellbore integrity in the geological storage of CO_2. ICC 2014 - The International Carbon Conference, Reykjavík, Iceland, August 25-29. 2014. Poster. https://www.or.is/sites/default/files/icc2014.pdf

- Hernández A., Montegrossi G., Virgili G., Vaselli O., Marini L. (2015) A study on well integrity in a natural analogue for the geological CO_2 storage. PhD Day University of Florence, May 27th 2015. Poster. http://phdday.lens.unifi.it/previous/6/img/abstract_booklet.pdf.

- Hernández-Rodríguez A., Montegrossi G., Virgili G., Vaselli O., Huet B., Marini L. (2015) Use of Reactive Transport Modelling to study well integrity in a natural analogue for the geological CO_2 storage. Proceedings, TOUGH Symposium 2015. Lawrence Berkeley National Laboratory, Berkeley, California, September 28-30, 2015. Oral Communication http://esd1.lbl.gov/files/research/projects/tough/events/symposia/toughsymposium15/Proceedings_TOUGHSymposium2015.pdf.

- Hernández-Rodríguez A., Montegrossi G., Virgili G., Vaselli O., Minardi I., Marini L. (2015) A study on well integrity in a natural analogue for the geological CO_2 storage. Goldschmidt 2015, Prague, August 16-21. Oral Communication. http://goldschmidt.info/2015/uploads/abstracts/finalPDFs/1247.pdf

- Hernández-Rodríguez A., Montegrossi G., Huet B., Virgili G., Orlando A., Vaselli O., Marini L.(2016) Experimental determination of carbonation rate in Portland cement at 25°C and relatively high CO_2 partial pressure. EGU 2016, Vienna, Austria 17-22 April. Poster.http://meetingorganizer.copernicus.org/EGU2016/EGU2016-14739.pdf

- Hernández-Rodríguez A., Montegrossi G., Orlando A., Huet B., Agnelli M., Venturi S., Virgili G., Orlando A., Vaselli O., Marini L. Experimental analysis of the reaction rate of hydrated Class G cement powder at 11 bar PCO2 and ambient temperature. Procedia, 15th Water Rock Interactions, 2016. Evora, 16-21 October, Portugal. Poster.

- Hernández-Rodríguez, A., Virgili, G., Continanza, D., Ferrante, L., Marini, L. (2016). Occurrence of a nearly constant air flux through the accumulation chamber during CO_2 flux measurements. Evidence from laboratory experiments and consequences. Journal of Volcanology and Geothermal Research (submitted).

- Hernández-Rodríguez A., Montegrossi G., Orlando A., Huet B., Virgili G., Orlando A., Vaselli O., Marini L. (2016). A study of wellbore cement alteration controlled by CO_2 leakage in a natural analogue for geological CO_2 storage. Chemical Geology (submitted).

MEDIA SCIENCE COMUNICATIONS

- Hernández-Rodríguez A., Sáinz-García A.(2015) Natural CO_2 emissions: Understanding the past to forecast the future http://www.co2-react.com/?p=129.

- Hernández-Rodríguez A. West Systems taking part in the climate change.

- Encourage young people in science: http://www.fqsaja.com/?p=8682, Santander, Spain.

In Florence, at 29/11/2016

Signed by Ana Hernández Rodríguez